

REMARKS/ARGUMENTS

The Office Action has rejected all claims under a combination of 35 U.S.C. § 112 first and second paragraphs. Each rejection raised by the Examiner is addressed separately below. In light of the amendments above and the arguments below, Applicants respectfully request reconsideration.

IN THE CLAIMS

Claims 26 and 27 are pending. Claims 1-25 and 28-30 have been withdrawn. Claims 26 and 27 have been amended herein, and support for the amendments can be found in the application as filed. No new matter has been added.

REJECTION UNDER 35 USC §112, FIRST PARAGRAPH-INDEFINITENESS

Claims 26 and 27 have been rejected as being indefinite for failing to particularly point out and distinctly claim the subject matter of the invention. Specifically, the Examiner alleges that the phrase "antiviral therapy" is vague and indefinite and that it is unclear how a substance can be an antiviral therapy. Without agreeing to the Examiner's characterization of the claims, and solely to move prosecution forward, Applicants have amended claims 26 and 27 to recite "A method of evaluating a substance as an antiviral agent". Support for this amendment can be found in the application as filed, see paragraph [0008] of the published application.

REJECTION UNDER 35 USC §112, SECOND PARAGRAPH-WRITTEN DESCRIPTION

Claims 26 and 27 have been rejected as failing to comply with the written description requirement. Specifically, the Examiner alleges that the claims read on using a $\Delta 9$ fatty acid desaturase enzyme derived from various organisms such as humans, rats, mice, canines, felines, sheep, cows, etc., but the specification only discusses using $\Delta 9$ fatty acid desaturase enzyme encoded by OLE1 gene in yeast. Without agreeing to the Examiner's characterization of the claims, and solely to move prosecution forward, Applicants have amended claims 26 and 27 to recite "exposing a substance to a yeast or mammalian $\Delta 9$ fatty acid desaturase enzyme." The application as filed discloses a close functional relationship between the yeast and mammalian enzymes. Support for this amendment can be found in the application as filed, see paragraph [0052] of the

published application. As paragraph [0052] discloses, $\Delta 9$ fatty acid desaturase enzyme name is generally applied to the class of homologous enzymes from yeast and other cells. There is much homology and functional equivalence among such genes. For instance, it is known that the corresponding $\Delta 9$ fatty acid desaturase from mammals can functionally replace the yeast protein, and conversely that expressing yeast $\Delta 9$ fatty acid desaturase in mammalian cells modulates the level of UFAs in those cells in the predictable manner expected from its function.

REJECTION UNDER 35 USC §112, SECOND PARAGRAPH-ENABLEMENT

Claims 26 and 27 have been rejected as failing to comply with the enablement requirement. Specifically, the Examiner alleges that the specification fails to provide adequate guidance as to whether affecting the stability or activity of various $\Delta 9$ desaturase enzymes (OLE1 proteins) would be indicative of potential antiviral therapy. Applicants disagree, and point to the specification as filed for support.

For instance, the specification clearly discloses that $\Delta 9$ desaturase enzyme is the desaturase that converts newly synthesized SFAs to UFAs (paragraph [0138]) and that positive strand RNA replication is strongly dependent on UFA levels (paragraph [0143]). When UFA was limited, RNA replication was blocked (paragraph [0143]), leading to the conclusion that modulating the lipid composition of membranes helps to identify useful antiviral agents (paragraph [0144]). In short, an agent that impacts the stability of the $\Delta 9$ desaturase enzyme impacts the stability of UFA levels and therefore impacts RNA replication, and is a possible antiviral agent. See for example, Exhibits A-D attached hereto, which provide further support, particularly (but not exclusively) in regards to positive strand RNA viruses, for the universal dependence of RNA replication on expanded, rearranged membranes, and thus on the synthesis and physical characteristics of these membranes, which are governed by their UFA-dominated lipid composition. Accordingly, Applicants submit that the specification as filed clearly provides adequate guidance as to whether decreasing the stability or inhibiting the activity of $\Delta 9$ desaturase enzymes is indicative of an antiviral agent.

The Examiner also alleges that there are numerous types of viruses and that infection caused by the different viruses vary greatly. The Examiner alleges that a substance identified through its effect in decreasing stability or inhibiting activity of

OLE1 proteins may be antiviral for one type of infection, but not necessarily antiviral for other types of infections. Without agreeing to the Examiner's characterization of the claims, and solely to move prosecution forward, Applicants have amended claims 26 and 27 to recite "A method of evaluating a substance as a positive strand RNA antiviral agent." The specification clearly discloses that positive strand viruses such as BMV are inhibited when the stability of the delta 9 desaturase enzyme is affected (see above). Accordingly, Applicants submit that as amended, claims 26 and 27 are fully enabled by the specification as filed.

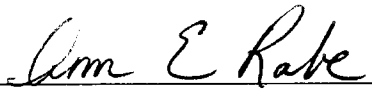
SUMMARY

A Petition for One-Months Extension of Time and Authorization to Charge Fees is included herewith. No additional fee is believed due in connection with this submission. However, if a fee is due in this or any subsequent response, please charge the fee to Deposit Account No. 17-0055.

Respectfully submitted,

Paul G. Ahlquist, *et al.*

Date: February 14, 2008

By: 
Ann E. Rabe, Reg. No. 56, 597
Attorney for Applicants
QUARLES & BRADY
411 East Wisconsin Avenue
Milwaukee, WI 53202
(414) 277-5613

Applicant's
Exhibit
A

Parallels among positive-strand RNA viruses, reverse-transcribing viruses and double-stranded RNA viruses

Paul Ahlquist

Abstract | Viruses are divided into seven classes on the basis of differing strategies for storing and replicating their genomes through RNA and/or DNA intermediates. Despite major differences among these classes, recent results reveal that the non-virion, intracellular RNA-replication complexes of some positive-strand RNA viruses share parallels with the structure, assembly and function of the replicative cores of extracellular virions of reverse-transcribing viruses and double-stranded RNA viruses. Therefore, at least four of seven principal virus classes share several underlying features in genome replication and might have emerged from common ancestors. This has implications for virus function, evolution and control.

Positive-strand RNA virus
A virus, the infectious virions of which contain the genome in a single-stranded, messenger-sense RNA form.

Despite continuing advances, established and emerging viruses remain major causes of human disease, with dramatic costs in mortality, morbidity and economic terms. In addition to acute diseases, viruses cause at least 15–20% of human cancers^{1,2} and are implicated in neurological and other chronic disorders. One of many challenges in controlling viruses and virus-mediated diseases is that viruses show an amazing diversity in basic characteristics and life cycles, including differences in virion structure, replication strategies, genetic organization, gene expression and many other fundamental processes. Therefore, even the very processes against which antivirals are targeted often differ radically among virus classes. Inherent in this remarkable variety are intriguing issues about the multiplicity of virus origins and the functional and evolutionary relations of existing viruses. Such issues have practical as well as academic importance, as underlying similarities among virus classes might serve as a foundation for broader-spectrum antiviral strategies.

One of the most elemental differences among viruses is their diversity in genome replication and encapsidation strategies, which define seven major classes (FIG. 1). Some viruses replicate their genomes solely through DNA intermediates, packaging these genomes in infectious virions either as double-stranded (ds)DNA or single-stranded (ss)DNA. By contrast, most viruses replicate their genomes solely through RNA intermediates. Such RNA viruses are divided into three classes based on whether their virions package the genome as mRNA-sense (positive-strand) ssRNA, antisense (negative-strand)

ssRNA or dsRNA. Other viruses replicate by interconverting their genomes between RNA and DNA. The virions of such reverse-transcribing viruses always initially package the RNA forms of their genomes, and either might (for example, hepadnaviruses and foamy retroviruses) or might not (for example, orthoretroviruses) reverse-transcribe the RNA into DNA before the virion exits the initially infected producer cell.

Viruses in each of these seven classes tend to share additional features, such as gene-expression strategies and so on, that further cluster and differentiate their members from the other classes, showing that these classes represent meaningful, functionally distinct groupings and probable evolutionary lineages. Some of these variations arise because the type of nucleic acid delivered by the virion to a target cell dictates early infection and gene-expression steps. For example, to initiate viral gene expression, dsRNA virus virions and negative-strand RNA ((-)RNA) virus virions contain viral polymerases that transcribe the genome into translatable mRNA, and reverse-transcribing-virus virions contain polymerases that copy the genome into cell-transcribable DNA (BOX 1). Positive-strand RNA ((+)RNA) viruses, the virions of which deliver immediately translatable messenger-sense RNAs, encapsidate their RNA without a polymerase and form strictly intracellular RNA-replication and mRNA transcription complexes (BOX 1).

Despite these and other differences, recent results have revealed fundamental parallels in the genome-replication processes of certain (+)RNA viruses, dsRNA viruses and reverse-transcribing viruses. In particular, the

Institute for Molecular Virology and Howard Hughes Medical Institute, University of Wisconsin–Madison, Madison, Wisconsin 53706, USA.
e-mail: ahlquist@wisc.edu
doi:10.1038/nrmicro1389
Published online 3 April 2006

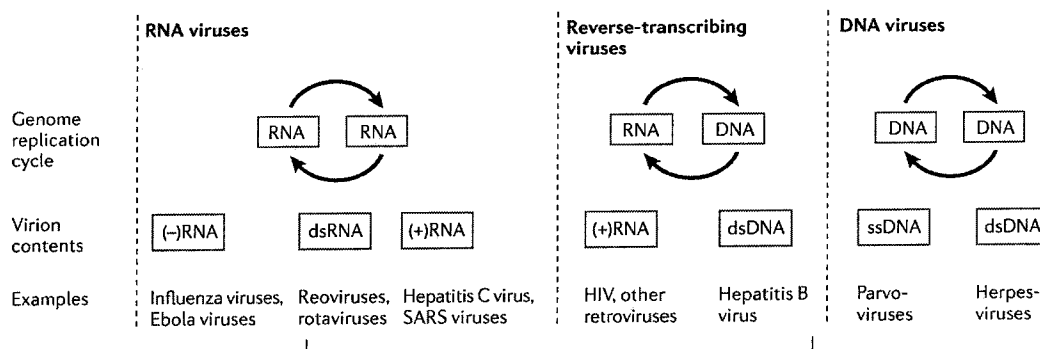


Figure 1 | Seven classes of virus distinguished by genome replication and encapsidation strategies. The bracket highlights the four virus classes emphasized in this review. (+)RNA, positive-strand RNA, which is single-stranded RNA of the same polarity as viral mRNA; (-)RNA, negative-strand RNA, which is single-stranded RNA of anti-mRNA polarity; dsRNA, double-stranded RNA; SARS, severe acute respiratory syndrome.

intracellular RNA-replication complexes of some, if not many, (+)RNA viruses share several similarities with the replicative cores of virions from both dsRNA viruses and reverse-transcribing viruses. This review outlines these similarities and their potential implications for virus function and evolution. As primary examples, we review similarities among (+)RNA viruses in the alphavirus-like superfamily, the dsRNA reoviruses and the retroviruses. Other shared characteristics with similar evolutionary implications have been recognized recently among certain other (+)RNA viruses, the dsRNA birnaviruses and the reverse-transcribing hepadnaviruses, including parallels in viral RNA-polymerase structure, capsid proteins and protein priming of genome replication³⁻⁷.

Negative-strand RNA ((-)RNA) viruses (FIG. 1) also share similarities with some of the basic features reviewed here, suggesting that the functional and evolutionary parallels discussed below might be extended further. These possibilities are not discussed here in detail for reasons of space. In addition, whereas (+)RNA viruses, dsRNA viruses and reverse-transcribing viruses each use identical (+)RNA molecules as genome-replication intermediates and mRNAs, (-)RNA viruses are distinguished by using different forms of (+)RNA for these functions.

(+)RNA virus and retrovirus parallels

tRNAs and genome replication. One of the first similarities recognized between the replication of retroviruses and (+)RNA viruses was the role of tRNAs in initiating retroviral reverse transcription and of tRNA-like elements in initiating RNA replication by a subset of (+)RNA viruses such as the bromoviruses^{8,9} (FIG. 2). Bromoviruses, discussed further below, have three genomic RNAs with highly conserved, structured, tRNA-like 3' ends (FIG. 2b). These 3' ends terminate in 3'-CCA_{OH} sequences that are completed by tRNA-nucleotidyl transferase, they are specifically aminoacylated *in vitro* and *in vivo* with tyrosine, and they contain the promoter for (-)RNA synthesis¹⁰⁻¹³.

tRNA-related sequences initiate negative-strand synthesis for genomic RNA replication in both retroviruses and (+)RNA viruses, but the mechanisms are distinct. For

retroviruses, a cellular tRNA covalently primes negative-strand cDNA synthesis, whereas for the relevant (+)RNA viruses, a viral tRNA-like element serves as a recognition site and template for (-)RNA synthesis that is initiated *de novo*, without a primer. A natural intermediate and potential evolutionary link between these processes was identified by Lambowitz and colleagues, who showed that a *Neurospora crassa* mitochondrial retroplasmid initiates reverse transcription without a primer at the tRNA-like 3' end of its genomic RNA, paralleling negative-strand initiation by (+)RNA viruses¹⁴.

Membrane-associated RNA-replication complexes. As noted above, (+)RNA viruses differ from retroviruses and other RNA viruses in that they do not encapsidate their polymerases in extracellular virions. Nevertheless, emerging results show that similarities between (+)RNA-virus RNA replication and retrovirus reverse transcription are not limited to aspects of negative-strand initiation and the general similarities of RNA and DNA polymerases. Instead, as detailed below, (+)RNA-virus RNA replication occurs in virus-induced compartments which have many similarities to the replicative cores or capsids of retrovirus virions.

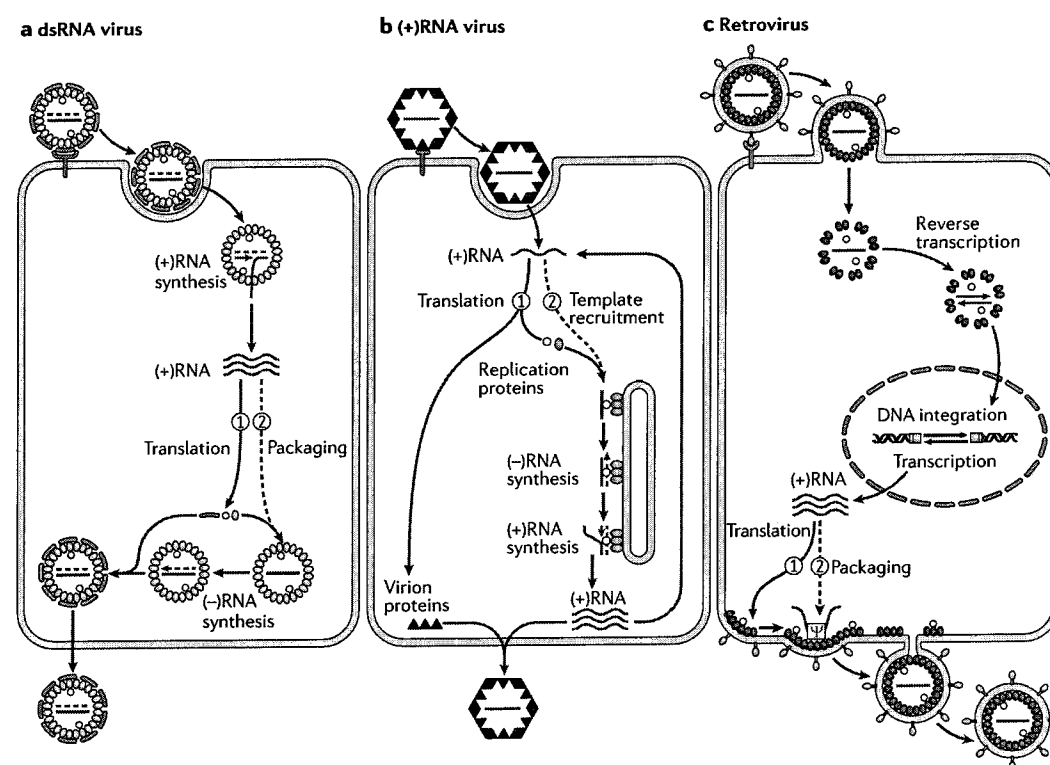
(+)RNA-virus replication is invariably localized to intracellular membranes. Different (+)RNA viruses target distinct but usually specific membranes, such as those of the endoplasmic reticulum (ER)¹⁵⁻¹⁹, endosomes^{20,21}, mitochondria²² or chloroplasts²³. RNA replication is usually associated with rearrangements of these target membranes, often giving rise to membrane invaginations, single- or double-membrane vesicles, membrane-bound vesicle packets and other structures.

For many (+)RNA viruses, RNA synthesis localizes to membranes bearing 50–70-nm vesicular compartments that are invaginated away from the cytoplasm into the lumen of the affected secretory compartment or organelle. Such invaginations, termed spherules, were first visualized in early electron microscopy (EM) studies of alphavirus-infected cells^{20,21}. There are many other examples of such invaginations in and beyond the alphavirus-like superfamily, such as those associated with bromoviruses^{24,25}, nodaviruses²² and tymoviruses²³.

Negative-strand RNA virus
A virus, the infectious virions of which contain the genome in a single-stranded, anti-messenger-sense RNA form.

Retroplasmid
A DNA plasmid that replicates by transcription and reverse transcription of an RNA intermediate.

Box 1 | Distinct life cycles of dsRNA viruses, (+)RNA viruses and retroviruses



All three classes of virus replicate through positive-strand RNA ((+)RNA) intermediates (red strands in the figure) that are templates for both translation and genome replication. For each class, the figure shows a simplified, representative life cycle.

Double-stranded (ds)RNA viruses

As shown in part **a** of the figure, virus attachment and endocytosis deliver a virion core that contains viral genomic dsRNA and viral RNA polymerase (yellow) into the cytoplasm. The core transcribes and extrudes (+)mRNAs that are first translated (1) and then packaged (2) by the resulting viral proteins into new virion cores. Cores mature by synthesizing negative-strand (-)RNA (dotted strand) and adding exterior proteins. They exit by cell lysis or secretion.

(+)RNA viruses

As shown in part **b** of the figure, endocytosed virions release messenger-sense genomic RNA into the cytoplasm for translation. Newly translated viral RNA-replication proteins recruit this genomic RNA into a membrane-associated, intracellular RNA-replication complex. Small amounts of (-)RNA are produced and used as templates to greatly amplify viral (+)RNA, which is encapsidated into new progeny virions.

Retroviruses

As shown in part **c** of the figure, virion attachment and envelope fusion release a subviral complex that contains viral genomic (+)RNA and reverse transcriptase (yellow). After cDNA synthesis by reverse transcription, proviral cDNA is integrated into the host chromosome and transcribed to produce (+)RNA that is translated (1) and then packaged (2) into new virions that are released by budding.

As illustrated in FIG. 3a–c, for nodaviruses and bromoviruses, such spherules frequently occur in contiguous clusters and are often light-bulb-shaped structures, the interiors of which are connected to the cytoplasm through membranous necks.

Parallels with retrovirus capsids. Retroviruses package their reverse transcriptase (also designated Pol) and their genomic RNA templates into membrane-enveloped capsid shells assembled by the major capsid protein, Gag^{26–28} (FIG. 4a). For most retroviruses, these capsids bud from the cell together with viral envelope proteins and are delivered to new cells by infection, giving rise to

intracellular complexes in which reverse transcription occurs^{29–31}. For foamy retroviruses and retrovirus-like LTR (long terminal repeat) retrotransposons, reverse transcription occurs in such capsids without leaving the producer cell^{32–34}. Such capsids contain hundreds³⁵ to thousands³⁶ of Gag proteins and approximately 10–20-fold fewer Gag–Pol fusion proteins^{28,37}. Retrovirus genomic RNAs are selectively packaged in these capsids by Gag interaction with specific *cis*-acting signals, often designated as Ψ ^{38,39}.

Recently, links between the intracellular spherules of (+)RNA viruses and retrovirus capsids emerged from studies of brome mosaic virus (BMV) RNA replication.

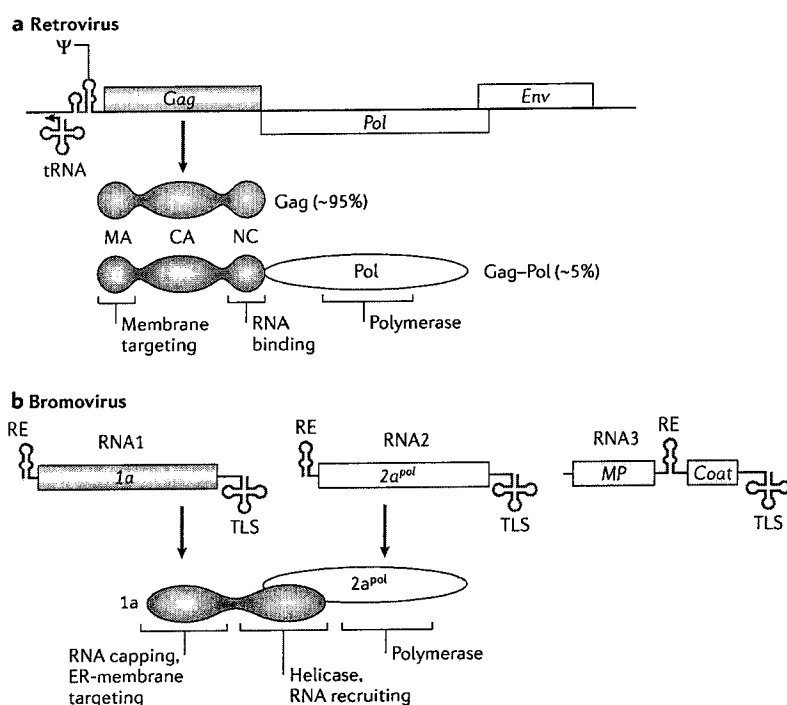


Figure 2 | Schematic overview of retrovirus and bromovirus genomes. **a** | Schematic of the genomic RNA of a simple retrovirus and encoded virion proteins Gag and Gag-Pol. **b** | Schematic of bromovirus genomic RNAs 1, 2 and 3 and encoded RNA-replication factors 1a and 2a^{pol}. CA, capsid; Env, envelope-protein gene; ER, endoplasmic reticulum; MA, matrix; NC, nucleocapsid; RE, RNA template recruiting element for genomic RNA replication; TLS, 3' tRNA-like sequence, which contains the promoter for negative-strand RNA synthesis; tRNA, host tRNA primer for negative-strand cDNA synthesis; Ψ , RNA-packaging signal.

BMV is the type member of the bromoviruses and a representative member of the alphavirus-like superfamily of (+)RNA viruses. This superfamily includes many viruses that infect animals or plants, all of which share three conserved protein domains that are involved in RNA replication^{40,41}. In BMV, these domains are distributed across two replication proteins, 1a and 2a^{pol} (FIG. 2b), that co-localize on ER membranes at the sites of viral RNA synthesis^{15,16}. 1a contains an RNA-helicase-like domain and an RNA-capping domain with m⁷G methyltransferase and covalent m⁷G binding activities required for capping of viral RNAs *in vivo*⁴²⁻⁴⁴. 2a^{pol} contains a central polymerase domain.

Protein 1a is a multifunctional protein with central roles in the genesis and operation of BMV RNA-replication complexes (FIG. 4b). In the absence of other viral factors, 1a localizes to ER membranes¹⁶ and induces invagination of the spherular replication compartments⁴⁵. 1a also recruits nascent or full-length 2a^{pol} to ER membranes by an interaction between the 1a helicase-like domain and the N-terminal extension that precedes the 2a^{pol} polymerase domain⁴⁶⁻⁴⁸.

Protein 1a also transfers BMV genomic RNA-replication templates to a new state, which was first recognized because the stability and accumulation of BMV genomic RNAs was dramatically increased by 1a co-expression in yeast⁴⁹⁻⁵¹. Subsequent work showed that 1a induces the transfer of BMV genomic RNAs to

a novel, membrane-associated, nuclease-resistant state⁴⁵. The location of the nuclease-resistant RNA and the site of RNA synthesis seem to be the spherule interior, as (+)RNA and (-)RNA templates and nascent BMV RNAs show identical membrane association and nuclease resistance, and immunogold EM localizes 5-bromo-UTP (BrUTP)-labelled nascent RNAs to the spherule interior⁴⁵.

Recruitment of BMV genomic RNAs to the RNA-replication complex by 1a is controlled in *cis* by internal (RNA3) or 5' proximal (RNA1 and RNA2) recruitment elements (REs) on each genomic RNA (FIG. 2b), which are necessary and sufficient for 1a responsiveness^{51,52}. Mutational studies show that the RE activity of BMV RNA derivatives in 1a-induced recruitment is closely linked to their relative template activity in (-)RNA synthesis and full RNA replication^{51,52}. Therefore, 1a-responsive RNA-template recruitment seems to be a crucial step that precedes replication.

As shown in FIG. 4a,b, the roles of 1a, 2a^{pol} and the *cis*-acting REs parallel the roles of Gag, Pol and Ψ in retrovirus replication. Similar to Gag, 1a localizes to the cytoplasmic face of membranes as a peripheral membrane protein⁵³, self-interacts⁵⁴, and is the sole viral factor required to induce membrane invagination⁴⁵. Immunogold EM labelling and biochemical analyses show that each spherule contains hundreds of 1a proteins⁴⁵. The resulting spherules (FIG. 3c) are remarkably similar to the necked vesicles that result when retrovirus budding is arrested by mutations in the Gag late domain that recruits host factors required for membrane breakage and fusion⁵⁵. Moreover, the high multiplicity of 1a in spherules, its strong membrane association and self-interaction, and the dependence of endocytic and secretory vesicle formation and enveloped-virion budding on protein coats or shells^{56,57} indicate that 1a might induce membrane invagination by forming a capsid-like shell similar to that of Gag. Similarly, the 1a-RE interaction in RNA-template recruitment parallels the Gag- Ψ interaction in retrovirus RNA packaging. Like retrovirus Pol, BMV 2a^{pol} is not required for spherule formation or RNA recruitment. However, when expressed, 2a^{pol} is incorporated into the replication complex in a 1a/2a^{pol} ratio of ~25, similar to the Gag/Pol ratio of 10/20 (REFS 37,45).

Similarities with other (+)RNA viruses

The universal association of (+)RNA-virus RNA replication with modified intracellular membranes, often in association with membrane invaginations, and other shared features imply that the RNA-replication complexes of a wide variety of (+)RNA viruses might use principles that are similar to those illustrated in FIG. 4b. Such parallels include the following: both alphavirus- and cucumovirus-induced membrane spherules contain dsRNA^{25,58}; BrUTP labelling implies that the interiors of alphavirus spherules are the sites of viral RNA synthesis⁵⁹; hepatitis C virus and coronavirus (-)RNA-replication templates are in a membrane-associated, nuclease-resistant state⁶⁰⁻⁶²; hepatitis C virus replication proteins are present in active replication complexes at >100-fold excess over viral RNA and are sequestered in a protease-resistant

BrUTP labelling

Labelling RNA by replacing the substrate UTP with 5-bromo-UTP (BrUTP). The labelled RNA can be localized using electron microscopy following immunogold labelling with an antibody directed against BrU.

state^{61,62}; poliovirus polymerase and possibly other replication factors self-oligomerize in extended lattices⁶³, and tombusvirus genomic RNA possesses an internal *cis* signal for initial template recruitment and separate 3' terminal sequences for negative-strand initiation⁶⁴.

Furthermore, just as for retrovirus Gag and BMV 1a, the membrane structures associated with genome replication by many (+)RNA viruses can be induced by a subset of viral RNA-replication proteins that do not include the polymerase. Examples include the RNA-replication-associated membrane structures induced by alphavirus nsP123 (REF. 65), arterivirus nsP2 and nsP3 (REF. 66), hepatitis C virus nsP4B (REFS 19,67) and picornavirus 2BC (REFS 18,68,69).

As explained further below, the parallels among (+)RNA-virus RNA-replication complexes, retrovirus capsids and dsRNA-virus capsids (FIG. 4) imply possible mechanistic explanations for several common features of (+)RNA-virus RNA replication, such as the ability of the replication complex to retain (–)RNA templates for positive-strand synthesis, differential regulation of (–)RNA and (+)RNA synthesis, and frequent down-regulation of polymerase expression.

Pol regulation in retroviruses and (+)RNA viruses. In retrovirus genomes, the Pol open reading frame (ORF) follows that of Gag and is expressed by a rare translational frameshift or translational readthrough event, generating an ~20-fold ratio of Gag/Gag–Pol (FIG. 2a) that is incorporated into the final virion (FIG. 4a). This highly asymmetric ratio regulates the free volume and other parameters of the capsid, and is functionally important, as increasing the level of Gag–Pol relative to Gag inhibits retrovirus virion assembly, release and infectivity^{37,70,71}.

Similarly, many (+)RNA viruses downregulate expression of their polymerase relative to RNA-replication proteins related in sequence and/or functions to 1a. The finding that BMV 1a parallels Gag in acting at high multiplicity to induce the RNA-replication compartment (FIG. 4a,b) implies that such polymerase downregulation might satisfy functional requirements similar to those governing the Gag/Gag–Pol ratio in retrovirus capsids. Like retroviruses, many (+)RNA viruses use translational readthrough or frameshift to downregulate polymerase expression. Well-studied examples include the animal alphaviruses and arteriviruses and plant tobamoviruses and tombusviruses. In each case, the ORF upstream to that of polymerase encodes a protein(s) with parallels to 1a. Specifically, alphavirus nsP123 and tobamovirus p130 are homologous to 1a (REF. 40), and nsP123 is sufficient to induce membrane spherules⁶⁵; arterivirus ORF1a proteins induce membrane rearrangements associated with RNA replication⁶⁶; and tombusvirus p33 self-interacts and directs membrane association of itself, viral RNA and polymerase⁷². As with Gag and Pol, increasing expression of the polymerase-containing fusion proteins at the expense of the upstream membrane-interacting proteins inhibits tobamovirus and alphavirus replication^{73,74}.

Unlike the above examples, bromoviruses express 1a and 2a^{pol} from separate genomic RNAs (FIG. 2b). In this

Nodavirus-modified mitochondria



Bromovirus-modified nuclear membranes

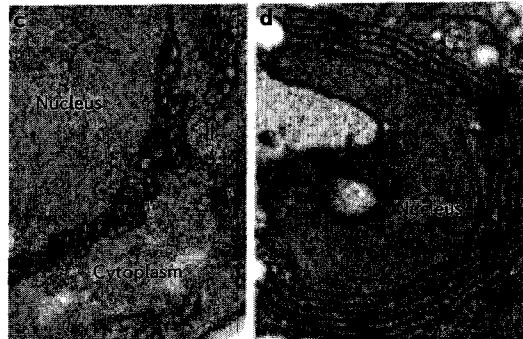


Figure 3 | Electron micrographs of membrane rearrangements associated with nodavirus and bromovirus RNA replication. **a** | Mitochondria in a flock-house-nodavirus-infected *Drosophila* cell, showing the typical 50–70-nm, light-bulb-shaped spherular invaginations of the outer mitochondrial membrane into the expanded lumen between the inner and outer membranes. Reproduced with permission from REF. 22 © (2001) American Society for Microbiology. **b** | Mitochondrion in a flock-house-nodavirus-infected *Drosophila* cell that has been sectioned perpendicular to the axis of the spherule necks, rather than parallel to these axes as in panel **a**. This view reveals a 'vesicle packet' appearance (B. Kopek and P.A., unpublished results). Note that invagination into the lumen of any closed membrane compartment such as the endoplasmic reticulum (ER) or mitochondrial envelope creates a spherule interior that remains connected to the cytoplasm, but that in the section shown in **b**, the spherule appears separated from the cytoplasm by two or more bounding membranes. **c** | Similar 50–70-nm spherular vesicles invaginated from the outer perinuclear ER membrane into the ER lumen, in a yeast cell expressing bromo mosaic virus (BMV) replication factor 1a in the absence of other viral components. Indistinguishable spherules occur in cells expressing 1a and BMV 2a^{pol} in a 20/1 ratio and replicating BMV RNA3. Reproduced with permission from REF. 45 © (2002) Elsevier. **d** | Karmellae-like layering of the outer perinuclear ER membrane in cells expressing BMV 1a plus elevated levels of BMV 2a^{pol}, and replicating BMV RNA3. Note at top and bottom left that the ~60-nm intermembrane space is contiguous with the cytoplasm. Reproduced with permission from REF. 84 © (2004) National Academy of Sciences, USA.

Translational frameshift

A site-specific, programmed shift of some translating ribosomes from one reading frame to another, allowing a fraction of translation products to be extended in the new frame.

Translational readthrough

Programmed translation of some ribosomes through a termination codon, allowing a fraction of translation products to be extended beyond the normal stop site.

regard, they parallel the foamy virus genus of retroviruses, which express Gag and Pol as independent proteins from separate mRNAs³⁴. Although expressed separately, direct *in vivo* interaction between the C-terminal 1a helicase domain and N-terminal sequences of nascent 2a^{pol} results in a 1a–2a^{pol} complex with a polarity that is reminiscent

of orthoretrovirus Gag–Pol^{46–48} (FIG. 2). Moreover, whereas translation from separate mRNAs precludes regulation by frameshift or readthrough, BMV downregulates 2a^{pol} at translation initiation⁷⁵ and by degradation of 2a^{pol} that is not complexed with 1a (REF. 76). 1a–2a^{pol} interaction itself is downregulated by competing 1a–1a interaction⁵⁴ and 2a^{pol} phosphorylation⁷⁷. Therefore, like alphaviruses⁷⁸, bromoviruses have evolved several mechanisms to reduce polymerase accumulation and incorporation to achieve the retrovirus-like 1a to 2a^{pol} ratio of 25/1 in RNA-replication complexes⁴⁵.

Some other (+)RNA viruses, such as hepatitis C virus and picornaviruses, use polyprotein expression strategies that translate all viral ORFs, including polymerase, at equimolar levels. In at least some of these cases, only a fraction of polymerase sequences might be active owing to production of processing intermediates that lack polymerase sequences or activity, polymerase-active and -inactive conformers, polymerase sequestration in the nucleus and/or inclusion bodies, and other effects^{62,79}. Some retrotransposons that produce equimolar levels of Gag and Pol appear to use related strategies to regulate polymerase incorporation or activity^{80,81}.

Alternative membrane rearrangements. Whereas RNA replication by many (+)RNA viruses induces spherular membrane invaginations similar to those shown in FIG. 3a–c, some (+)RNA viruses induce alternative membrane rearrangements. In many cases, the topologies of these rearranged membranes remain under investigation and, as discussed below, some superficially distinct membrane structures might share underlying parallels in topology, assembly and function. Similarly, depending on the conditions, retrovirus Gag not only assembles normal capsids but also sheets, tubes and other structures⁸².

Flavivirus RNA replication localizes to packets in which an outer bounding membrane surrounds 50–100-nm vesicles that label with antibodies to viral RNA-replication proteins and dsRNA⁸³. These vesicle packets are similar to EM views of BMV spherules invaginated into the ER lumen⁸⁴ or nodavirus spherules invaginated into the lumen between the inner and outer mitochondrial membranes²², when sectioned perpendicular to the direction of invagination (FIG. 3b). BrUTP-labelled RNA synthesis by the related hepatitis C virus localizes to potentially similar clusters of ~85-nm vesicles surrounded by undulating membranes, termed

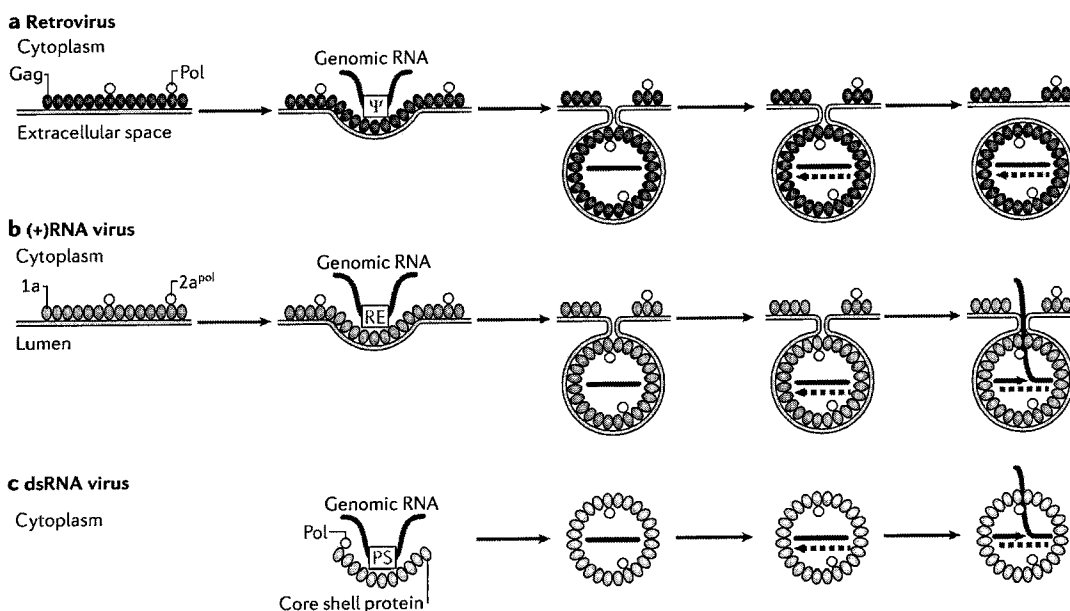


Figure 4 | Parallels between structure, assembly and function of retrovirus capsids, dsRNA-virus capsids and (+)RNA-virus RNA-replication complexes. Highly simplified schematics are shown in each case. **a** | Assembly of a retrovirus capsid includes the interaction of membrane-associated Gag and Gag–Pol. Gag-dependent genomic RNA encapsidation takes place through packaging signal Ψ, and this is followed by budding. To emphasize similarities with panels **b** and **c**, synthesis of negative-strand cDNA (dashed lines) is shown prior to budding, as occurs for foamy retroviruses. **b** | Assembly and function of a bromovirus RNA-replication complex at the outer endoplasmic-reticulum membrane includes interaction of membrane-associated 1a and 2a^{pol}. 1a-dependent genomic RNA encapsidation takes place through the recruitment element (RE) template recruitment signal. This is followed by synthesis and retention of negative-strand RNA (dashed black lines), and asymmetric synthesis and export of positive-strand progeny RNA (red lines), which for at least some positive-strand RNA ((+)RNA) viruses proceeds by a semi-conservative mechanism as shown¹⁴³. **c** | Assembly and function of the capsid core of a generalized double-stranded (ds)RNA virus includes encapsidation of genomic RNAs by a packaging signal (PS), synthesis and retention of negative-strand RNA (dashed black lines) and subsequent asymmetric synthesis and export of positive-strand progeny RNA (red lines). (+)RNA synthesis by dsRNA viruses can be either semi-conservative¹⁴⁴, as shown, or conservative^{90,145}.

the membranous web^{19,67}. Recently, models with strong parallels to bromovirus replication complexes have been proposed for RNA-replication complexes of hepatitis C virus^{62,85}.

RNA replication by picornaviruses, arteriviruses and coronaviruses occurs in conjunction with double-membrane vesicles, that is, vesicles bearing two closely appressed bounding membranes^{17,18,86}. Similar to spherules, arterivirus double-membrane vesicles are thought to form by invagination of appressed ER membranes¹⁷. Some EM sections of poliovirus double-membrane vesicles display a narrow neck that connects the inner and outer membranes to each other, and that also connects the vesicle interior to the cytoplasm⁸⁷, indicating possible genesis by invagination, continuing connection with the cytoplasm, or both.

Interconversion of membrane rearrangements. Further evidence linking seemingly distinct membrane rearrangements in RNA replication is that altering the relative levels and interactions of BMV replication factors 1a and 2a^{pol} shifts the associated membrane rearrangements between two dramatically distinct forms⁸⁴. Expressing 1a plus low levels of 2a^{pol} (1a/2a^{pol} ≈ 20) induces spherular replication complexes matching those of natural bromovirus^{24,25} and alphavirus²¹ infections (FIG. 3c). By contrast, expressing 1a plus higher levels of 2a^{pol} induces stacks of appressed double membranes that support RNA replication to levels as high as spherules⁸⁴ (FIG. 3d). The spaces between these double membrane layers parallel spherule interiors in being 50–60 nm wide, containing 1a and 2a^{pol}, and being directly connected to the cytoplasm. Therefore, BMV-induced spherules and double membrane layers seem to be functionally and topologically equivalent forms that are built from the same protein–protein and protein–membrane interactions, but in altered proportions.

Similar stacked, double-membrane ER layers and other ordered ER membrane arrays are induced by over-expression of membrane-associated picornavirus replication factors 2B and 2BC (REFS 68,88). Moreover, the double-membrane vesicles associated with picornavirus RNA replication, the spherule-bearing mitochondrial membranes associated with nodavirus RNA replication and the spherule-bearing chloroplast membranes associated with tymovirus RNA replication all cluster by interaction of surface membranes bearing viral replication factors^{22,23,63,89}. Therefore, a continuum of vesicle-forming and planar membrane interactions seems to be a normal part of RNA replication by many (+)RNA viruses.

(+)RNA virus and dsRNA virus parallels

Many of the above parallels between (+)RNA viruses and retroviruses extend to dsRNA viruses, which also sequester genomic RNA templates, viral polymerase and, often, RNA-capping functions in a protein shell for genome replication^{90,91} (FIG. 4c). Possible connections between certain (+)RNA and dsRNA viruses were recognized previously, based on conservation of polymerase^{5,92} and, in one case, on additional replication-factor sequences⁹³.

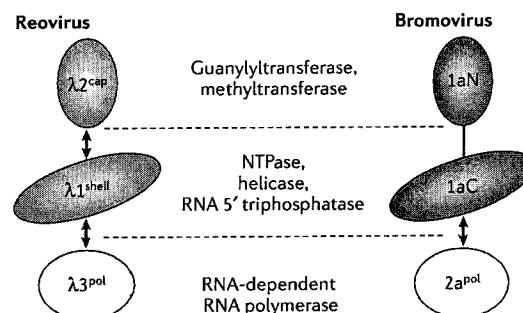


Figure 5 | Structure–function parallels between reovirus and bromovirus RNA-replication factors. The schematics illustrate similarities between interaction and function of reovirus core shell-forming protein $\lambda 1$, RNA-capping protein $\lambda 2$ and RNA-dependent polymerase $\lambda 3$, and the interactions and functions of the brome mosaic virus (BMV) 1a C-proximal NTPase/helicase domain (1aC), 1a N-proximal RNA-capping domain (1aN) and 2a^{pol} RNA-dependent RNA polymerase. The reovirus $\lambda 1$ – $\lambda 2$ – $\lambda 3$ interactions shown in the schematic occur at each of the twelve 5-fold axes of the reovirus core.

Similarities with Reoviridae cores. BMV RNA-replication factors and replication complexes share several similarities with the icosahedrally symmetric replicative cores of the dsRNA-virus family *Reoviridae* (FIG. 4). *Reoviridae* virions consist of one or more outer-protein shells that are shed during cell entry, surrounding an RNA-containing core that synthesizes RNA *in vivo* and *in vitro*⁹⁰. For the Orthoreovirus genus of the *Reoviridae*, the transcriptionally active, dsRNA-containing core is bound by an ~60-nm icosahedral shell made from 60 dimers of protein $\lambda 1$ (REF. 94). At each of the twelve 5-fold axes of the core, one copy of the $\lambda 3$ polymerase resides inside the shell⁹⁵, whereas on the shell exterior, a pentamer turret of the $\lambda 2$ capping proteins surrounds the 5-fold axis⁹⁴. The $\lambda 3$ polymerase copies the genomic dsRNA templates into new (+)RNA progeny, exporting the nascent RNAs to the cytoplasm through the $\lambda 2$ pentamer turret, which adds m⁷G caps to the 5' ends.

BMV 1a shows many parallels in function and protein–protein interactions with reovirus core proteins $\lambda 1$ and $\lambda 2$, implying potentially similar roles in RNA synthesis (FIG. 5). 1a parallels $\lambda 1$ as the self-interacting, high-copy-number inducer of the viral RNA-replication compartment, yielding the spherular BMV replication complexes. The 50–70-nm intra-membrane diameter of these spherules is similar to the reovirus $\lambda 1$ core-protein shell. The C-terminal 1a NTPase/helicase domain and its alphavirus homologues have NTPase, RNA 5'-triphosphatase and helicase activities^{96–99}, matching $\lambda 1$ (REFS 100,101). The 1a NTPase/helicase domain also anchors BMV RNA polymerase 2a^{pol} to the replication complex by direct interaction¹⁰², whereas $\lambda 1$ performs the same role for reovirus RNA polymerase $\lambda 3$ (REF. 95). The resulting twelve $\lambda 3$ polymerases per core are similar to the estimated 10–15 2a^{pol} per BMV RNA-replication complex⁴⁵. Continuing these parallels, $\lambda 1$ and the 1a NTPase/helicase domain each anchor RNA-capping

functions to the RNA-synthesis complex in the form of reovirus $\lambda 2$ protein and the BMV 1a N-terminal domain, respectively. $\lambda 2$ (REFS 103,104) and the 1a N-terminal domain^{42–44,105} both possess guanylyltransferase and methyltransferase activities that add m⁷G caps to the 5' ends of the (+)RNA products of their respective RNA-synthesis complexes.

RNA packaging, synthesis and export. Recent results indicate possible parallels between the recruitment of (+)RNA templates to BMV RNA-replication complexes and the packaging of (+)RNAs in dsRNA viruses. For dsRNA bacteriophage $\phi 6$, viral (+)RNAs are translocated into a pre-formed, empty core by a hexameric viral NTPase/helicase, P4 (REFS 106,107). Similarly, recruitment of BMV genomic RNAs from a membrane-bound, nuclease-sensitive state into the nuclease-resistant spherule replication complex, but not formation of the membrane-invaginated spherules themselves, is blocked by single amino-acid substitutions that inhibit the NTPase activity of the 1a NTPase/helicase domain⁹⁹. Also, like $\phi 6$ P4, the 1a-homologous NTPase/helicase domain of protein p126 of tobacco mosaic virus forms hexamers¹⁰⁸. For the *Reoviridae*, packaging viral (+)RNAs for replication also involves a viral protein with NTPase, RNA-binding and helix-destabilizing activities — the octameric NSP2 for the Rotavirus genus^{109,110} and, potentially, $\mu 2$ for the Orthoreovirus genus^{90,110,111}. Like $\phi 6$ P4 (REF. 106) and BMV 1a (REF. 112), $\mu 2$ also seems to be a co-factor for (+)RNA synthesis¹¹¹.

For dsRNA viruses, packaging of (+)RNAs is associated with, or followed by, (–)RNA synthesis, yielding dsRNAs that are protected in cores or core-like precursors^{90,91}. Similarly, BMV (–)RNA synthesis depends on 1a-mediated (+)RNA recruitment^{51,52}, and the resulting (–)RNA products are exclusively

retained in the nuclease-resistant, membrane-associated RNA-replication compartment⁴⁵. This retention in a virus-induced RNA-replication compartment explains the efficient, repetitive *in vivo* use of (–)RNAs as templates for (+)RNA synthesis, and the lack of (–)RNA exchange between RNA-replication complexes in the same cell¹¹³. Compartmentalization of RNA templates also seems to be important in protecting dsRNA-virus genomes and the potentially dsRNA-replication intermediates of (+)RNA viruses^{25,58} from dsRNA-induced host defences, including interferon responses and RNA interference^{90,91,114–116}.

A reovirus-like pathway for (+)RNA replication (FIG. 4b,c) would also explain the common early shutoff of (–)RNA synthesis in BMV and other (+)RNA viruses, while (+)RNA synthesis continues unabated^{112,117,118}, and the dependence of (–)RNA synthesis on continuing protein synthesis¹¹⁸. In such a model, (–)RNAs might be synthesized primarily during or immediately after replication-complex assembly from newly synthesized proteins, forming dsRNAs that would preferentially or exclusively be templates for (+)RNA synthesis in the resulting stable replication complexes. Replication-complex assembly and negative-strand synthesis seem to cease on exhaustion of a limiting host factor, possibly the target membrane for replication-complex formation^{15,118}. Pre-formed replication complexes, however, remain active in (+)RNA synthesis^{112,118}.

For both the *Reoviridae*⁹⁰ and the alphavirus-like superfamily^{119,120}, (–)RNAs are not capped. By contrast, (+)RNA products are modified with 5' m⁷G caps and exported to the cytoplasm from both dsRNA virus cores^{94,95,121} and BMV spherules^{43–45}. This and the parallels noted above between the capping functions and polymerase interactions of the responsible reovirus proteins and 1a suggest that the transcription/capping/export complexes at the 5-fold axes of dsRNA-virus cores might provide models for at least some aspects of the corresponding processes at the spherule necks of BMV and other (+)RNA-virus replication complexes.

Possible evolutionary relationships

The above results show that reverse-transcribing viruses, dsRNA viruses and many, if not all, (+)RNA viruses share central features of genome replication (FIG. 6). Most fundamentally, all replicate their genome through an RNA intermediate that also functions as an mRNA. In all three cases, viral proteins that are translated from these mRNAs capture the mRNA template with its polymerase in a multi-subunit core, sequestering viral RNA from competing processes such as translation and degradation, and sequestering polymerase from competing templates. The polymerase then copies the mRNA into a complementary template from which more mRNA is produced.

The variations on this theme that distinguish the three virus classes primarily relate to possessing an RNA-dependent RNA or DNA polymerase, and to deriving infectious virions from different intermediates in the common replication cycle. Orthoretroviruses, such as HIV, export the replicative core prior to copying

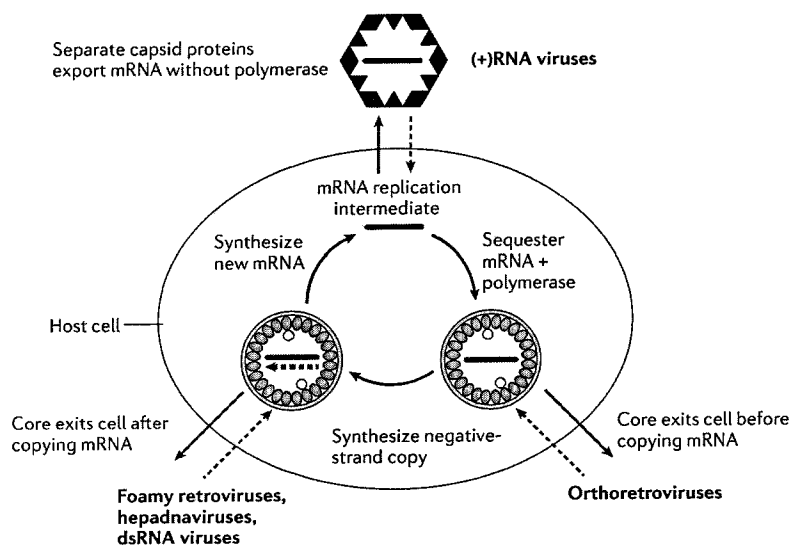


Figure 6 | Parallels and distinctions among the life cycles of reverse-transcribing viruses, (+)RNA viruses and dsRNA viruses. All three classes of virus share a similar replication cycle for their genomic RNA (central cyclical steps) but derive their infectious virions from different intermediates in that cycle (radial arrows). See text for further details. (+)RNA, positive-strand RNA; dsRNA, double-stranded RNA.

the mRNA intermediate (FIG. 6, bottom right). By contrast, foamy viruses, hepadnaviruses and dsRNA viruses export the replicative core after copying the mRNA intermediate (FIG. 6, bottom left). For (+)RNA viruses, the virion is separate from the replication complex, and capsid proteins that are not involved in RNA replication package and export the mRNA intermediate before it is sequestered with polymerase (FIG. 6, top). These distinct virion-assembly choices have important consequences, as noted in the introduction, but from some perspectives could be considered temporary extracellular excursions because, as soon as the next cell is infected, each virus re-enters the central, shared replication pathway.

Although no set of shared features can distinguish divergent from convergent evolution, the many parallels summarized here suggest that (+)RNA viruses, dsRNA viruses and reverse-transcribing viruses might have arisen from common ancestors. The transitions required for such evolution can be readily envisioned, and in some cases have precedents. RNA-dependent RNA and DNA polymerases, for example, have related structures^{122,123}, and a shift between the two has generally been postulated as the basis for the emergence of DNA-based biology from the RNA world⁹. In keeping with the potential for such transitions, BMV RNA-dependent RNA polymerase can copy DNA templates¹²⁴, and reverse transcriptase can, with single point mutations, incorporate ribonucleotide triphosphates (rNTPs) to produce RNA¹²⁵.

Established and emerging results further indicate that the intracellular RNA-replication complexes of (+)RNA viruses might evolve into infectious extracellular virions, similar to those of dsRNA or reverse-transcribing viruses, by relatively simple modifications. The spherule RNA-replication complexes of alphaviruses, for example, occur on endosomal membranes and, in lesser numbers, at the plasma membrane, where their appearance closely mimics budding virions⁵⁹. Such spherules are released into the medium at low frequency⁵⁹, which might explain the novel infectious particles released from cells replicating alphavirus derivatives with all natural virion proteins deleted and replaced by envelope protein G of vesicular stomatitis virus¹²⁶. As G protein is readily incorporated into many particles that bud from the plasma membrane and confers the ability to attach to, and fuse membranes with, many cells, incorporation of G protein into spherule membranes might confer infectivity by allowing released replication complexes or their RNAs to enter new cells.

Once acquired, infectivity might be enhanced and optimized through subsequently selected events. For retroviruses and other enveloped viruses, efficient virion budding requires recruiting functions from the host-cell multivesicular-body pathway⁵⁷. This host machinery can be recruited by incorporating into viral proteins any of a range of short protein-interaction motifs or L domains, which function in a largely position-independent manner⁵⁵. RNA-recombination events that are suitable to acquire such L domains, favourable envelope-protein genes or other relevant functions from cellular or other viral RNAs are rampant in (+)RNA viruses and retroviruses, representing a major force in virus evolution^{127–129}.

Additional pathways for evolutionary transitions between the intracellular RNA-replication complexes of (+)RNA viruses and dsRNA virions have recently been suggested^{6,130}. As the replication complexes of (+)RNA viruses are invariably membrane-associated, it is notable that virions of the Rotavirus genus of the dsRNA *Reoviridae* bud through membranes during assembly and exit from cells¹³¹. Moreover, rotavirus transmembrane protein nsP4, which mediates virion-core association with ER membranes, is required for correct assembly of the viroplasms in which core assembly and replicative RNA synthesis occur, indicating linkage of these processes with membranes^{132,133}. dsRNA bacteriophage $\phi 6$ virions also become membrane-enveloped during exit¹³⁴.

Whereas most views of virus relationships have tended to emphasize the features and classes depicted in FIG. 1, it is intriguing that several alternative, orthogonal virus groupings are defined and mutually distinguished by features that are more strongly conserved across two or more of the classes in FIG. 1. Selected examples include the conservation of an unusual polymerase-sequence rearrangement between (+)RNA tetraviruses and dsRNA birnaviruses⁵, or the use of protein-primed genome replication by the (+)RNA picornaviruses, dsRNA birnaviruses and reverse-transcribing hepadnaviruses^{3,4,7}, in contrast to the use of tRNA-like elements by bromoviruses and retroviruses. Such relationships suggest that transitions between the virus classes depicted in FIG. 1 might have evolved on more than one occasion, and that links between viruses within a class might not always be as strong as links between classes.

Implications for virus control

The emergence of common underlying principles in the central replication processes of (+)RNA viruses, reverse-transcribing viruses and dsRNA viruses suggests that some of these shared features might provide useful targets for broader-spectrum or generalizable approaches for virus control. One approach might be to modulate membrane lipid composition, as recent results show that assembly and function of membrane-associated (+)RNA-virus replication complexes and retrovirus capsids are highly sensitive to the lipid composition of their target membranes, which in at least some cases can be manipulated by small-molecule therapeutics^{135–138}. Another general approach might be to interfere with oligomerization or function of oligomerizing replication factors such as retrovirus Gag and BMV 1a by dominant negative mutants^{43,99}, inhibition of required chaperones^{139,140}, targeted incorporation of destructive ligands or other approaches. Further interventions might be based on interfering with viral RNA interactions that are essential for genome packaging, replication and other steps, using nucleic-acid aptamers or other inhibitors¹⁴¹. Other approaches might interfere with the trafficking of viral replication factors and RNAs to their required intracellular sites of assembly¹⁴². Opportunities for such interference will continue to increase as further aspects of these processes are understood in greater detail.

Concluding remarks

An exciting aspect of current virology is that advancing results have not only continued to enrich our understanding of individual viruses, but also to reveal unifying principles that link many aspects of virus infection, replication and host interactions across a surprisingly wide breadth of virus–host systems. The resulting insights display a fundamental order within the vast and sometimes apparently chaotic diversity of known

viruses, with important ramifications for virus function and evolution. As the full extent of this tapestry of relations is still emerging, ongoing studies will continue to extend and refine the underlying mechanistic connections. In association with their mechanistic importance, the results should have a growing impact on our abilities to limit the continuing toll and emerging threat of viral diseases, and to develop the beneficial uses of viruses.

- Butel, J. S. Viral carcinogenesis: revelation of molecular mechanisms and etiology of human disease. *Carcinogenesis* **21**, 405–426 (2000).
- Talbot, S. J. & Crawford, D. H. Viruses and tumours — an update. *Eur. J. Cancer* **40**, 1998–2005 (2004).
- Paul, A. V., Rieder, E., Kim, D. W., van Boom, J. H. & Wimmer, E. Identification of an RNA hairpin in poliovirus RNA that serves as the primary template in the *in vitro* uridylation of VPg. *J. Virol.* **74**, 10359–10370 (2000).
- Murray, K. E. & Barton, D. J. Poliovirus CRE-dependent VPg uridylation is required for positive-strand RNA synthesis but not for negative-strand RNA synthesis. *J. Virol.* **77**, 4739–4750 (2003).
- References 3 and 4 reveal and refine parallels in protein-primed genome replication by RNA picornaviruses and reverse-transcribing hepatitis B virus.
- Gorbalenya, A. E. *et al.* The palm subdomain-based active site is internally permuted in viral RNA-dependent RNA polymerases of an ancient lineage. *J. Mol. Biol.* **324**, 47–62 (2002).
- Reveals that an unusual re-ordering of polymerase domains is shared by certain (+)RNA viruses and dsRNA viruses.
- Coulibaly, F. *et al.* The birnavirus crystal structure reveals structural relationships among icosahedral viruses. *Cell* **120**, 761–772 (2005).
- Ahlquist, P. Virus evolution: fitting lifestyles to a T. *Curr. Biol.* **15**, R465–R467 (2005).
- Weiner, A. M. & Maizels, N. tRNA-like structures tag the 3' ends of genomic RNA molecules for replication: implications for the origin of protein synthesis. *Proc. Natl Acad. Sci. USA* **84**, 7385–7387 (1987).
- Proposes evolutionary relationships among tRNA-like 3' ends of certain (+)RNA-virus genomic RNAs, retroviral tRNA priming and chromosomal telomeres.
- Maizels, N. & Weiner, A. M. in *The RNA World* (eds Gesteland, R. F., Cech, T. R. & Atkins, J. F.) 79–111 (Cold Spring Harbor Laboratory Press, Cold Spring Harbor, 1999).
- Miller, W. A., Bujarski, J. J., Dreher, T. W. & Hall, T. C. Minus-strand initiation by brome mosaic virus replicase within the 3' tRNA-like structure of native and modified RNA templates. *J. Mol. Biol.* **187**, 537–546 (1986).
- Dreher, T. W. & Hall, T. C. Mutational analysis of the tRNA mimicry of brome mosaic virus RNA. Sequence and structural requirements for aminoacylation and 3'-adenylation. *J. Mol. Biol.* **201**, 41–55 (1988).
- Dreher, T. W. & Hall, T. C. Mutational analysis of the sequence and structural requirements in brome mosaic virus RNA for minus strand promoter activity. *J. Mol. Biol.* **201**, 31–40 (1988).
- Choi, S. K., Hema, M., Gopinath, K., Santos, J. & Kao, C. Replicase-binding sites on plus- and minus-strand brome mosaic virus RNAs and their roles in RNA replication in plant cells. *J. Virol.* **78**, 13420–13429 (2004).
- Wang, H. & Lambowitz, A. M. The Mauriceville plasmid reverse transcriptase can initiate cDNA synthesis *de novo* and may be related to reverse transcriptase and DNA polymerase progenitor. *Cell* **75**, 1071–1081 (1993).
- Identifies a natural intermediate between tRNA-primed retrovirus reverse transcription and *de novo* RNA synthesis on tRNA-like 3' ends of some RNA viruses.
- Restrepo-Hartwig, M. & Ahlquist, P. Brome mosaic virus helicase- and polymerase-like proteins colocalize on the endoplasmic reticulum at sites of viral RNA synthesis. *J. Virol.* **70**, 8908–8916 (1996).
- Restrepo-Hartwig, M. & Ahlquist, P. Brome mosaic virus RNA replication proteins 1a and 2a colocalize and 1a independently localizes on the yeast endoplasmic reticulum. *J. Virol.* **73**, 10303–10309 (1999).
- Pedersen, K. W., van der Meer, Y., Roos, N. & Snijder, E. J. Open reading frame 1-a-encoded subunits of the arterivirus replicase induce endoplasmic reticulum-derived double-membrane vesicles which carry the viral replication complex. *J. Virol.* **73**, 2016–2026 (1999).
- Suh, D. A., Giddings, T. H., Jr & Kirkegaard, K. Remodeling the endoplasmic reticulum by poliovirus infection and by individual viral proteins: an autophagy-like origin for virus-induced vesicles. *J. Virol.* **74**, 8953–8965 (2000).
- Gosert, R. *et al.* Identification of the hepatitis C virus RNA replication complex in Huh-7 cells harboring subgenomic replicons. *J. Virol.* **77**, 5487–5492 (2003).
- Grimley, P. M., Berezsky, I. & Friedman, R. M. Cytoplasmic structures associated with an arbovirus infection: loci of viral ribonucleic acid synthesis. *J. Virol.* **2**, 1326–1338 (1968).
- Froshauer, S., Kartenbeck, J. & Helenius, A. Alphavirus RNA replicase is located on the cytoplasmic surface of endosomes and lysosomes. *J. Cell Biol.* **107**, 2075–2086 (1988).
- References 20 and 21 are classic papers showing association of alphavirus RNA synthesis with modified intracellular membranes.
- Miller, D. J., Schwartz, M. D. & Ahlquist, P. Flock house virus RNA replicates on outer mitochondrial membranes in *Drosophila* cells. *J. Virol.* **75**, 11664–11676 (2001).
- Prod'homme, D., Le Panse, S., Drugeon, G. & Jupin, I. Detection and subcellular localization of the turnip yellow mosaic virus 66K replication protein in infected cells. *Virology* **281**, 88–101 (2001).
- Kim, K. S. An ultrastructural study of inclusions and disease in plant cells infected by cowpea chlorotic mottle virus. *J. Gen. Virol.* **35**, 535–543 (1977).
- Hatta, T. & Francki, R. I. B. Cytopathic structures associated with tonoplasts of plant cells infected with cucumber mosaic and tomato aspermy viruses. *J. Gen. Virol.* **53**, 343–346 (1981).
- Morikawa, Y. HIV capsid assembly. *Curr. HIV Res.* **1**, 1–14 (2003).
- Scarlata, S. & Carter, C. Role of HIV-1 Gag domains in viral assembly. *Biochim. Biophys. Acta* **1614**, 62–72 (2003).
- Swanstrom, R. & Wills, J. W. in *Retroviruses* (eds Coffin, J. M., Hughes, S. H. & Varmus, H. E.) 263–334 (Cold Spring Harbor Laboratory Press, Cold Spring Harbor, 1997).
- Ansari-Lari, M. A. & Gibbs, R. A. Expression of human immunodeficiency virus type 1 reverse transcriptase in *trans* during virion release and after infection. *J. Virol.* **70**, 3870–3805 (1996).
- Yuan, B., Fassati, A., Yueh, A. & Goff, S. P. Characterization of Moloney murine leukemia virus p12 mutants blocked during early events of infection. *J. Virol.* **76**, 10801–10810 (2002).
- Nermut, M. V. & Fassati, A. Structural analyses of purified human immunodeficiency virus type 1 intracellular reverse transcription complexes. *J. Virol.* **77**, 8196–8206 (2003).
- Garfinkel, D. J., Boeke, J. D. & Fink, G. R. Ty element transposition: reverse transcriptase and virus-like particles. *Cell* **42**, 507–517 (1985).
- Eichinger, D. J. & Boeke, J. D. The DNA intermediate in yeast Ty1 element transposition copurifies with virus-like particles: cell-free Ty1 transposition. *Cell* **54**, 955–966 (1988).
- Linial, M. L. Foamy viruses are unconventional retroviruses. *J. Virol.* **73**, 1747–1755 (1999).
- Palmer, K. J. *et al.* Cryo-electron microscopy structure of yeast Ty retrotransposon virus-like particles. *J. Virol.* **71**, 6863–6868 (1997).
- Briggs, J. A. *et al.* The stoichiometry of Gag protein in HIV-1. *Nature Struct. Mol. Biol.* **11**, 672–675 (2004).
- Shehu-Xhilaga, M., Crowe, S. M. & Mak, J. Maintenance of the Gag/Gag-Pol ratio is important for human immunodeficiency virus type 1 RNA dimerization and viral infectivity. *J. Virol.* **75**, 1834–1841 (2001).
- Berkowitz, R., Fisher, J. & Goff, S. P. RNA packaging. *Curr. Top. Microbiol. Immunol.* **214**, 177–218 (1996).
- D'Souza, V. & Summers, M. F. Structural basis for packaging the dimeric genome of Moloney murine leukaemia virus. *Nature* **431**, 586–590 (2004).
- Ahlquist, P. *et al.* Sindbis virus proteins nsP1 and nsP2 contain homology to nonstructural proteins from several RNA plant viruses. *J. Virol.* **53**, 536–542 (1985).
- van Regenmortel, M. H. V. [ed.] *Virus Taxonomy* (Academic Press, San Diego, 2000).
- Ahola, T. & Ahlquist, P. Putative RNA capping activities encoded by brome mosaic virus: methylation and covalent binding of guanylate by replicase protein 1a. *J. Virol.* **73**, 10061–10069 (1999).
- Ahola, T., den Boon, J. A. & Ahlquist, P. Helicase and capping enzyme active site mutations in brome mosaic virus protein 1a cause defects in template recruitment, negative-strand RNA synthesis, and viral RNA capping. *J. Virol.* **74**, 8803–8811 (2000).
- Kong, F., Sivakumaran, K. & Kao, C. The N-terminal half of the brome mosaic virus 1a protein has RNA capping-associated activities: specificity for GTP and S-adenosylmethionine. *Virology* **259**, 200–210 (1999).
- Schwartz, M. *et al.* A positive-strand RNA virus replication complex parallels form and function of retrovirus capsids. *Mol. Cell* **9**, 505–514 (2002).
- Reveals parallels between the structure, assembly and function of bromovirus RNA-replication complexes and retrovirus virions.
- Kao, C. C. & Ahlquist, P. Identification of the domains required for direct interaction of the helicase-like and polymerase-like RNA replication proteins of brome mosaic virus. *J. Virol.* **66**, 7293–7302 (1992).
- Chen, J. & Ahlquist, P. Brome mosaic virus polymerase-like protein 2a is directed to the endoplasmic reticulum by helicase-like viral protein 1a. *J. Virol.* **74**, 4310–4318 (2000).
- Chen, J., Noueiry, A. & Ahlquist, P. An alternate pathway for recruiting template RNA to the brome mosaic virus RNA replication complex. *J. Virol.* **77**, 2568–2577 (2003).
- Janda, M. & Ahlquist, P. Brome mosaic virus RNA replication protein 1a dramatically increases *in vivo* stability but not translation of viral genomic RNA3. *Proc. Natl Acad. Sci. USA* **95**, 2227–2232 (1998).
- Sullivan, M. & Ahlquist, P. Cis-acting signals in bromovirus RNA replication and gene expression: networking with viral proteins and host factors. *Semin. Virol.* **8**, 221–230 (1997).
- Chen, J., Noueiry, A. & Ahlquist, P. Brome mosaic virus protein 1a recruits viral RNA2 to RNA replication through a 5' proximal RNA2 signal. *J. Virol.* **75**, 3207–3219 (2001).
- Sullivan, M. & Ahlquist, P. A brome mosaic virus intergenic RNA3 replication signal functions with viral replication protein 1a to dramatically stabilize RNA *in vivo*. *J. Virol.* **73**, 2622–2632 (1999).
- den Boon, J., Chen, J. & Ahlquist, P. Identification of sequences in brome mosaic virus replicase protein 1a that mediate association with endoplasmic reticulum membranes. *J. Virol.* **75**, 12370–12381 (2001).

54. O'Reilly, E. K., Wang, Z., French, R. & Kao, C. C. Interactions between the structural domains of the RNA replication proteins of plant-infecting RNA viruses. *J. Virol.* **72**, 7160–7169 (1998).
55. Freed, E. O. Viral late domains. *J. Virol.* **76**, 4679–4687 (2002).
56. McMahon, H. T. & Mills, I. G. COP and clathrin-coated vesicle budding: different pathways, common approaches. *Curr. Opin. Cell Biol.* **16**, 379–391 (2004).
57. Morita, E. & Sundquist, W. I. Retrovirus budding. *Annu. Rev. Cell Dev. Biol.* **20**, 395–425 (2004).
58. Lee, J.-Y., Marshall, J. A. & Bowden, D. S. Characterization of rubella virus replication complexes using antibodies to double-stranded RNA. *Virology* **200**, 307–312 (1994).
59. Kujala, P. *et al.* Biogenesis of the Semliki Forest virus RNA replication complex. *J. Virol.* **75**, 3873–3884 (2001).
60. Sethna, P. B. & Brian, D. A. Coronavirus genomic and subgenomic minus-strand RNAs copartition in membrane-protected replication complexes. *J. Virol.* **71**, 7744–7749 (1997).
61. Miyazaki, Y. *et al.* Hepatitis C virus non-structural proteins in the probable membranous compartment function in viral genome replication. *J. Biol. Chem.* **278**, 50301–50308 (2003).
62. Quinkert, D., Bartschlag, R. & Lohmann, V. Quantitative analysis of the hepatitis C virus replication complex. *J. Virol.* **79**, 13594–13605 (2005).
63. Lyle, J. M., Bullitt, E., Bienz, K. & Kirkegaard, K. Visualization and functional analysis of RNA-dependent RNA polymerase lattices. *Science* **296**, 2218–2222 (2002).
Shows that poliovirus RNA polymerase can self-interact in extended networks consistent with RNA replication on membrane surfaces.
64. Panaviene, Z., Panavas, T. & Nagy, P. D. Role of an internal and two 3'-terminal RNA elements in assembly of tombusvirus replicase. *J. Virol.* **79**, 10608–10618 (2005).
65. Salonen, A. *et al.* Properly folded nonstructural polyprotein directs the Semliki Forest virus replication complex to the endosomal compartment. *J. Virol.* **77**, 1691–1702 (2003).
66. Snijder, E. J., van Tol, H., Roos, N. & Pedersen, K. W. Non-structural proteins 2 and 3 interact to modify host cell membranes during the formation of the arterivirus replication complex. *J. Gen. Virol.* **82**, 985–994 (2001).
67. Egger, D. *et al.* Expression of hepatitis C virus proteins induces distinct membrane alterations including a candidate viral replication complex. *J. Virol.* **76**, 5974–5984 (2002).
68. Cho, M. W., Teterina, N., Egger, D., Bienz, K. & Ehrenfeld, E. Membrane rearrangement and vesicle induction by recombinant poliovirus 2C and 2BC in human cells. *Virology* **202**, 129–145 (1994).
69. Teterina, N. L. *et al.* Requirements for assembly of poliovirus replication complexes and negative-strand RNA synthesis. *J. Virol.* **75**, 3841–3850 (2001).
70. Felsenstein, K. M. & Goff, S. P. Expression of the Gag–Pol fusion protein of Moloney murine leukemia virus without Gag protein does not induce virion formation or proteolytic processing. *J. Virol.* **62**, 2179–2182 (1988).
71. Karacostas, V., Wolfe, E. J., Nagashima, K., Gonda, M. A. & Moss, B. Overexpression of the HIV-1 Gag–Pol polyprotein results in intracellular activation of HIV-1 protease and inhibition of assembly and budding of virus-like particles. *Virology* **193**, 661–671 (1993).
72. Panavas, T., Hawkins, C. M., Panaviene, Z. & Nagy, P. D. The role of the p33/p33/p92 interaction domain in RNA replication and intracellular localization of p33 and p92 proteins of Cucumber necrosis tombusvirus. *Virology* **338**, 81–95 (2005).
73. Ishikawa, M., Meshi, T., Motoyoshi, F., Takamatsu, N. & Okada, Y. *In vitro* motility of the putative replicase genes of tobacco mosaic virus. *Nucleic Acids Res.* **14**, 8291–8305 (1986).
74. Li, G. & Rice, C. M. Mutagenesis of the in-frame opal termination codon preceding nsP4 of Sindbis virus: studies of translational readthrough and its effect on virus replication. *J. Virol.* **63**, 1326–1337 (1989).
75. Noueiry, A. O., Chen, J. & Ahlquist, P. A mutant allele of essential, general translation initiation factor DED1 selectively inhibits translation of a viral mRNA. *Proc. Natl Acad. Sci. USA* **97**, 12985–12990 (2000).
76. Ishikawa, M., Diez, J., Restrepo-Hartwig, M. & Ahlquist, P. Yeast mutations in multiple complementation groups inhibit brome mosaic virus RNA replication and transcription and perturb regulated expression of the viral polymerase-like gene. *Proc. Natl Acad. Sci. USA* **94**, 13810–13815 (1997).
77. Kim, S. H., Palukaitis, P. & Park, Y. I. Phosphorylation of cucumber mosaic virus RNA polymerase 2a protein inhibits formation of replicase complex. *EMBO J.* **21**, 2292–2300 (2002).
78. deGroot, R. J., Rumenapf, T., Kuhn, R. J., Strauss, E. G. & Strauss, J. H. Sindbis virus RNA polymerase is degraded by the N-end rule pathway. *Biochemistry* **88**, 8967–8971 (1991).
79. Hajimorad, M. R. *et al.* Nla and Nlb of peanut stripe potyvirus are present in the nucleus of infected cells, but do not form inclusions. *Virology* **224**, 368–379 (1996).
80. Levin, H. L., Weaver, D. C. & Boeke, J. D. Novel gene expression mechanism in a fission yeast retroelement: TFI proteins are derived from a single primary translation product. *EMBO J.* **12**, 4885–4895 (1993).
81. Teyssier, L., Dang, V. D., Kim, M. K. & Levin, H. L. A long terminal repeat-containing retrotransposon of *Schizosaccharomyces pombe* expresses a Gag-like protein that assembles into virus-like particles which mediate reverse transcription. *J. Virol.* **77**, 5451–5463 (2003).
82. Ganser, B. K., Cheng, A., Sundquist, W. I. & Yeager, M. Three-dimensional structure of the M-MuLV CA protein on a lipid monolayer: a general model for retroviral capsid assembly. *EMBO J.* **22**, 2886–2892 (2003).
83. Westaway, E., Mackenzie, J., Kenney, M., Jones, M. & Khromykh, A. Ultrastructure of Kunjin virus-infected cells: colocalization of NS1 and NS3 with double-stranded RNA, and of NS2B with NS3, in virus-induced membrane structures. *J. Virol.* **71**, 6650–6661 (1997).
84. Schwartz, M., Chen, J., Lee, W. M., Janda, M. & Ahlquist, P. Alternate, virus-induced membrane rearrangements support positive-strand RNA virus genome replication. *Proc. Natl Acad. Sci. USA* **101**, 11263–11268 (2004).
Shows that outwardly distinct membrane rearrangements, similar to those associated with RNA replication by different viruses, can be induced by the same viral replication proteins.
85. Aizaki, H., Lee, K. J., Sung, V. M., Ishiko, H. & Lai, M. M. Characterization of the hepatitis C virus RNA replication complex associated with lipid rafts. *Virology* **324**, 450–461 (2004).
86. Gosert, R., Kanjanahualthai, A., Egger, D., Bienz, K. & Baker, S. C. RNA replication of mouse hepatitis virus takes place at double-membrane vesicles. *J. Virol.* **76**, 3697–3708 (2002).
87. Schlegel, A., Giddings, J., T., Ladinsky, M. & Kirkegaard, K. Cellular origin and ultrastructure of membranes induced during poliovirus infection. *J. Virol.* **70**, 6576–6588 (1996).
88. Teterina, N. L., Bienz, K., Egger, D., Gorbalenya, A. E. & Ehrenfeld, E. Induction of intracellular membrane rearrangements by HAV proteins 2C and 2BC. *Virology* **237**, 66–77 (1997).
89. Egger, D., Pasamontes, L., Bolten, R., Boyko, V. & Bienz, K. Reversible dissociation of the poliovirus replication complex: functions and interactions of its components in viral RNA synthesis. *J. Virol.* **70**, 8675–8683 (1996).
90. Nibert, M. L. & Schiff, L. A. In *Fields Virology* (eds Knipe, D. M. & Howley, P. M.) 1679–1728 (Lippincott, Williams & Wilkins, Philadelphia, 2001).
91. Patton, J. T. & Spencer, E. Genome replication and packaging of segmented double-stranded RNA viruses. *Virology* **277**, 217–225 (2000).
92. Koonin, E. V., Gorbalenya, A. E. & Chumakov, K. M. Tentative identification of RNA-dependent RNA polymerases of dsRNA viruses and their relationship to positive strand RNA viral polymerases. *FEBS Lett.* **252**, 42–46 (1989).
93. Koonin, E. V., Choi, G. H., Nuss, D. L., Shapira, R. & Carrington, J. C. Evidence for common ancestry of a chestnut blight virulence-associated double-stranded RNA and a group of positive-strand RNA plant viruses. *Proc. Natl Acad. Sci. USA* **88**, 10647–10651 (1991).
94. Reinisch, K. M., Nibert, M. L. & Harrison, S. C. Structure of the reovirus core at 3.6 Å resolution. *Nature* **404**, 960–967 (2000).
95. Zhang, X., Walker, S. B., Chipman, P. R., Nibert, M. L. & Baker, T. S. Reovirus polymerase $\lambda 3$ localized by cryo-electron microscopy of virions at a resolution of 7.6 Å. *Nature Struct. Biol.* **10**, 1011–1018 (2003).
References 94 and 95 define the structure of transcriptionally active cores of dsRNA reovirus.
96. Gomez de Cedron, M., Ehsani, N., Mikkola, M. L., Garcia, J. A. & Kaariainen, L. RNA helicase activity of Semliki Forest virus replicase protein NSP2. *FEBS Lett.* **448**, 19–22 (1999).
97. Vasiljeva, L., Merits, A., Auvinen, P. & Kaariainen, L. Identification of a novel function of the alphavirus capping apparatus. RNA 5'-triphosphatase activity of Nsp2. *J. Biol. Chem.* **275**, 17281–17287 (2000).
98. Li, Y. I. *et al.* The helicase-like domain of plant potyvirus replicase participates in formation of RNA 5' cap structure by exhibiting RNA 5'-triphosphatase activity. *J. Virol.* **75**, 12114–12120 (2001).
99. Wang, X. *et al.* Brome mosaic virus 1a nucleoside triphosphatase/helicase domain plays crucial roles in recruiting RNA replication templates. *J. Virol.* **79**, 13747–13758 (2005).
100. Bisailon, M., Bergeron, J. & Lemay, G. Characterization of the nucleoside triphosphate phosphohydrolase and helicase activities of the reovirus $\lambda 1$ protein. *J. Biol. Chem.* **272**, 18298–18303 (1997).
101. Bisailon, M. & Lemay, G. Characterization of the reovirus $\lambda 1$ protein RNA 5'-triphosphatase activity. *J. Biol. Chem.* **272**, 29954–29957 (1997).
102. Kao, C. C., Quadt, R., Hershberger, R. P. & Ahlquist, P. Brome mosaic virus RNA replication proteins 1a and 2a form a complex *in vitro*. *J. Virol.* **66**, 6322–6329 (1992).
103. Luongo, C. L., Contreras, C. M., Farsetta, D. L. & Nibert, M. L. Binding site for S-adenosyl-L-methionine in a central region of mammalian reovirus $\lambda 2$ protein. Evidence for activities in mRNA cap methylation. *J. Biol. Chem.* **273**, 23773–23780 (1998).
104. Luongo, C. L., Reinisch, K. M., Harrison, S. C. & Nibert, M. L. Identification of the guanylyltransferase region and active site in reovirus mRNA capping protein $\lambda 2$. *J. Biol. Chem.* **275**, 2804–2810 (2000).
105. Li, Y. I., Chen, Y. J., Hsu, Y. H. & Meng, M. Characterization of the AdoMet-dependent guanylyltransferase activity that is associated with the N terminus of bamboo mosaic virus replicase. *J. Virol.* **75**, 782–788 (2001).
106. Pirttimaa, M. J., Paatero, A. O., Frilander, M. J. & Bamford, D. H. Nonspecific nucleoside triphosphatase P4 of double-stranded RNA bacteriophage $\phi 6$ is required for single-stranded RNA packaging and transcription. *J. Virol.* **76**, 10122–10127 (2002).
107. Kainov, D. E. *et al.* RNA packaging device of double-stranded RNA bacteriophages, possibly as simple as hexamer of P4 protein. *J. Biol. Chem.* **278**, 48084–48091 (2003).
108. Goregaoker, S. P. & Culver, J. N. Oligomerization and activity of the helicase domain of the tobacco mosaic virus 126- and 183-kilodalton replicase proteins. *J. Virol.* **77**, 3549–3556 (2003).
109. Jayaram, H., Taraporewala, Z., Patton, J. T. & Prasad, B. V. Rotavirus protein involved in genome replication and packaging exhibits a HIT-like fold. *Nature* **417**, 311–315 (2002).
110. Taraporewala, Z. F. & Patton, J. T. Nonstructural proteins involved in genome packaging and replication of rotaviruses and other members of the *Reoviridae*. *Virus Res.* **101**, 57–66 (2004).
111. Kim, J., Parker, J. S., Murray, K. E. & Nibert, M. L. Nucleoside and RNA triphosphatase activities of orthoreovirus transcriptase cofactor $\mu 2$. *J. Biol. Chem.* **279**, 4394–4403 (2004).
112. Kroner, P. A., Young, B. M. & Ahlquist, P. Analysis of the role of brome mosaic virus 1a protein domains in RNA replication, using linker insertion mutagenesis. *J. Virol.* **64**, 6110–6120 (1990).
113. Ishikawa, M., Kroner, P., Ahlquist, P. & Meshi, T. Biological activities of hybrid RNAs generated by 3'-end exchanges between tobacco mosaic and brome mosaic viruses. *J. Virol.* **65**, 3451–3459 (1991).
114. Ahlquist, P. RNA-dependent RNA polymerases, viruses, and RNA silencing. *Science* **296**, 1270–1273 (2002).
115. Silvestri, L. S., Taraporewala, Z. F. & Patton, J. T. Rotavirus replication: plus-sense templates for double-stranded RNA synthesis are made in viroplasm. *J. Virol.* **78**, 7763–7774 (2004).
116. Gitlin, L., Stone, J. K. & Andino, R. Poliovirus escape from RNA interference: short interfering RNA-target recognition and implications for therapeutic approaches. *J. Virol.* **79**, 1027–1035 (2005).

117. Ishikawa, M., Meshi, T., Ohno, T. & Okada, Y. Specific cessation of minus-strand RNA accumulation at an early stage of tobacco mosaic virus infection. *J. Virol.* **65**, 861–868 (1991).
118. Strauss, J. H. & Strauss, E. G. The alphaviruses: gene expression, replication, and evolution. *Microbiol. Rev.* **58**, 491–562 (1994).
119. Wengler, G., Wengler, G. & Gross, H. J. Terminal sequences of Sindbis virus-specific nucleic acids: identity in molecules synthesized in vertebrate and insect cells and characteristic properties of the replicative form RNA. *Virology* **123**, 273–283 (1985).
120. Collmer, C. W. & Kaper, J. M. Double-stranded RNAs of cucumber mosaic virus and its satellite contain an unpaired terminal guanosine: implications for replication. *Virology* **145**, 249–259 (1985).
121. Diprose, J. M. *et al.* Translocation portals for the substrates and products of a viral transcription complex: the bluetongue virus core. *EMBO J.* **20**, 7229–7239 (2001).
122. Hansen, J., Long, A. & Schultz, S. Structure of the RNA-dependent RNA polymerase of poliovirus. *Structure* **5**, 1109–1122 (1997).
123. Lesburg, C. A. *et al.* Crystal structure of the RNA-dependent RNA polymerase from hepatitis C virus reveals a fully encircled active site. *Nature Struct. Biol.* **6**, 937–943 (1999).
124. Siegel, R. W., Bellon, L., Beigelman, L. & Kao, C. C. Use of DNA, RNA, and chimeric templates by a viral RNA-dependent RNA polymerase: evolutionary implications for the transition from the RNA to the DNA world. *J. Virol.* **73**, 6424–6429 (1999).
Shows that a (+)RNA-virus RNA-dependent RNA polymerase has substantial activity on DNA templates.
125. Gao, G., Orlova, M., Georgiadis, M. M., Hendrickson, W. A. & Goff, S. P. Conferring RNA polymerase activity to a DNA polymerase: a single residue in reverse transcriptase controls substrate selection. *Proc. Natl Acad. Sci. USA* **94**, 407–411 (1997).
126. Rolls, M. M., Webster, P., Balba, N. H. & Rose, J. K. Novel infectious particles generated by expression of the vesicular stomatitis virus glycoprotein from a self-replicating RNA. *Cell* **79**, 497–506 (1994).
127. Lai, M. M. RNA recombination in animal and plant viruses. *Microbiol. Rev.* **56**, 61–79 (1992).
128. Nagy, P. D. & Simon, A. E. New insights into the mechanisms of RNA recombination. *Virology* **235**, 1–9 (1997).
129. Worobey, M. & Holmes, E. C. Evolutionary aspects of recombination in RNA viruses. *J. Gen. Virol.* **80**, 2535–2543 (1999).
130. Ahlquist, P. *et al.* Viral and host determinants of RNA virus vector replication and expression. *Vaccine* **23**, 1784–1787 (2005).
131. Estes, M. K. in *Fields Virology* (eds Knipe, D. M. & Howley, P. M.) 1747–1785 (Lippincott, Williams & Wilkins, Philadelphia, 2001).
132. Lopez, T. *et al.* Silencing the morphogenesis of rotavirus. *J. Virol.* **79**, 184–192 (2005).
133. Silvestri, L. S., Tortorici, M. A., Vasquez-Del Carpio, R. & Patton, J. T. Rotavirus glycoprotein NSP4 is a modulator of viral transcription in the infected cell. *J. Virol.* **79**, 15165–15174 (2005).
References 132 and 133 reveal links between rotavirus transmembrane protein nsP4 and formation of viroplasm in which dsRNA virion-core assembly occurs.
134. Laurinavicius, S., Kakela, R., Bamford, D. H. & Somerharju, P. The origin of phospholipids of the enveloped bacteriophage $\phi 6$. *Virology* **326**, 182–190 (2004).
135. Lee, W. M., Ishikawa, M. & Ahlquist, P. Mutation of host $\Delta 9$ fatty acid desaturase inhibits brome mosaic virus RNA replication between template recognition and RNA synthesis. *J. Virol.* **75**, 2097–2106 (2001).
136. Lee, W. M. & Ahlquist, P. Membrane synthesis, specific lipid requirements, and localized lipid composition changes associated with a positive-strand RNA virus RNA replication protein. *J. Virol.* **77**, 12819–12828 (2003).
137. Ono, A. & Freed, E. O. Plasma membrane rafts play a critical role in HIV-1 assembly and release. *Proc. Natl Acad. Sci. USA* **98**, 13925–13930 (2001).
138. Kushner, D. B. *et al.* Systematic, genome-wide identification of host genes affecting replication of a positive-strand RNA virus. *Proc. Natl Acad. Sci. USA* **100**, 15764–15769 (2003).
139. Hu, J., Toft, D. O. & Seeger, C. Hepadnavirus assembly and reverse transcription require a multi-component chaperone complex which is incorporated into nucleocapsids. *EMBO J.* **16**, 59–68 (1997).
140. Tomita, Y. *et al.* Mutation of host *dnaJ* homolog inhibits brome mosaic virus negative-strand RNA synthesis. *J. Virol.* **77**, 2990–2997 (2003).
141. Held, D. M., Kissel, J. D., Patterson, J. T., Nickens, D. G. & Burke, D. H. HIV-1 inactivation by nucleic acid aptamers. *Front. Biosci.* **11**, 89–112 (2006).
142. Resh, M. D. Intracellular trafficking of HIV-1 Gag: how Gag interacts with cell membranes and makes viral particles. *AIDS Rev.* **7**, 84–91 (2005).
143. Khromykh, A. A., Kondratieva, N., Sgro, J. Y., Palmenberg, A. & Westaway, E. G. Significance in replication of the terminal nucleotides of the flavivirus genome. *J. Virol.* **77**, 10623–10629 (2003).
144. Yang, H., Makeyev, E. V., Butcher, S. J., Gaidelyte, A. & Bamford, D. H. Two distinct mechanisms ensure transcriptional polarity in double-stranded RNA bacteriophages. *J. Virol.* **77**, 1195–1203 (2003).
145. Wickner, R. B. Double-stranded RNA viruses of *Saccharomyces cerevisiae*. *Microbiol. Rev.* **60**, 250–265 (1996).

Acknowledgements

We thank all members of our laboratory for helpful discussions. This work was supported by the National Institutes of Health.

Competing interests statement

The author declares no competing financial interests.

DATABASES

The following terms in this article are linked online to:
Entrez Genome: <http://www.ncbi.nlm.nih.gov/entrez/query.fcgi?db=genome>
hepatitis C virus | HIV | poliovirus | RNA1 | RNA2 | RNA3 | tobacco mosaic virus | vesicular stomatitis virus
UniProtKB: <http://ca.expasy.org/sprot>
1a | 2a^{pol} | $\lambda 1$ | $\lambda 2$ | $\lambda 3$ | P4

FURTHER INFORMATION

Paul Ahlquist's homepage: http://mcardle.oncology.wisc.edu/faculty/bio/ahlquist_p.html
Access to this links box is available online.

Three-Dimensional Analysis of a Viral RNA Replication Complex Reveals a Virus-Induced Mini-Organelle

Applicant's
Exhibit
B

Benjamin G. Kopek¹, Guy Perkins^{2,3}, David J. Miller^{4,5}, Mark H. Ellisman^{2,3}, Paul Ahlquist^{1,6*}

1 Institute for Molecular Virology, University of Wisconsin–Madison, Madison, Wisconsin, United States of America, **2** National Center for Microscopy and Imaging Research, University of California San Diego, La Jolla, California, United States of America, **3** Department of Neurosciences, University of California San Diego, La Jolla, California, United States of America, **4** Department of Medicine, University of Michigan Medical School, Ann Arbor, Michigan, United States of America, **5** Department of Microbiology and Immunology, University of Michigan Medical School, Ann Arbor, Michigan, United States of America, **6** Howard Hughes Medical Institute, University of Wisconsin–Madison, Madison, Wisconsin, United States of America,

Positive-strand RNA viruses are the largest genetic class of viruses and include many serious human pathogens. All positive-strand RNA viruses replicate their genomes in association with intracellular membrane rearrangements such as single- or double-membrane vesicles. However, the exact sites of RNA synthesis and crucial topological relationships between relevant membranes, vesicle interiors, surrounding lumens, and cytoplasm generally are poorly defined. We applied electron microscope tomography and complementary approaches to flock house virus (FHV)-infected *Drosophila* cells to provide the first 3-D analysis of such replication complexes. The sole FHV RNA replication factor, protein A, and FHV-specific 5-bromouridine 5'-triphosphate incorporation localized between inner and outer mitochondrial membranes inside ~50-nm vesicles (spherules), which thus are FHV-induced compartments for viral RNA synthesis. All such FHV spherules were outer mitochondrial membrane invaginations with interiors connected to the cytoplasm by a necked channel of ~10-nm diameter, which is sufficient for ribonucleotide import and product RNA export. Tomographic, biochemical, and other results imply that FHV spherules contain, on average, three RNA replication intermediates and an interior shell of ~100 membrane-spanning, self-interacting protein As. The results identify spherules as the site of protein A and nascent RNA accumulation and define spherule topology, dimensions, and stoichiometry to reveal the nature and many details of the organization and function of the FHV RNA replication complex. The resulting insights appear relevant to many other positive-strand RNA viruses and support recently proposed structural and likely evolutionary parallels with retrovirus and double-stranded RNA virus virions.

Citation: Kopek BG, Perkins G, Miller DJ, Ellisman MH, Ahlquist P (2007) Three-dimensional analysis of a viral RNA replication complex reveals a virus-induced mini-organelle. *PLoS Biol* 5(9): e220. doi:10.1371/journal.pbio.0050220

Introduction

Positive-strand RNA [(+)RNA] viruses contain messenger-sense, single-stranded RNA in their virions; they represent over a third of known virus genera; and they include many important human, animal, and plant pathogens [1]. A common, if not universal, feature of (+)RNA virus replication is the association of their RNA replication complexes with infection-specific host intracellular membrane rearrangements [2–19]. Characterizing the features of these membrane-associated RNA replication complexes should identify general principles and mechanisms of (+)RNA virus replication and could lead to broadly applicable control strategies for (+)RNA viruses including, e.g., hepatitis C virus and the SARS coronavirus.

For many (+)RNA viruses—including alphaviruses [5], other members of the alphavirus-like superfamily [15], rubiviruses [7,20], flaviviruses [21], tombusviruses [22], and others [4,23–25]—RNA replication occurs in association with ~50–70-nm diameter membranous vesicles or spherules that form in the lumen of specific secretory compartments or organelles. The similarity of these structures suggests that RNA replication by such otherwise distinct viruses involves important conserved features related to membranes. For some viruses, the localization of viral replicase proteins [11,17,23,26–28] or viral RNA synthesis [5,15,29] suggest that such spherules may

contain or comprise the viral RNA replication complex. For brome mosaic virus (BMV) and some other viruses, two-dimensional (2-D) electron microscopy (EM) reveals that a fraction of such spherules have interiors that appear to be connected to the cytoplasm by membranous necks [15,25,28]. However, limitations inherent in random sectioning and 2-D analysis prevent standard EM from resolving many issues crucial to understanding spherule structure and function, such as the range of spherule diameter and volume, and whether all spherule interiors are connected to the cytoplasm or if some bud free from their adjacent bounding membranes.

To resolve these and other issues central to the mechanism

Academic Editor: Skip Virgin, Washington University School of Medicine, United States of America

Received March 30, 2007; **Accepted** June 15, 2007; **Published** August 14, 2007

Copyright: © 2007 Kopek et al. This is an open-access article distributed under the terms of the Creative Commons Attribution License, which permits unrestricted use, distribution, and reproduction in any medium, provided the original author and source are credited.

Abbreviations: (–)RNA, negative-strand RNA; (+)RNA, positive-strand RNA; BMV, brome mosaic virus; BrUTP, 5-bromouridine 5'-triphosphate; dsRNA, double-stranded RNA; EM, electron microscopy; EMT, electron microscope tomography; FHV, flock house virus; hpi, h post infection;

* To whom correspondence should be addressed. E-mail: ahlquist@wisc.edu

Author Summary

Whereas cells store and replicate their genomes as DNA, most viruses have RNA genomes that replicate by using virus-specific pathways in the host cell. The largest class of RNA viruses, the positive-strand RNA viruses, replicate their genomes on intracellular membranes. However, little is understood about how and why these viruses use membranes in RNA replication. The well-studied flock house virus (FHV) replicates its RNA on mitochondrial membranes. We found that the single FHV RNA replication factor and newly synthesized FHV RNA localized predominantly in numerous infection-specific membrane vesicles inside the outer mitochondrial membrane. We used electron microscope tomography to image these membranes in three dimensions and found that the interior of each vesicle was connected to the cytoplasm by a single necked channel large enough to import ribonucleotide substrates and to export product RNA. The results suggest that FHV uses these vesicles as replication compartments, which may also protect replicating RNA from competing processes and host defenses. These findings complement results from other viruses to support possible parallels between genome replication by positive-strand RNA viruses and two distinct virus classes, double-stranded RNA and reverse-transcribing viruses.

of RNA replication, we used EM tomography (EMT) to provide the first, to our knowledge, three-dimensional (3-D) ultrastructural study of the membrane-bound RNA replication complexes of a (+)RNA virus. EMT generates high-resolution, 3-D images or tomograms by digitally processing a series of 50–100 electron micrographs collected as a specimen is tilted in 1–2° increments on an axis perpendicular to the electron beam [30]. Similar 3-D EMT analyses have been crucial to reveal many important features of complex cellular organelles such as the Golgi apparatus [31–34], endoplasmic reticulum [33,34], and mitochondria [35–37].

We chose flock house virus (FHV), the best characterized member of the *Nodaviridae*, as a (+)RNA virus with advantageous features for such studies. FHV has been used as a model to study RNA replication [8,9,38–40], virion structure and assembly [41,42], and genomic packaging [42–46]. FHV has a 4.5-kb bipartite RNA genome in which RNA2 (1.4 kb) encodes the capsid precursor [47] whereas RNA1 (3.1 kb) encodes an RNA silencing inhibitor [48,49] and a multifunctional RNA replication factor, protein A [40,50,51]. Protein A, the only FHV protein needed for RNA replication, is directed by an N-terminal targeting and transmembrane sequence to outer mitochondrial membranes, where it colocalizes by immunofluorescence with the sites of viral RNA synthesis [8,38]. Gradient flotation and dissociation assays showed that protein A behaves as an integral transmembrane protein [38]. Additionally, protease digestion and selective permeabilization after differential epitope tagging demonstrated that protein A is inserted into the outer mitochondrial membrane with the N terminus in the inner membrane space or matrix, while the majority of the protein A sequence is exposed to the cytoplasm [38]. Protein A also self-interacts in vivo in ways that are important for RNA replication [52]. Like many other (+)RNA viruses [4,5,7,15,20–25], FHV infection induces the formation of ~50-nm membranous vesicles or spherules, which, for the case of FHV, are found between the mitochondrial outer and inner membranes [8].

Here we use EMT and multiple complementary approaches

to provide 3-D visualization of a (+)RNA virus replication complex. Among other findings, the results show that FHV spherules are compartments or mini-organelles for viral RNA synthesis, which form by invagination of the outer mitochondrial membrane and communicate with the cytoplasm through ~10-nm diameter necks. The results further indicate that each spherule contains, on average, ~100 membrane-spanning, self-interacting protein A molecules and that FHV-infected cells contain 2–4 genomic RNA replication intermediates per spherule. These observations define a new level of understanding of the nature, structure, and organization of a viral RNA replication complex, including principles that are likely relevant to many other (+)RNA viruses.

Results

FHV RNA Replication Protein A and RNA Synthesis Are Located within Membrane-Bound Spherules

Protein A is the only FHV protein needed for RNA replication and so must co-localize with viral RNA replication complexes. Prior immunofluorescence and immunogold labeling EM localized protein A to the outer mitochondrial membrane in FHV-infected cells [8]. However, in those prior attempts at immunogold labeling, fixation conditions needed to preserve spherule ultrastructure abolished protein A antigenicity for the polyclonal antibody used, hence blocking protein A localization relative to spherules. To overcome this, we identified a monoclonal antibody against protein A [9] that was able to detect protein A under fixation conditions that sufficiently retained spherule ultrastructure. Immunogold EM with this protein A monoclonal antibody revealed that nearly all protein A was in or on mitochondrial spherules in FHV-infected cells (Figure 1). Over 900 gold particles in 25 different electron micrographs were counted and $88\% \pm 5\%$ of the specific gold labeling density above background (see Materials and Methods) was associated with spherules. Cytoplasmic labeling, presumably including protein A being translated and/or trafficked in the cytoplasm, was just $2\% \pm 7\%$ above background labeling levels. The remaining $10\% \pm 5\%$ of immunogold label was associated with mitochondria but not discernable spherules, including gold particles on the cytoplasmic face of the outer mitochondrial membrane where some protein A might have been localized that was not, or not yet, internalized into spherules. The clustering pattern of immunogold particles in a subset of spherules may be due to nonuniform epitope exposure or signal amplification by secondary antibodies. To avoid over-weighting the calculations due to such clustering effects, we also analyzed the same 25 micrographs counting each cluster as one event. The resulting count of clusters gave a very similar pattern to the one described above (94% spherule associated).

By immunofluorescence microscopy, we found that 5-bromouridine (BrU)-labeled FHV RNA synthesis occurs exclusively at outer mitochondrial membranes in infected *Drosophila* cells [8]. To localize more precisely FHV RNA synthesis in relation to spherules, we incubated mitochondria isolated from uninfected and FHV-infected *Drosophila* cells with a nucleotide mix including 5-bromouridine 5'-triphosphate (BrUTP) and performed immunogold labeling EM with an antibody recognizing BrU incorporated into RNA, but not unincorporated BrUTP.

For mitochondrial preparations from FHV-infected cells,

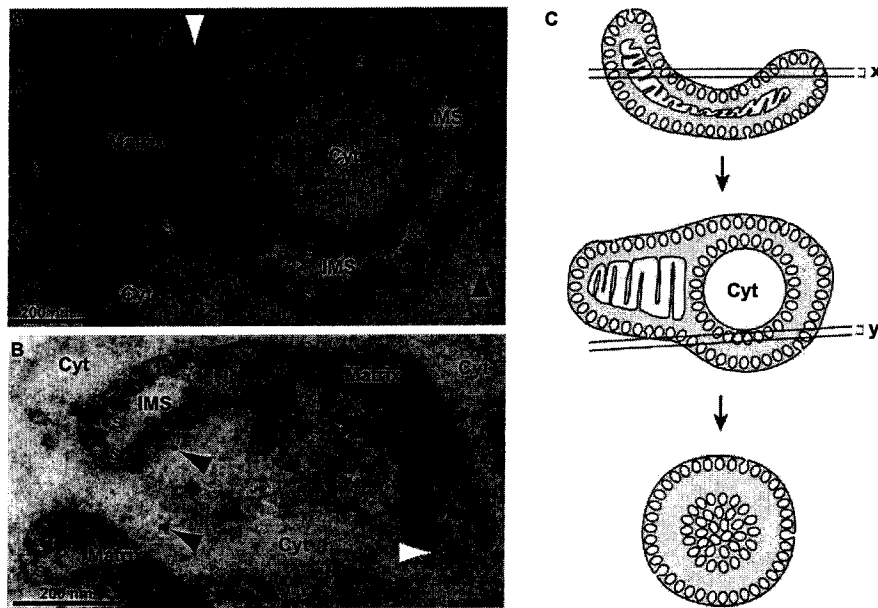


Figure 1. FHV Protein A Is Localized in Virus-Induced Mitochondrial Spherules

(A and B) Examples of anti-protein A immunogold labeling of mitochondrial spherules in FHV-infected cells. Cells were fixed in 4% paraformaldehyde and 0.2% glutaraldehyde, postfixed in 0.1% osmium, dehydrated and embedded in LR Gold resin, sectioned and placed on nickel-grids, immunostained with protein A antisera and a secondary antibody conjugated to ultrasmall gold particles, and silver-enhanced. The mitochondrial matrix, cytoplasm (Cyt) and examples of the many spherules (S) in the mitochondrial intermembrane space (IMS) are labeled for reference. White arrowheads indicate gold particles at a mitochondrial membrane but not directly over a spherule. Black arrowheads indicate gold particles in the cytoplasm. As illustrated in panel A, islands of cytoplasm surrounded by a mitochondrial ring are seen frequently in EM sections of FHV-infected mitochondria.

(C) A schematic, based on 3-D tomographic analysis shown below, of how such cytoplasmic islands are generated by EM sectioning of the frequently cup-shaped, FHV-modified mitochondria [see panel (B)]. The bottom image in (C) further shows how some planes of sectioning give rise to “vesicle packet” structures seen in Figures 2C and 3D below. White, cytoplasm; blue, space between outer and inner mitochondrial membranes; yellow, matrix. doi:10.1371/journal.pbio.0050220.g001

spherules were the major site of immunogold labeling (Figure 2A and 2B). Of 221 gold particles examined, $70\% \pm 18\%$ were on spherules. The remaining 30% of gold particles that fell outside of spherules may include mature RNA products released from spherules and nonspecific background labeling. For mitochondria from uninfected cells, background labeling levels were independent of the addition or omission of BrUTP and averaged 15% of the total immunogold labeling of BrUTP-treated mitochondria from FHV-infected cells. We found that using isolated mitochondria was advantageous for the BrUTP-labeling experiments because of low transfection efficiencies of BrUTP into whole *Drosophila* cells. Nevertheless, we were able to obtain some immunogold labeling results using intact *Drosophila* cells, which also showed that spherules were the major sites of BrUTP-labeling (Figure 2C). Gold particles in the intermembrane space of the mitochondrion in the lower right are well within the distance (20 nm) from spherules that may be spanned by the primary and secondary antibodies linking the immunogold particles to their target epitopes [53].

All Replication Spherules Retain an Open Connection to the Cytoplasm

Having shown that spherules were the sites of protein A accumulation and FHV RNA synthesis, we applied 3-D EMT to provide a new level of analysis of spherule morphology and topology. As noted in the Introduction, the 3-D nature of EMT overcomes many serious limitations of 2-D EM analysis to reveal possible connections to surrounding membranes and compartments, complete dimensions, and other funda-

mental characteristics not accessible from conventional transmission EM analyses of random sections. For example, along the z-axis parallel to the electron beam, standard transmission EM projects a 50–70-nm section into a single view, whereas EMT allows computationally dissecting an entire ~250-nm-thick sample volume into successively viewable planes spaced with a resolution of just a few nanometers [54].

To produce 3-D reconstructions of FHV-infected cells including modified mitochondria, *Drosophila* S2 cells were harvested 12 h post infection (hpi) and fixed, embedded, and sectioned as described under Materials and Methods. For each reconstruction, a tilt series of 60 images was collected by rotating a 250-nm-thick section of resin-embedded sample in 2° increments between -60° to $+60^\circ$ relative to the plane perpendicular to the beam, and was digitally processed to produce a tomographic reconstruction. Using *Drosophila* cells from three independent FHV infection experiments, five independent reconstructions were generated using a single-tilt series technique (Figure 3C–3D and additional unpublished data) and one reconstruction was performed using a double tilt technique (Figure 3A and 3B) to improve tomographic resolution further [55]. Representative results are shown in the figures.

For one such tomogram, Figure 3A shows the image of a computationally dissected, 2.2-nm-thick virtual section, revealing an FHV-modified mitochondrion containing spherules in the mitochondrial intermembrane space. This 2-D image shows a typical view of randomly sectioned, FHV-

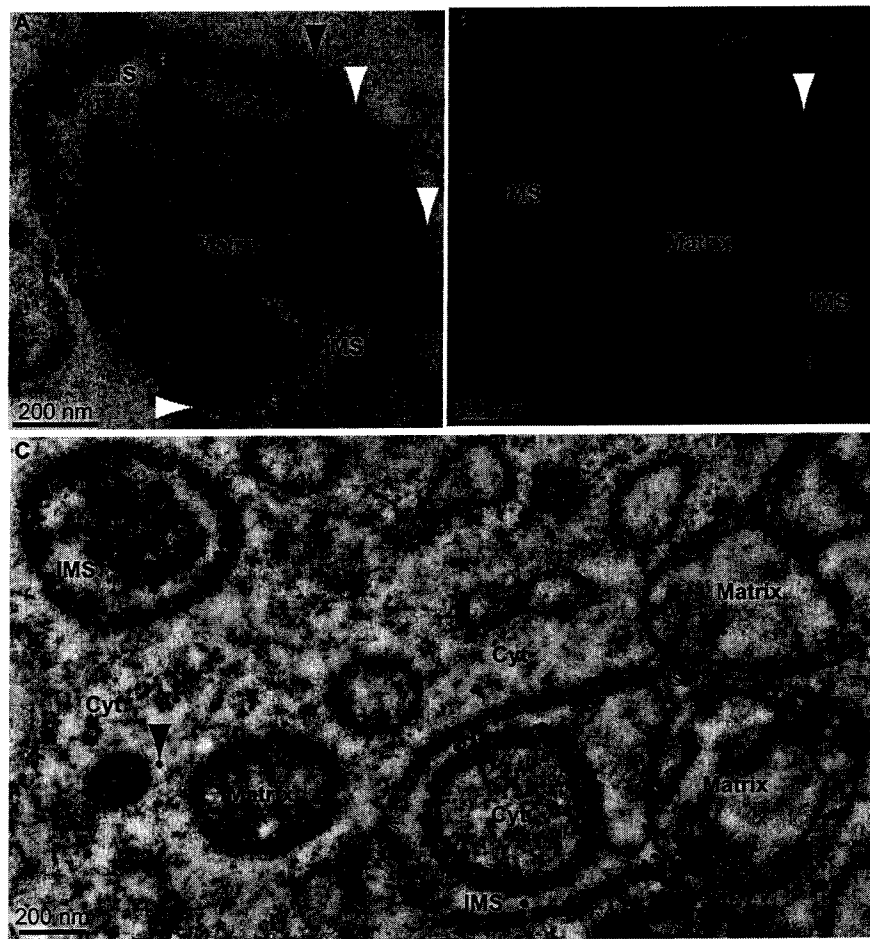


Figure 2. Association of Viral RNA Synthesis with FHV Spherules

(A and B) Examples of incorporated BrUTP immunogold labeling of mitochondrial spherules from cells infected with FHV. Isolated mitochondria were incubated for 1 h at 28 °C with a transcription mix that included BrUTP.

(C) Localization of RNA synthesis to spherules in FHV-infected cells into which BrUTP was introduced by transfection. Length of labeling period was 15 min. Samples were prepared for EM and immunogold labeling as in Figure 1, except that anti-BrU antibody was used instead of anti-protein A. See Figure 1C for an explanation of the nonstandard mitochondrial morphologies seen in the upper left and lower right of (C). The arrowheads and labeling of mitochondria, spherules, and cytoplasm are as in Figure 1. In interpreting the immunogold localization, note that the primary-secondary antibody complex linking the gold particles to their target epitopes may span up to 20 nm.

doi:10.1371/journal.pbio.0050220.g002

modified mitochondria, in which some spherules appear to be light bulb-shaped invaginations attached to the outer membrane by small diameter necks (white arrowheads), whereas others appear to be free vesicles in the intermembrane space (asterisks). Figure 3B shows another virtual section from the same tomogram, displaced down the perpendicular z-axis by ~15 nm to a point where those spherules that appeared to be free vesicles in Figure 3A (asterisks) now show necked attachments to the outer membrane. To determine if all spherules were attached to the outer mitochondrial membrane, or if a population of spherules budded free of this membrane, we followed individual spherules through dozens of successive 2.2-nm-spaced adjacent planes perpendicular to the electron beam (a “z-series” of sections). When all six reconstructions were examined in this way, all ~500 spherules in all ~8 FHV-modified mitochondria examined were found to be connected to the outer mitochondrial membrane by a membranous neck observable in some plane of the sample. The red arrowhead in

Figure 3A points to a channel through the spherule neck that connects the interior of a spherule to the cytoplasm.

Thus, all spherules are necked invaginations of the outer mitochondrial membrane whose interiors remain connected to the cytoplasm, and sections in which a given spherule appears to be a free vesicle simply represent planes that did not pass through the smaller diameter neck linking the spherule membrane to the mitochondrial outer membrane. This is illustrated more dynamically in Video S1, which animates the progression through a z-series of sections of the tomogram of Figure 3A and 3B.

Figure 3C–3D shows two virtual sections from another tomogram, which are displaced ~150 nm down the perpendicular z-axis from each other. As shown in a video through this z-series (Video S2), mitochondrion 1 curves significantly in the space between these two sections, such that the plane of Figure 3C sections mitochondrion 1 spherules parallel to an axis through the spherule necks, whereas the parallel plane of Figure 3D sections the spherules on another part of the

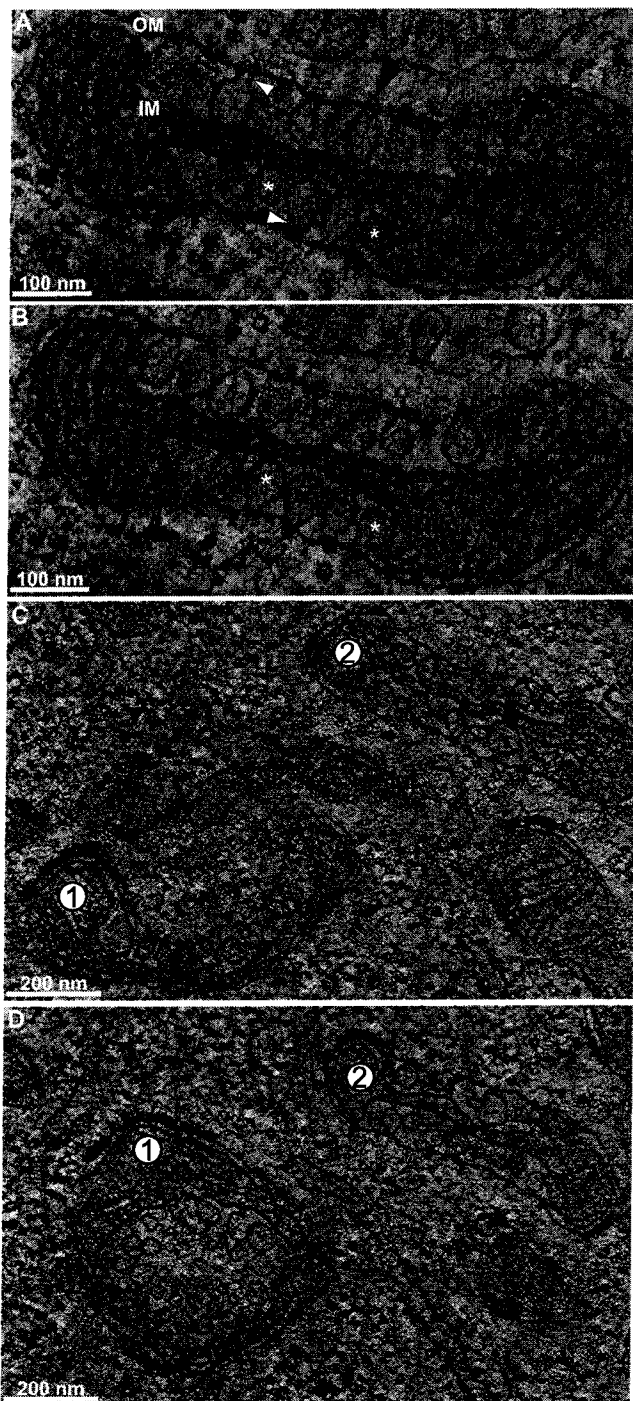


Figure 3. EMT Reconstructions of Mitochondria from FHV-Infected *Drosophila* Cells

Labels denote outer mitochondrial membrane (OM) and inner mitochondrial membrane (IM). (A and B) Slices through a tomographic reconstruction showing FHV-induced spherule rearrangements of a mitochondrion (see Video S1 to view the entire z-series). (B) is a slice that is ~15 nm down the z-axis (perpendicular to the plane of the image) from the slice in (A). White arrowheads indicate the necks that connect spherules to the OM. Asterisks mark two spherules that appear to be free vesicles in (A) but are shown to have necked connections to the outer membrane in (B). A red arrow marks the ~10-nm channel connecting a representative spherule interior to the cytoplasm. This red arrow also corresponds to the same spherule and connection as the red arrow in Figure 4B–4C.

(C and D) Images from another tomogram that are displaced from each

other in the z-axis by ~150 nm. Note the change in morphology of mitochondrion 1 where spherules that appear to be connected to the outer mitochondrial membrane in (C) appear as a vesicle packet in (D). doi:10.1371/journal.pbio.0050220.g003

mitochondrion 1 surface tangential to the axes through their necks. These two perpendicular views of similar spherules on the same mitochondrion are notable because Figure 3C strongly resembles images of spherules induced by alphaviruses, nodaviruses, etc. [8,28], whereas Figure 3D resembles images of apparently distinct “vesicle packets” described for flaviviruses [3]. Thus, some apparently distinct membrane rearrangements and vesicle structures observed in connection with RNA replication by different (+)RNA viruses may represent related structures distinguished in part by the perspective from which they were viewed.

3-D Mapping of Spherule Membranes

To generate 3-D surface maps of the virus-induced membrane rearrangements associated with FHV RNA replication, we manually traced the inner and outer mitochondrial membranes (including spherules) over ~100 adjacent, 2.2-nm-spaced virtual sections of selected tomographic reconstructions, and we used a computer-generated mesh overlay to join these tracings into continuous surfaces (Figure 4). Figure 4A shows part of the relationship between the electron density of the mitochondrion in Figure 3A and its 3-D map, and Video S3 provides a much more dynamic visualization of this relationship and the complete 3-D map. For clarity, the cytoplasmic faces of outer mitochondrial membranes are colored blue, spherule membranes are white, and inner mitochondrial membranes are yellow.

Figure 4B shows a close-up view of a portion of the 3-D map in Figure 4A that demonstrates the connection of the spherules to the outer mitochondrial membrane. This and other similar maps confirmed as noted above that the spherule membranes (white) are continuous with the outer mitochondrial membrane (blue). Figure 4C is a 90° rotation of Figure 4B that shows a view looking down on the surface of an FHV-modified mitochondrion, with the outer membrane (blue) rendered translucent to reveal the spherules beneath (Video S4). The necked channels connecting the interior of each spherule to the cytoplasm (red arrowhead) are clearly visible as circular openings in the outer membrane. For 150 individual spherules in four mitochondria from four cells and three experiments, we measured the interior diameters of these neck channels as the distance between the two lipid bilayers, from inner leaflet to inner leaflet, at the point where the tomographic plane sliced through the center of the neck. The resulting distribution of neck diameters is shown in Figure 5A. The average diameter of the neck channel was 10.5 ± 1.8 nm (Figure 5A), which is more than large enough to allow import of ribonucleotides and export of RNA products (diameter < 2 nm).

Surface-rendered, 3-D maps of the two mitochondria from Figure 3C are shown in Figure 4D, illustrating also the inner mitochondrial membrane (yellow). Using such surface-rendered maps (Figure 4 and other unpublished data), we also measured the interior volume and membrane surface area of 175 spherules. As illustrated in Figure 5C, the spherule volumes spanned a range of ~15,000 to 50,000 nm³. A range of spherule sizes is seen in Figure 4E, which is a rotated view

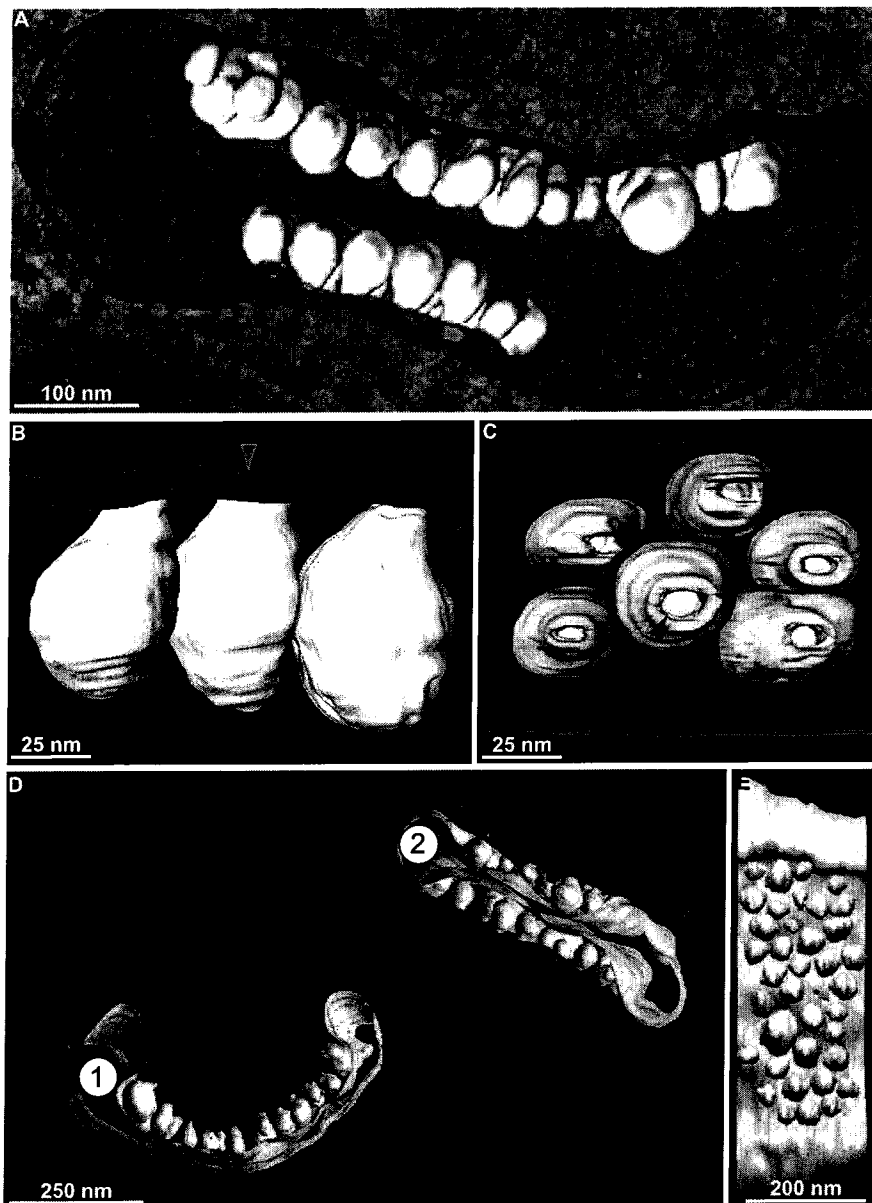


Figure 4. 3-D Maps of FHV-Modified Mitochondria

Blue indicates outer mitochondrial membrane, white indicates FHV spherules, yellow indicates inner mitochondrial membrane.

(A) Merged image of a 3-D map of the outer membrane and spherules of the mitochondrion from Figure 3A and 3B and a slice of the tomogram showing the electron density map from which it was derived.

(B) A portion of the map in (A) showing a close-up view of the connections between the outer mitochondrial membrane and the spherules. The red arrow marks that same spherule as the one depicted by the red arrow in Figure 3A.

(C) A 90° rotation of (B) showing the channels that connect the spherule interiors to the cytoplasm. The outer membrane has been made translucent to show the spherules behind it. Again, the red arrow corresponds to the red arrows in Figures 3A and 4B.

(D) 3-D maps of the mitochondria shown in Figure 3C.

(E) A view of mitochondrion 2 from (D) that has been rotated and has had the outer membrane removed to show the range of spherule sizes.

doi:10.1371/journal.pbio.0050220.g004

of mitochondrion 2 in Figure 4D, with the outer membrane removed. The average spherule interior volume was $\sim 33,000 \text{ nm}^3$ (Figure 5C), and the average interior spherule membrane surface area was $\sim 6,000 \text{ nm}^2$ (Figure 5B).

Stoichiometry of FHV RNA Replication Components Reveals High Protein A Copy Number

Since both protein A (Figure 1) and nascent FHV RNA (Figure 2) localized predominantly or exclusively to spherules,

the relative numbers of protein A, RNA replication templates, and spherules could provide important insights into the structure and organization of FHV RNA replication complexes. Accordingly, we measured the number of molecules of protein A and FHV RNAs per cell in *Drosophila* S2 cells at 4, 8, 12, and 24 hpi with FHV. The numbers of positive- and negative-strand genomic RNAs per cell were measured by quantitative Northern blotting calibrated with known amounts of in vitro transcripts (Figure 6A and 6B). The number of

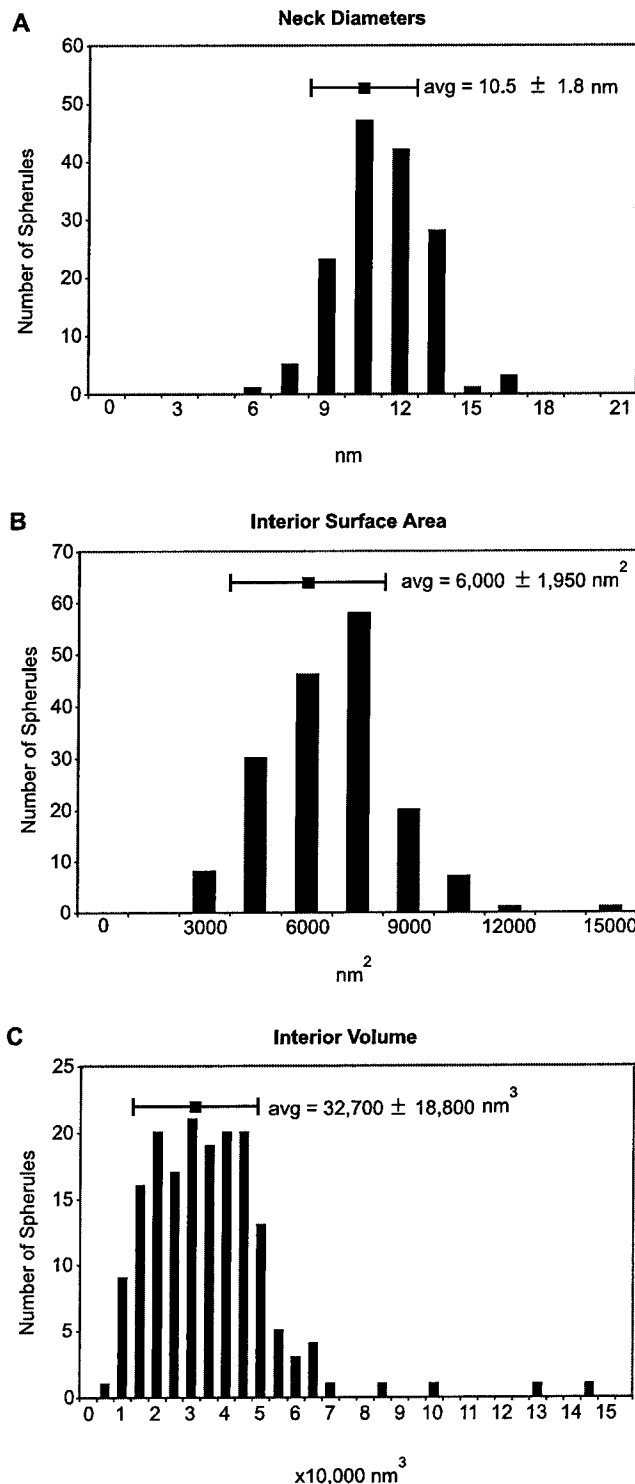


Figure 5. Spherule Dimensions

Distribution of spherule neck channel diameters (A), interior surface areas (B), and interior volumes (C). The data shown represents measurements of 150 (A) and 175 (B and C) individual spherules. doi:10.1371/journal.pbio.0050220.g005

protein A molecules per cell was measured by quantitative Western blotting calibrated with known amounts of co-electrophoresed, purified protein A standards (Figure 6E).

Starting before 4 hpi and continuing thereafter in FHV-

infected *Drosophila* cells, the primary mode of viral RNA synthesis is (+)RNA synthesis from negative-strand RNA [(-)RNA] templates (Figure 6A–6D). The number of (+)RNA1 and (+)RNA2 per cell increased from ~40,000 molecules of each RNA species at 4 hpi to ~2–3 million each by 24 hpi (Figure 6C). Such (+)RNA products primarily accumulate in the cytoplasm for translation and encapsidation, and only a minor fraction of (+)RNAs fractionate with the membrane-associated RNA replication complex (P. Van Wynsberghe, P. Ahlquist, unpublished data).

By contrast to positive-strand export and accumulation in the cytoplasm, FHV (-)RNAs appear to function only as RNA replication intermediates and are completely membrane-associated (P. Van Wynsberghe, P. Ahlquist, unpublished data). (-)RNA thus is a key measure of a minimal RNA replication complex, because every mature RNA replication complex, active in (+)RNA synthesis, must contain at least one (-)RNA template. Therefore, the number of (-)RNAs gives an estimate of the maximal number of replication complexes per cell. (-)RNA1 accumulation plateaued by 8 hpi at ~16,000 copies per cell (Figure 6D). (-)RNA2 accumulation increased throughout the first 24 hpi, although more slowly after 12 hpi, reaching ~50,000 molecules per cell by 24 hpi (Figure 6D).

The number of protein A molecules plateaued by 8 hpi (Figure 6F), which is consistent with prior results that protein A synthesis occurs early in infection and then declines [47]. Intriguingly, the peak level of protein A was ~2 million molecules per cell (Figure 6F). Protein A was thus present at dramatically higher levels than (-) RNA templates were. The ratio of protein A to (-)RNAs was relatively consistent over all time points examined, with averages throughout infection of 118 ± 23 and 64 ± 20 protein A copies per (-)RNA1 and (-)RNA2, respectively (Figure 6G).

To understand the organization of the replication complex in relation to the spherules better, we compared the number of spherules per cell with the number of protein A and (-)RNA molecules per cell. To measure the number of spherules per cell, we collected FHV-infected *Drosophila* S2 cells at 12 hpi, processed them for transmission EM, and imaged 25 randomly sectioned cell profiles. All spherules in each imaged cell section were counted and divided by the cell section volume, which was calculated by measuring the cell area using ImageJ (National Institutes of Health) and multiplying by the effective section thickness (see Materials and Methods). The number of spherules per cell was calculated by multiplying the resulting density of spherules by the average volume of the almost perfectly round, 10 μm -diameter *Drosophila* S2 cells [56] (and our independent, matching measurements).

These calculations revealed the average number of spherules per cell at 12 hpi to be $\sim 20,000 \pm 11,000$ (Table 1). The ratio of protein A per cell to spherules per cell revealed that on average, there are ~100 copies of protein A per spherule (Table 1). Further comparison to the Figure 6 data shows that, on average there are ~1 (-)RNA1 and ~2 (-)RNA2 molecules per spherule (Table 1). The implications of these results for the organization of replication complexes are considered further in the Discussion.

Discussion

To advance understanding of the crucial relationship between (+)RNA viruses and the intracellular membranes

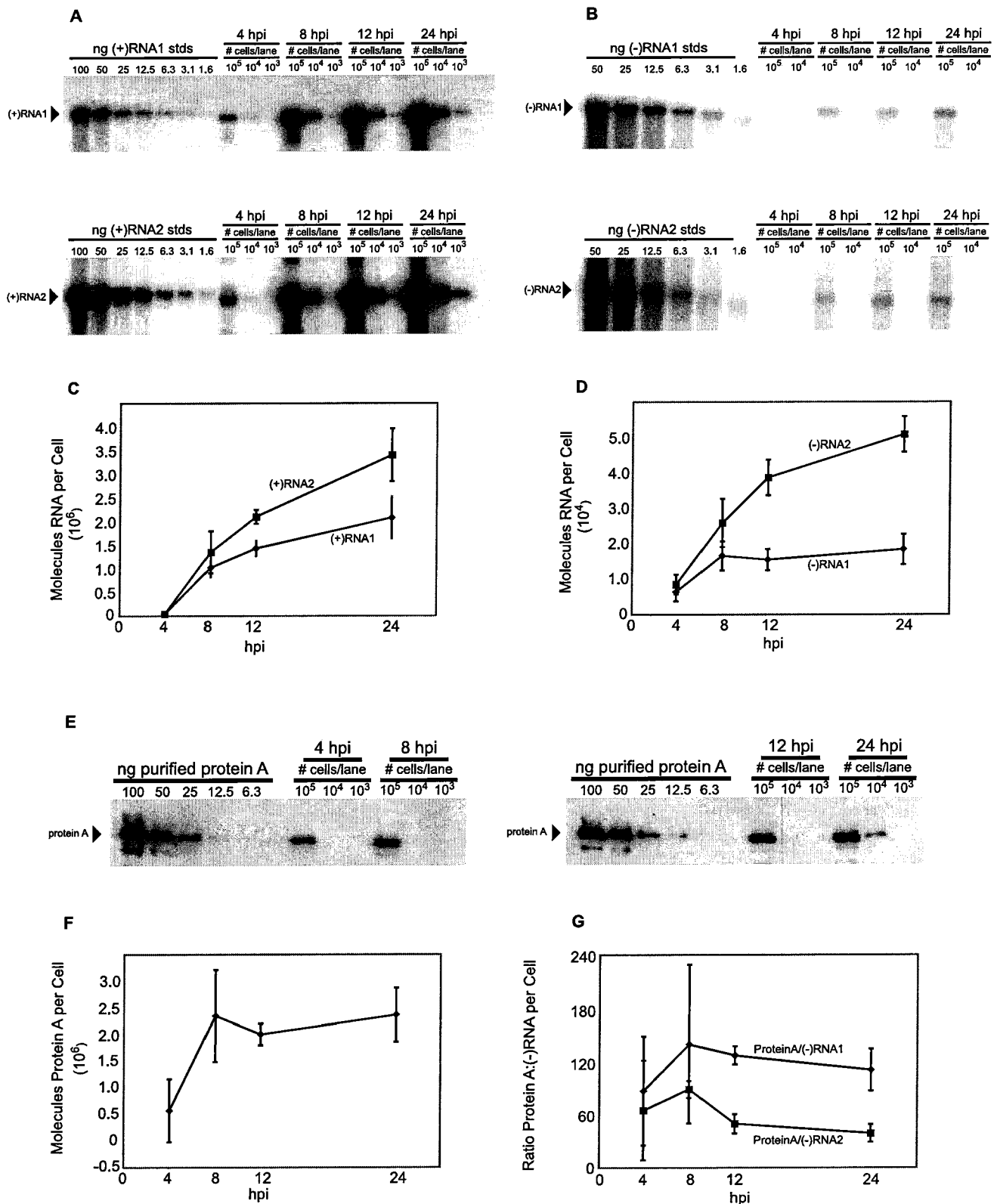


Figure 6. Measurements of the number of molecules of FHV (+)RNAs and (-)RNAs and protein A per cell in FHV-infected *Drosophila* cells

(A and B) Cells were harvested and counted at the time points indicated above the figure, and total RNA was extracted. An amount of RNA corresponding to 1.0×10^5 , 1.0×10^4 , or 1.0×10^3 cell equivalents was loaded as indicated above each lane and subjected to Northern blot hybridization with radio-labeled probes specific for the detection of (+)RNA1 (top panel of A), (-)RNA1 (top panel of B), (+)RNA2 (bottom panel of A), or (-)RNA2 (bottom panel of B). Specific signals are indicated by the arrowheads.

(C) Graph of the number of molecules of (+)RNA1 (diamond) and (+)RNA2 (squares) per cell over a 24-h time course.

(D) Graph of the number of molecules of (-)RNA1 and (-)RNA2 per cell over a 24-h time course.

(E) An aliquot of the same cells harvested for the RNA analysis at the indicated time points was lysed in Laemmli sample buffer and subjected to immunoblot analysis with polyclonal antisera for protein A. Protein A levels were measured by comparison with the signal intensities derived from known amounts of purified protein A.

(F) Graph of the number of molecules of protein A per cell over a 24-h time course.

(G) Graph of the ratios of protein A versus (–)RNA1 (diamonds) and (–)RNA2 during the course of infection. The 24 hpi data shown represent the mean and standard deviation for three independent experiments. The data shown for 4, 8, and 12 hpi represent the mean and standard deviation for two independent experiments.

doi:10.1371/journal.pbio.0050220.g006

on which they replicate their RNA genomes, we combined 3-D ultrastructural imaging with quantitative biochemical data and other results to model the architecture and organization of a nodavirus RNA replication complex. Immunogold labeling identified virus-induced membranous spherules as the sites of accumulation of the sole FHV RNA replication protein, protein A, and of FHV RNA synthesis (Figures 1 and 2). EMT revealed that all FHV spherules maintain an open connection with the cytoplasm with a diameter of ~10 nm, which is wide enough to allow the exchange of ribonucleotides and RNA products (Figures 4C and 5A). Our stoichiometry measurements further revealed the presence of, on average, 100 copies of the viral replicase protein A and 2–4 RNA replication intermediates per spherule (Table 1). As discussed further below, these findings have substantial implications for the structure, assembly, and function of the FHV RNA replication complex and likely also for the organization of many similar membrane-associated viral RNA replication complexes. In addition to advancing understanding of viral replication mechanisms, such insights also should prove valuable for developing additional antiviral strategies or agents.

Organization of the FHV RNA Replication Complex

Protein A is a transmembrane protein in outer mitochondrial membranes [38] and is ~90% localized within spherules (Figure 1). Therefore, protein A must line the interior membrane surface of spherules. If protein A is similar to typical globular proteins, its volume would be ~183 nm³, based on the protein A molecular weight of 112 kDa [57] and the average partial specific volume of typical proteins [58]. If globular, protein A then would have a diameter of ~7 nm and cover a surface area of ~40 nm². Thus, the average spherule interior membrane surface area of 6,000 nm² (Figure 5B) provides enough space to accommodate at most ~150 protein A molecules, under a perfect close-packing arrangement. Therefore, the measured value of ~100 protein A molecules per spherule (Table 1) is near saturation for the spherule interior membrane surface area. We modeled 50 7-nm-diameter spheres representing protein A adjacent to the membrane surface within a tomographic model of half a

typical spherule (Figure 7) to demonstrate how protein A may pack into the spherules.

The resulting near-full occupancy of the interior membrane surface area by protein A (Figure 7) and the nature of protein A as a transmembrane protein whose self-interaction is required for RNA replication [38,52] imply that the ~100 copies of protein A form an inner network or shell within the spherule (Figure 7B). Such a shell would explain the formation and maintenance of the high-energy membrane deformation of spherules. A shell of these dimensions appears reasonable, given that the main shell of a reovirus core is 60 nm in diameter and is composed of 120 copies of a slightly larger protein λ 1 (142 kDa) [59]. The distribution of FHV spherule size spans a defined range of ~30–45-nm intra-membrane diameter, suggesting some flexibility in the assembly of the protein A shell. Other examples of high-density protein shells of flexible size and shape include the capsids of retroviruses, influenza, and retrotransposons [60–62]. For example, one species of Ty retrotransposon forms virus-like capsids that have a 30–50-nm range of diameters, similar to FHV spherules, and contain on average 300 copies of a 381-amino acid protein subunit [62], a protein content very close to the FHV spherule average of 100 copies of 998-amino acid protein A. Endocytic vesicles, secretory transport vesicles, and synaptic vesicles are further examples of protein-induced membrane vesicles that each have a range of variable sizes (50–100-nm diameter), despite being formed by regular arrays of uniform proteins [63,64].

Because ~90% of protein A, the FHV RNA polymerase (Figure 1), and ~70% of newly synthesized FHV RNA (Figure 2) are spherule-associated, and essentially all FHV (–)RNA templates are membrane associated (P. Van Wynsberghe, P. Ahlquist, unpublished data), it appears likely that (–)RNAs, and thus any double-stranded RNAs (dsRNAs) are within spherules. Sequestration of dsRNA within such a compartment may allow the virus to avoid, minimize, or delay dsRNA-induced host–cell defense responses such as protein kinase, RNA activated (PKR) and RNase L [65] or RNA interference (RNAi) [66]. Such dsRNA localization is consistent with earlier observations of virus-induced membrane spherules containing fibrils with salt-dependent nuclease sensitivity [25,67].

The ~100 protein A molecules per spherule (Table 1) would consume ~18,300 nm³ of interior volume, leaving ~14,000 nm³ within an average spherule to accommodate FHV RNA. Based on 0.655 nm³ per hydrated nucleotide for the crystal structure of duplex RNA [43,68,69], the volumes of FHV RNA1, RNA2, and RNA3 would be 2035, 917, and 254 nm³, respectively. Thus, in addition to ~100 protein A molecules, a spherule of average size has enough interior space to contain at most four single-stranded RNA (ssRNA) or two dsRNA copies of all three FHV RNA species. Given this maximal occupancy, the estimate from biochemical data of an average of one (–)RNA1 and two (–)RNA2 templates per

Table 1. Ratio of Spherules per Cell to Protein A and (–)RNA at 12 hpi

| Parameter | Ratio |
|--------------------|-----------------|
| spherules per cell | 20,000 ± 11,000 |
| protein A:spherule | 101 ± 51 |
| (–)RNA1:spherule | 0.9 ± 0.4 |
| (–)RNA2:spherule | 2.2 ± 1.0 |

doi:10.1371/journal.pbio.0050220.t001

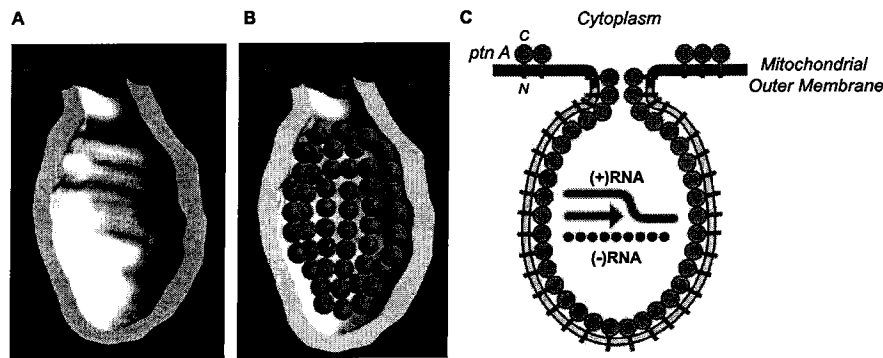


Figure 7. Modeling of FHV Transmembrane Protein A into a Spherule

(A) 3-D map of a single spherule where half of the membrane has been removed to show the interior. As in Figure 4, the spherule membrane is white and the contiguous outer mitochondrial membrane is blue.

(B) Schematic of likely protein A organization within a spherule. Based on the average density of globular proteins, FHV protein A (112 kDa) is modeled in as a green sphere of ~7 nm in diameter. Based on the average of ~100 protein A molecules per spherule (Table 1), the figure shows the potential packing arrangement of 50 protein A molecules in half a spherule. The spheres are shown lining the interior surface area of the spherule membrane because protein A is a transmembrane protein [38].

(C) Schematic representation of the structure and organization of the FHV RNA replication complex. Protein A (*ptn A*; green spheres) forms a shell within the mitochondrial membrane spherule within which RNA synthesis occurs (*N* = N terminus; *C* = C terminus). Protein A is also shown as possibly extending into the spherule neck, since it may be a determinant of the relatively constant 10-nm diameter neck. As noted in Figure 1 (white arrowheads), a small fraction of protein A may reside on the outer mitochondrial membrane external to spherules. The diagram shows (+)RNA synthesis (red arrow) from (-)RNA templates (black segmented line), which is the predominant form of FHV RNA synthesis throughout all but the earliest phases of FHV infection (Figure 6A–6D).

doi:10.1371/journal.pbio.0050220.g007

spherule (Table 1), together with at least one nascent (+)RNA progeny strand for each, appears fully reasonable.

Currently, it is not known if FHV RNA1 and RNA2 are replicated in separate or common spherules. If RNA1 and RNA2 were in separate spherules (i.e., 50% of spherules containing RNA1 and 50% containing RNA2), then the ratios of (-)RNA1 and (-)RNA2 to total spherules (Table 1) imply each RNA1-containing spherule would have two replication intermediates, and each RNA2-containing spherule would have approximately four replication intermediates. Because RNA1 (3.1 kb) is twice as long as RNA2 (1.4 kb), the total RNA content in both cases then would be nearly equal. If RNA1 and RNA2 were together in the same spherule, then each spherule would hold on average three replication intermediates (one RNA1 and two RNA2). The possibility of spherules containing both species of RNAs is intriguing, considering the interactions of FHV RNAs required for replication: FHV subgenomic RNA3, which is templated from RNA1, transactivates RNA2 replication and, in turn, RNA3 replication is suppressed by the resulting progeny RNA2 [70]. RNA3, and not its protein product, is responsible for transactivating RNA2 [70]. However, it is also possible that RNA3 is produced in one spherule during RNA1 replication and then exported to the cytoplasm prior to transactivating RNA2.

Parallels with Other Viral RNA Replication Complexes

Membrane spherules similar to those of FHV are induced by many other (+)RNA viruses including alphaviruses [5], other members of the alphavirus-like superfamily [15], rubiviruses [7,20], flaviviruses [21], tombusviruses [22], and others [4,23–25]. Among these, one of the best-studied with regard to the localization and stoichiometry of RNA replication complex components is BMV. BMV and FHV differ in many important respects including that BMV encodes a much larger complement of RNA replication proteins [15,19]. Nevertheless, although the understanding

that we present here for FHV RNA replication complexes is more advanced in many ways, the known characteristics of BMV RNA replication complexes are strikingly similar to those for FHV. Both BMV and FHV induce spherules of similar dimensions where viral RNA synthesis and viral replication proteins are localized [15]. BMV replication protein 1a, which is sufficient to induce spherules [15], is also a strongly membrane-associated [71], self-interacting [72,73] protein that is present at high copy number per spherule [15]. Similarly, whereas the ultrastructural organization of hepatitis C virus RNA replication complexes has not been defined, recent results suggest that these may also involve a dramatic excess of nonstructural protein copies per (-)RNA [74].

In addition to the many (+)RNA viruses whose RNA replication is associated with spherules, other (+)RNA viruses induce various, apparently distinct membrane rearrangements [4,17,21,26,27,75,76]. Although some or most of this variability reflects real ultrastructural differences, at least some of the perceived differences may be due to differences in perspective under conventional 2-D imaging. Our tomography results demonstrated that equivalent FHV spherules appeared to vary in morphology and topological relation to adjacent membranes when viewed in two dimensions from different perspectives (Figures 3C and 3D). A greater understanding of the 3-D nature of membrane rearrangements associated with RNA replication by other (+)RNA viruses may reveal shared features or common underlying principles.

Based on results with BMV, Schwartz et al. identified potential parallels between the assembly, structure, and function of membrane-associated RNA replication complexes and the cores of reverse-transcribing and dsRNA virus virions, including the sequestration of genomic RNA templates within a virus-induced compartment for replication [15,19]. The results presented here for FHV validate and extend these parallels by showing that all FHV spherules are

membrane invaginations topologically equivalent to a budding, enveloped virion (Figure 4), and that self-interacting, transmembrane protein A is present at levels sufficient to coat the inner spherule membrane in a multi-subunit shell similar to the capsids of retrovirus and dsRNA virus cores (Figure 7). As with dsRNA viruses, hepadnaviruses, and retroviruses, the high copy of protein A per spherule suggests that there may be threshold effects in replication protein expression to initiate replication. Further analysis of the structure, interactions, and function of FHV RNA replication complexes should provide additional insights into the basic mechanisms of (+)RNA virus replication and potentially identify new approaches for antiviral interference.

Materials and Methods

Cells and infection protocol. *Drosophila* S2 cells were grown at 28 °C in Gibco *Drosophila* serum-free media (SFM). Cells were dislodged by gentle scraping, pelleted, and resuspended at 10^7 cells/ml. FHV was added at a multiplicity of infection of 10 for all experiments. The cells and virus were incubated at 26 °C on a rotary shaker at 1,000 revolutions per minute (rpm) for 1 h to let the virus attach. After the hour incubation, the cells were plated onto a tissue culture dish and further incubated at 28 °C.

Mitochondria isolation. Mitochondria were isolated from *Drosophila* cells as described by Echaliar [77]. Briefly, cells were recovered by scraping and centrifugation and resuspended in a hypotonic buffer that contained 20 mM *N*-2-hydroxyethylpiperazine-*N'*-2-ethanesulfonic acid (HEPES; pH 7.4), 1 mM EGTA, and a protease inhibitor cocktail (1 mM phenylmethanesulfonylfluoride, 5 µg/ml pepstatin A, 1 µg/ml chymostatin, 10 mM benzamidin, 10 µg/ml leupeptin, and 0.5 µg/ml bestatin). After a 10 min incubation at room temperature, an equal volume of double isotonic buffer was added that consisted of the hypotonic buffer plus 0.5 M mannitol. The cells were lysed for 7 min using a pre-chilled Potter-Elvehjem homogenizer fitted with a Teflon pestle (Kimble-Kontes; www.kimble-kontes.com) and attached to a stirrer motor spinning at 250 rpm. The lysate was transferred to a Dounce homogenizer fitted with a type B glass pestle (Kimble-Kontes) and disrupted manually for 100 strokes on ice. Unbroken cells and nuclei were removed by two 10 min centrifugation steps at 500g at 4 °C. Mitochondria were pelleted by centrifugation at 3700g for 10 min at 4 °C, resuspended in an isotonic buffer containing 0.25 M mannitol, and washed by a second centrifugation at 7000g. BrUTP incorporation on the isolated mitochondria was performed at 28 °C for 1 h as described previously [15].

BrUTP transfection. *Drosophila* cells were infected with FHV as above. At 8 hpi, cells were treated with 20 µg/ml actinomycin D for 30 min. FuGENE 6 (Roche; http://www.roche.com) was diluted 10-fold in phosphate buffered saline pH 7.4 and mixed with BrUTP and actinomycin D to final concentrations of 10 mM and 20 µg/ml, respectively. The FuGENE/BrUTP/actinomycin D mix was incubated for 15 min at room temperature then added to the cells and incubated at 4 °C for 15 min. After the 4 °C incubation, the cells were moved to 28 °C for a 15-min labeling period and then immediately fixed and processed for EM.

Monoclonal antibody. Mouse monoclonal antibodies against FHV protein A have been described previously [9]. MAb clone 2–1.1.2.4.8, which recognizes the protein A epitope between amino acids 230 and 399, was used for immunogold EM labeling.

Immunogold EM labeling. BrUTP immunolabeling fixation was performed as described previously [15], except that samples were embedded in LR Gold resin. Samples were sectioned and placed on nickel grids. Sections were blocked with a goat-blocking solution (Aurion; http://www.aurion.nl), and incubated for 1 h with an anti-BrUTP antibody (PRB-1; Molecular Probes; http://probes.invitrogen.com), diluted 1:100 in an incubation solution containing 100 mM phosphate-buffered saline pH 7.4 and 0.1% BSA-c (Aurion). Grids were washed six times in incubation solution without antibody, then incubated for 2 h with a goat-anti-mouse antibody conjugated to an ultrasmall gold particle (Aurion) that was diluted 1:100 in incubation solution, and washed six times again with incubation solution. Silver enhancement was performed for 30 min using R-GENT SE-EM (Aurion). Protein A immunogold EM was performed in the same manner using the mouse monoclonal antibody at a dilution of 1:100. Background labeling was determined using uninfected control cells.

Labeling density was determined by calculating the surface area of spherules, mitochondria, and cytoplasm using the point-hit method [78]. Specific labeling was determined by subtracting the background labeling density.

Northern blot analysis and quantitation of FHV RNA. Northern blotting was done as described previously [8]. The number of molecules of FHV RNAs was determined by comparison with a serial dilution of a known amount of in vitro transcripts representing a known amount of (+)RNA or (–)RNA molecules. RNA levels were quantitated with ImageQuant software (Molecular Dynamics; http://www.mdyn.com/).

Western blot analysis and quantitation of FHV protein A. Western blotting was done as described previously [8]. The number of molecules of protein A was determined by comparison with a purified protein A standard. To generate the standard for quantitation, protein A was expressed in *Escherichia coli* as described previously [8]. To purify protein A, the hydrophobic transmembrane domain of protein A was deleted (amino acids 8–89), replaced with a C-terminal His₆ tag, and purified by talon column (Clontech; http://www.clontech.com) affinity chromatography. To further purify protein A, we performed preparative electrophoresis using a BioRad mini-prep cell. A 6%, 9.5-cm gel was run at 200 V for 9 h with an elution speed of 150 µl/min. Fractions containing the purified, truncated protein A standard were collected and quantitated based on comparison with known standards of bovine serum albumin and β-galactosidase. We quantitated protein levels with Lumi-imager software (Roche).

EM. For conventional transmission EM, cells were fixed and embedded as previously described [8]. For electron tomography, cells were fixed in 2% paraformaldehyde and 2.5% glutaraldehyde in 0.1 M sodium cacodylate, pH 7.4, post-fixed in 1% osmium tetroxide with 0.8% potassium ferrocyanide in sodium cacodylate buffer, stained with 2% uranyl acetate, dehydrated in a graded series of ethanol, and embedded in Durcupan ACM resin.

To calculate the total number of FHV-induced mitochondrial spherules per cell, FHV-infected *Drosophila* S2 cells were collected at 12 hpi, processed for transmission EM, and sectioned into 70-nm-thick slices. For each of 25 randomly selected cells imaged in these sections, we then counted all observable spherules with diameters larger than 20 nm. The number of spherules counted for each cell then was divided by the relevant section volume, which was calculated by measuring the cell area using ImageJ (National Institutes of Health) and multiplying by the effective section thickness. The effective section thickness is a correction used to avoid overcounting spherules with centers outside of the 70-nm physical section, which would otherwise be counted twice if adjacent sections were analyzed. As previously used to calculate synaptic vesicles per cell [79], this effective section thickness is the thickness that would encompass the centers of all counted spherules. In this case, the effective section thickness was 116 nm, based on adding 23 nm (the distance from the spherule center to a radius-perpendicular plane bisecting the spherule to yield a 20-nm-diameter section) to each face of the 70-nm section. The number of spherules per cell was calculated by multiplying the resulting density of spherules by the average volume of the almost perfectly round, 10 µm-diameter *Drosophila* S2 cells [56] (and our independent, matching measurements).

EMT. Three separate FHV infections produced samples for six independent tomograms. To survey the preservation quality and FHV-infection efficiency of the *Drosophila* cells, thin-sectioned material (~80 nm thick) was examined using a JEOL 1200FX electron microscope. 3-D reconstructions of portions of the cell containing FHV-infected mitochondria were generated using current techniques of electron tomography [80]. Sections were cut with a thickness of ~250 nm from blocks exhibiting well-preserved ultrastructure. These sections were stained for 30 min in 2% aqueous uranyl acetate, followed by 30 min in lead salts. Fiducial cues consisting of 20-nm colloidal gold particles were deposited on both sides of the section. For each reconstruction, a series of images was collected with a JEOL 4000EX intermediate-voltage electron microscope operated at 400 kV. The specimens were irradiated before initiating a tilt series in order to limit anisotropic specimen thinning during image collection. Pre-irradiation in this manner subjected the specimen to the steepest portion of the nonlinear shrinkage profile before images were collected. Six tilt series were collected: five single-tilt and one double-tilt. “FHV2” was the highest resolution single-tilt reconstruction and “FHV6” was the high-resolution double-tilt reconstruction; the majority of the analyses were conducted on these two reconstructions. The single-tilt series were recorded at 40,000 magnification with an angular increment of 2° from –60° to +60° about an axis perpendicular to the optical axis of the microscope using a

computer-controlled goniometer to increment accurately the angular steps. These single-axis tilt series were collected using a CCD camera with pixel dimensions $1,960 \times 2,560$. The pixel resolution was 0.55 nm. The illumination was held to near parallel beam conditions and optical density maintained constant by varying the exposure time. The IMOD package was used for generating the reconstructions [81].

Double-tilt tomography was performed by first collecting two tilt series of the same cellular region around orthogonal axes. After the first tilt series was complete using an angular increment of 2° from -66° to $+66^\circ$, the specimen grid was rotated 90° , and the second tilt series was acquired from -60° to $+66^\circ$. The IMOD software suite was used for fiducial mark tracking and alignment. The positions of 30 gold particles were tracked in both tilt series. After alignment, the tomographic reconstruction was generated by a projective algorithm [82].

Volume segmentation was performed by manual tracing in the planes of highest resolution with the program Xvotrace [83]. The mitochondrial reconstructions were visualized using Analyze (Mayo Foundation, Rochester, MN, United States), ImageJ (National Institutes of Health), or the surface-rendering graphics of Synu (National Center for Microscopy and Imaging Research, San Diego, CA, United States) as described by Perkins et al. 2001 [84]. These programs allow one to step through slices of the reconstruction in any orientation and to track or model features of interest in three dimensions. Measurements of structural features were made from planes within the reconstructed volume with the program ImageJ (National Institutes of Health) or within segmented volumes by the programs Synuarea and Synuvolume (National Center for Microscopy and Imaging Research). Some 3-D maps, images, and videos were created using the software Amira (Mercury TGS; <http://www.tgs.com>).

Supporting Information

Video S1. Animation through a z-Series of Slices of a Double-Tilt Tomogram Showing FHV-Induced Spherule Rearrangements of a Mitochondrion

Found at doi:10.1371/journal.pbio.0050220.sv001 (8.1 MB MOV).

Video S2. Z-Series Animation Illustrating the Varied Appearance of Spherule Clusters when Sectioned Parallel and Perpendicular to the Axes through Spherule Necks

Note how the morphology of the mitochondrion near the center changes during the progression through the z-series.

Found at doi:10.1371/journal.pbio.0050220.sv002 (1.3 MB MOV).

Video S3. Relationship of a 3-D Map of FHV-Induced Spherule Rearrangements of a Mitochondrion and the Electron Density from which the Map was Derived

Blue indicates outer mitochondrial membrane, white indicates FHV spherules, yellow indicates inner mitochondrial membrane. The red arrow points along the y-axis and the green arrow points along the x-axis of the tomogram. The boundary of the total tomographic volume is outlined by the orange bounding box.

Found at doi:10.1371/journal.pbio.0050220.sv003 (5.8 MB MOV).

Video S4. A 90° Rotation of Figure 4B to Figure 4C

Found at doi:10.1371/journal.pbio.0050220.sv004 (1.0 MB MOV).

Acknowledgments

We thank Randall Massey and Benjamin August of the University of Wisconsin Medical School Electron Microscopy Facility for assistance with electron microscopy; Priscilla Van Wynsberghe and Billy Dye for helpful discussions; Dan Lautenschlager, Steve Lamont, and Jean Yves-Sgro for computer assistance; and Johan den Boon for critical reading of the manuscript.

Author contributions. All authors conceived and designed the experiments and analyzed the data. BGK, GP, and DJM performed the experiments. BGK and PA wrote the paper.

Funding. This work was supported by NIH grants GM35072 to PA and P41 RR04050 to MHE. PA is an Investigator of the Howard Hughes Medical Institute.

Competing interests. The authors have declared that no competing interests exist.

References

- van Regenmortel MHV, editor (2000) Virus taxonomy. San Diego: Academic Press. 1162 p.
- Carette JE, van Lent J, MacFarlane SA, Wellink J, van Kammen A (2002) Cowpea mosaic virus 32- and 60-kilodalton replication proteins target and change the morphology of endoplasmic reticulum membranes. *J Virol* 76: 6293–6301.
- Egger D, Wolk B, Gosert R, Bianchi L, Blum HE, et al. (2002) Expression of hepatitis C virus proteins induces distinct membrane alterations including a candidate viral replication complex. *J Virol* 76: 5974–5984.
- Gosert R, Kanjanahualathai A, Egger D, Bienz K, Baker SC (2002) RNA replication of mouse hepatitis virus takes place at double-membrane vesicles. *J Virol* 76: 3697–3708.
- Kujala P, Ikaheimonen A, Ehsani N, Vihinen H, Auvinen P, et al. (2001) Biogenesis of the Semliki Forest virus RNA replication complex. *J Virol* 75: 3873–3884.
- Mackenzie JM, Jones MK, Westaway EG (1999) Markers for trans-Golgi membranes and the intermediate compartment localize to induced membranes with distinct replication functions in flavivirus-infected cells. *J Virol* 73: 9555–9567.
- Magliano D, Marshall JA, Bowden DS, Vardaxis N, Meanger J, et al. (1998) Rubella virus replication complexes are virus-modified lysosomes. *Virology* 240: 57–63.
- Miller DJ, Schwartz MD, Ahlquist P (2001) Flock house virus RNA replicates on outer mitochondrial membranes in *Drosophila* cells. *J Virol* 75: 11664–11676.
- Miller DJ, Schwartz MD, Dye BT, Ahlquist P (2003) Engineered retargeting of viral RNA replication complexes to an alternative intracellular membrane. *J Virol* 77: 12193–12202.
- Reichel C, Beachy RN (1998) Tobacco mosaic virus infection induces severe morphological changes of the endoplasmic reticulum. *Proc Natl Acad Sci U S A* 95: 11169–11174.
- Restrepo-Hartwig M, Ahlquist P (1996) Brome mosaic virus helicase- and polymerase-like proteins colocalize on the endoplasmic reticulum at sites of viral RNA synthesis. *J Virol* 70: 8908–8916.
- Ritzenthaler C, Laporte C, Gaire F, Dunoyer P, Schmitt C, et al. (2002) Grapevine fanleaf virus replication occurs on endoplasmic reticulum-derived membranes. *J Virol* 76: 8808–8819.
- Rubino L, Di Franco A, Russo M (2000) Expression of a plant virus non-structural protein in *Saccharomyces cerevisiae* causes membrane proliferation and altered mitochondrial morphology. *J Gen Virol* 81: 279–286.
- Schwartz M, Chen J, Lee WM, Janda M, Ahlquist P (2004) Alternate, virus-induced membrane rearrangements support positive-strand RNA virus genome replication. *Proc Natl Acad Sci U S A* 101: 11263–11268.
- Schwartz M, Chen J, Janda M, Sullivan M, den Boon J, et al. (2002) A positive-strand RNA virus replication complex parallels form and function of retrovirus capsids. *Mol Cell* 9: 505–514.
- Snijder EJ, van Tol H, Roos N, Pedersen KW (2001) Non-structural proteins 2 and 3 interact to modify host cell membranes during the formation of the arterivirus replication complex. *J Gen Virol* 82: 985–994.
- Suhly DA, Giddings TH Jr., Kirkegaard K (2000) Remodeling the endoplasmic reticulum by poliovirus infection and by individual viral proteins: An autophagy-like origin for virus-induced vesicles. *J Virol* 74: 8953–8965.
- Cho MW, Teterina N, Egger D, Bienz K, Ehrenfeld E (1994) Membrane rearrangement and vesicle induction by recombinant poliovirus 2C and 2BC in human cells. *Virology* 202: 129–145.
- Ahlquist P (2006) Parallels among positive-strand RNA viruses, reverse-transcribing viruses and double-stranded RNA viruses. *Nat Rev Microbiol* 4: 371–382.
- Lee J-Y, Marshall JA, Bowden DS (1994) Characterization of rubella virus replication complexes using antibodies to double-stranded RNA. *Virology* 200: 307–312.
- Westaway E, Mackenzie J, Kenney M, Jones M, Khromykh A (1997) Ultrastructure of Kunjin virus-infected cells: colocalization of NS1 and NS3 with double-stranded RNA, and of NS2B with NS3, in virus-induced membrane structures. *J Virol* 71: 6650–6661.
- Russo M, Di Franco A, Martelli GP (1987) Cytopathology in the identification and classification of tombusviruses. *Intervirology* 2: 134–143.
- Prod'homme D, Le Panse S, Druegon G, Jupin I (2001) Detection and subcellular localization of the turnip yellow mosaic virus 66K replication protein in infected cells. *Virology* 281: 88–101.
- Kim KS (1977) An ultrastructural study of inclusions and disease in plant cells infected by cowpea chlorotic mottle virus. *J Gen Virol* 35: 535–543.
- Hatta T, Francki RIB (1981) Cytopathic structures associated with tomatoplasts of plant cells infected with cucumber mosaic and tomato aspermy viruses. *J Gen Virol* 53: 343–346.
- Pedersen KW, van der Meer Y, Roos N, Snijder EJ (1999) Open reading frame 1-a-encoded subunits of the arterivirus replicase induce endoplasmic reticulum-derived double-membrane vesicles which carry the viral replication complex. *J Virol* 73: 2016–2026.
- Gosert R, Egger D, Lohmann V, Bartenschlager R, Blum HE, et al. (2003)

- Identification of the hepatitis C virus RNA replication complex in Huh-7 cells harboring subgenomic replicons. *J Virol* 77: 5487–5492.
28. Froshauer S, Kartenbeck J, Helenius A (1988) Alphavirus RNA replicase is located on the cytoplasmic surface of endosomes and lysosomes. *J Cell Biol* 107: 2075–2086.
 29. Kujala P, Ahola T, Ehsani N, Auvinen P, Vihinen H, et al. (1999) Intracellular distribution of rubella virus nonstructural protein P150. *J Virol* 73: 7805–7811.
 30. Frank J, editor (1992) Electron tomography. New York: Plenum Press. 399 p.
 31. Soto GE, Young SJ, Martone ME, Deerinck TJ, Lamont S, et al. (1994) Serial section electron tomography: A method for three-dimensional reconstruction of large structures. *Neuroimage* 1: 230–243.
 32. Ladinsky MS, Mastrorade DN, McIntosh JR, Howell KE, Stachelin LA (1999) Golgi structure in three dimensions: Functional insights from the normal rat kidney cell. *J Cell Biol* 144: 1135–1149.
 33. Mogelsvang S, Gomez-Ospina N, Soderholm J, Glick BS, Stachelin LA (2003) Tomographic evidence for continuous turnover of Golgi cisternae in *Pichia pastoris*. *Mol Biol Cell* 14: 2277–2291.
 34. Mironov AA, Mironov AA Jr., Beznoussenko GV, Trucco A, Lupetti P, et al. (2003) ER-to-Golgi carriers arise through direct en bloc protrusion and multistage maturation of specialized ER exit domains. *Dev Cell* 5: 583–594.
 35. Frey TG, Mannella CA (2000) The internal structure of mitochondria. *Trends Biochem Sci* 25: 319–324.
 36. Perkins G, Renken C, Martone ME, Young SJ, Ellisman M, et al. (1997) Electron tomography of neuronal mitochondria: three-dimensional structure and organization of cristae and membrane contacts. *J Struct Biol* 119: 260–272.
 37. Frey TG, Perkins GA, Ellisman MH (2006) Electron tomography of membrane-bound cellular organelles. *Annu Rev Biophys Biomol Struct* 35: 199–224.
 38. Miller DJ, Ahlquist P (2002) Flock house virus RNA polymerase is a transmembrane protein with amino-terminal sequences sufficient for mitochondrial localization and membrane insertion. *J Virol* 76: 9856–9867.
 39. Kampmuller KM, Miller DJ (2005) The cellular chaperone heat shock protein 90 facilitates Flock House virus RNA replication in *Drosophila* cells. *J Virol* 79: 6827–6837.
 40. Ball LA (1995) Requirements for the self-directed replication of flock house virus RNA 1 [published erratum appears in *J Virol* 69:2722]. *J Virol* 69: 720–727.
 41. Schneemann A, Reddy V, Johnson JE (1998) The structure and function of nodavirus particles: A paradigm for understanding chemical biology. *Adv Virus Res* 50: 381–446.
 42. Schneemann A, Zhong W, Gallagher TM, Rueckert RR (1992) Maturation cleavage required for infectivity of a nodavirus. *J Virol* 66: 6728–6734.
 43. Tihova M, Dryden KA, Le TV, Harvey SC, Johnson JE, et al. (2004) Nodavirus coat protein imposes dodecahedral RNA structure independent of nucleotide sequence and length. *J Virol* 78: 2897–2905.
 44. Krishna NK, Marshall D, Schneemann A (2003) Analysis of RNA packaging in wild-type and mosaic protein capsids of flock house virus using recombinant baculovirus vectors. *Virology* 305: 10–24.
 45. Zhong W, Dasgupta R, Rueckert R (1992) Evidence that the packaging signal for nodaviral RNA2 is a bulged stem-loop. *Proc Natl Acad Sci U S A* 89: 11146–11150.
 46. Venter PA, Krishna NK, Schneemann A (2005) Capsid protein synthesis from replicating RNA directs specific packaging of the genome of a multipartite, positive-strand RNA virus. *J Virol* 79: 6239–6248.
 47. Friesen P, Rueckert RR (1981) Synthesis of black beetle virus proteins in cultured *Drosophila* cells—differential expression of RNAs 1 and 2. *J Virol* 37: 876–886.
 48. Friesen PD, Rueckert RR (1982) Black beetle virus: Messenger for protein B is a subgenomic viral RNA. *J Virol* 42: 986–995.
 49. Li H, Li WX, Ding SW (2002) Induction and suppression of RNA silencing by an animal virus. *Science* 296: 1319–1321.
 50. Johnson KL, Ball LA (1997) Replication of flock house virus RNAs from primary transcripts made in cells by RNA polymerase II. *J Virol* 71: 3323–3327.
 51. Price BD, Roeder M, Ahlquist P (2000) DNA-directed expression of functional flock house virus RNA1 derivatives in *Saccharomyces cerevisiae*, heterologous gene expression, and selective effects on subgenomic mRNA synthesis. *J Virol* 74: 11724–11733.
 52. Dye BT, Miller DJ, Ahlquist P (2005) In vivo self-interaction of nodavirus RNA replicase protein A revealed by fluorescence resonance energy transfer. *J Virol* 79: 8909–8919.
 53. Hayat MA, editor (1991) Colloidal gold: Principles, methods and applications. Vol. 3. San Diego: Academic Press. 421 p.
 54. Baumeister W (2005) From proteomic inventory to architecture. *FEBS Lett* 579: 933–937.
 55. Penczek P, Marko M, Buttle K, Frank J (1995) Double-tilt electron tomography. *Ultramicroscopy* 60: 393–410.
 56. Rogers SL, Wiedemann U, Stuurman N, Vale RD (2003) Molecular requirements for actin-based lamella formation in *Drosophila* S2 cells. *J Cell Biol* 162: 1079–1088.
 57. Ball LA, Johnson KL (1998) Nodaviruses of insects. In: Miller LK, Ball LA, editors. *The insect viruses*. New York: Plenum Publishing. pp. 225–267.
 58. Richards FM (1977) Areas, volumes, packing and protein structure. *Annu Rev Biophys Bioeng* 6: 151–176.
 59. Reinisch KM, Nibert ML, Harrison SC (2000) Structure of the reovirus core at 3.6 Å resolution. *Nature* 404: 960–967.
 60. Goff SP (2001) *Retroviridae*: The retroviruses and their replication. In: Knipe DM, Howley PM, editors. *Fields virology*. 4th ed. Philadelphia: Lippincott Williams & Wilkins. pp. 1871–1939.
 61. Lamb RA, Krug RM (2001) *Orthomyxoviridae*: The viruses and their replication. In: Knipe DM, Howley PM, editors. *Fields virology*. 4th ed. Philadelphia: Lippincott Williams & Wilkins. pp. 1487–1579.
 62. Burns NR, Saibil HR, White NS, Pardon JF, Timmins PA, et al. (1992) Symmetry, flexibility and permeability in the structure of yeast retrotransposon virus-like particles. *Embo J* 11: 1155–1164.
 63. Huttner WB, Zimmerberg J (2001) Implications of lipid microdomains for membrane curvature, budding and fission. *Curr Opin Cell Biol* 13: 478–484.
 64. McNiven MA, Thompson HM (2006) Vesicle formation at the plasma membrane and trans-Golgi network: The same but different. *Science* 313: 1591–1594.
 65. Biron CA, Sen GC (2001) Interferons and other cytokines. In: Knipe DM, Howley PM, editors. *Fields Virology*. 4th ed. Philadelphia: Lippincott Williams & Wilkins. pp. 321–351.
 66. Bass BL (2000) Double-stranded RNA as a template for gene silencing. *Cell* 101: 235–238.
 67. Di Franco AM, Russo M, Martelli GP (1984) Ultrastructure and origin of cytoplasmic multivesicular bodies induced by carnation Italian ringspot virus. *J Gen Virol* 65: 1233–1237.
 68. Johnson JE, Rueckert R. R. (1997) Packaging and release of the viral genome. In: W. Chiu RMB, Garcea RL, editors. *Structural biology of viruses*. New York: Oxford University Press. pp. 269–287.
 69. Dong XF, Natarajan P, Tihova M, Johnson JE, Schneemann A (1998) Particle polymorphism caused by deletion of a peptide molecular switch in a quasispherical icosahedral virus. *J Virol* 72: 6024–6033.
 70. Eckerle LD, Albarino CG, Ball LA (2003) Flock House virus subgenomic RNA3 is replicated and its replication correlates with transactivation of RNA2. *Virology* 317: 95–108.
 71. den Boon J, Chen J, Ahlquist P (2001) Identification of sequences in brome mosaic virus replicase protein 1a that mediate association with endoplasmic reticulum membranes. *J Virol* 75: 12370–12381.
 72. O'Reilly EK, Wang Z, French R, Kao CC (1998) Interactions between the structural domains of the RNA replication proteins of plant-infecting RNA viruses. *J Virol* 72: 7160–7169.
 73. O'Reilly EK, Paul JD, Kao CC (1997) Analysis of the interaction of viral RNA replication proteins by using the yeast two-hybrid assay. *J Virol* 71: 7526–7532.
 74. Quinkert D, Bartenschlager R, Lohmann V (2005) Quantitative analysis of the hepatitis C virus replication complex. *J Virol* 79: 13594–13605.
 75. Egger D, Teterina N, Ehrenfeld E, Bienz K (2000) Formation of the poliovirus replication complex requires coupled viral translation, vesicle production, and viral RNA synthesis. *J Virol* 74: 6570–6580.
 76. Egger D, Pasamontes L, Bolten R, Boyko V, Bienz K (1996) Reversible dissociation of the poliovirus replication complex: functions and interactions of its components in viral RNA synthesis. *J Virol* 70: 8675–8683.
 77. Echallier G (1997) *Drosophila* cells in culture. New York: Academic Press. 702 p.
 78. Hajibagheri MAN, editor (1999) Electron microscopy methods and protocols. Totowa (New Jersey): Humana Press. 283 p.
 79. Lenzi D, Runyon JW, Crum J, Ellisman MH, Roberts WM (1999) Synaptic vesicle populations in saccular hair cells reconstructed by electron tomography. *J Neurosci* 19: 119–132.
 80. Perkins GA, Ellisman MH, Fox DA (2003) Three-dimensional analysis of mouse rod and cone mitochondrial cristae architecture: bioenergetic and functional implications. *Mol Vis* 9: 60–73.
 81. Mastrorade DN (1997) Dual-axis tomography: An approach with alignment methods that preserve resolution. *J Struct Biol* 120: 343–352.
 82. Lawrence A, Bouwer JC, Perkins G, Ellisman MH (2006) Transform-based backprojection for volume reconstruction of large format electron microscope tilt series. *J Struct Biol* 154: 144–167.
 83. Perkins GA, Renken CW, Song JY, Frey TG, Young SJ, et al. (1997) Electron tomography of large, multicomponent biological structures. *J Struct Biol* 120: 219–227.
 84. Perkins GA, Renken CW, van der Klei IJ, Ellisman MH, Neupert W, et al. (2001) Electron tomography of mitochondria after the arrest of protein import associated with Tom19 depletion. *Eur J Cell Biol* 80: 139–150.

Modulation of Lipid Unsaturation and Membrane Fluid State in Mammalian Cells by Stable Transformation with the Δ^9 -Desaturase Gene of *Saccharomyces cerevisiae*

Zs. Györfy, I. Horváth, G. Balogh, Á. Domonkos, E. Duda,^{*1} B. Maresca,* and L. Vigh
*Institute of Biochemistry, BRC, Szeged, Hungary; and *IIGB, Naples, Italy*

Received July 21, 1997

The composition and physical state of membrane lipids determine the dynamic nature of membranes, which in turn, could directly be linked to the activity of various membrane-associated cellular functions. To better understand the molecular basis of different membrane-related phenomena we established a novel strategy to alter unsaturation of mammalian cell membranes with an identical genetic background. We transfected L929 mouse fibroblastoid cells with DNA constructs containing the Δ^9 -fatty acid desaturase gene (*Ole1*) of *S. cerevisiae* under the control of desaturase promoters derived either from wild type or mutant strains of the dimorphic fungus *H. capsulatum*.

© 1997 Academic Press

In animal and fungal cells unsaturated fatty acids (UFA) are formed via an aerobic process by a microsomal three-component enzyme system, that involve cytochrome b_5 , NADH-dependent cytochrome b_5 reductase and the Δ^9 -fatty acid desaturase (1,2,3). The Δ^9 -desaturase gene product is the major enzyme for converting saturated fatty acids (SFA) into UFA and is responsible for the introduction of the first double bond between carbon 9 and 10 of palmitoyl (16:0) or stearoyl (18:0) -CoA to form palmitoleic (16:1) or oleic (18:1) acids (4). Desaturases are responsible for the regulation of the appropriate level of unsaturation of the acyl chains of membrane lipids and are presumed to be the key enzymes in modulating membrane fluid state. Δ^9 -desaturase genes have been cloned from several organisms such as *S. cerevisiae* (4), *Tetrahymena thermophila* (5), *H. capsulatum* (6), mouse (7), rat (8) and man (9).

The physical properties of lipids are related in a near-

linear fashion with the number of unsaturation bonds of membrane lipids. There is strong evidence that insertion of the first double bond in the middle of a SFA has the greatest effect on membrane physical properties, while successive bonds have progressively smaller effects (10, 11). Indeed, introduction of a fourth or fifth bond to otherwise UFA has no measurable effect upon bulk membrane properties detected by differential scanning calorimetry or fluorescence polarization spectroscopy (12, 13). This supports the general conclusion that the type of UFA incorporated into membrane phospholipids is of secondary importance compared to the balance between saturated and unsaturated fatty acids.

We have recently characterized two Δ^9 -desaturase genes from a virulent and a non-virulent strain of *H. capsulatum* (6). The coding sequences of these genes, both containing an intron of 93 nucleotides are virtually identical and analogous to the Δ^9 -desaturase genes of *S. cerevisiae* and similar to other eukaryotic desaturase genes.

We have more recently identified a 240 nt region of the proximal region of the promoter involved in a phase-specific binding *in vitro* (14). By sequence analysis we have distinguished one regulatory-like element that coincides with an AP1 binding site (TGATAA) that is located at -740 nt of 5'-upstream from the ATG (14). We have also identified by dissecting the promoter the presence of 11 nt, also present in the promoter of *S. cerevisiae* but not in those of higher eukaryotes, that is responsible for transcriptional regulation *in vivo* (Gargano et al., manuscript in preparation). *Ole1* transcription of the virulent, thermotolerant (G217B) and non-virulent, thermosensitive (Downs) strains of *H. capsulatum* is similar in yeast phase cells and during the temperature downshift (from 34 °C, 37 °C or 40 °C to 25 °C, yeast-to-mycelia transition).

Nevertheless, Δ^9 -desaturase gene is transcriptionally inactive in mycelia of G217B at 25 °C while it is actively transcribed in the Downs strain at the same

¹ Corresponding author: Biological Research Center, Szeged, POB. 521, 6701 Hungary. Fax: +36 62 432 506. E-mail: duda@everx.szbk.u-szeged.hu.

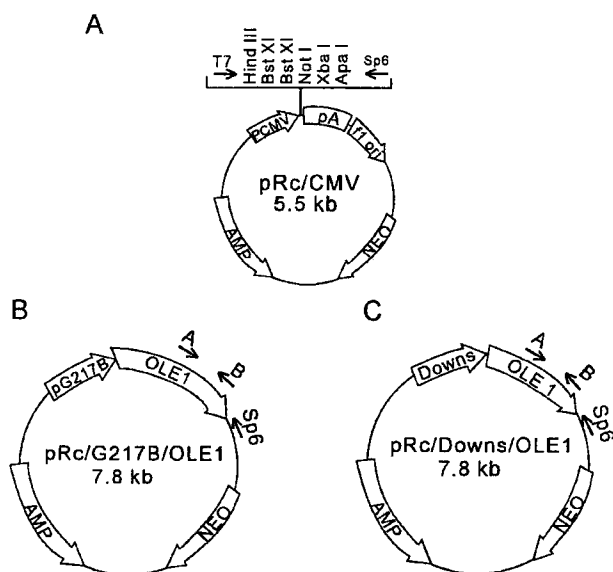


FIG. 1. Maps of transforming plasmids derived from the Invitrogen pRc/CMV mammalian expression vector. (A) The original pRc/CMV plasmid. (B) pRc/G217B/Ole1 plasmid, contains the promoter region of the desaturase gene of the wild type yeast *H. capsulatum* and the *S. cerevisiae* Δ^9 -desaturase gene. (C) pRc/Downs/Ole1 that contains the promoter region of the mutant *H. capsulatum* and the *S. cerevisiae* Δ^9 -desaturase gene.

temperature. These results were in agreement with the finding that membranes of the Downs strain have higher level of oleic acid.

We used wild type and mutant promoters of *H. capsulatum* Δ^9 -desaturase to control the expression of *S. cerevisiae* desaturase gene in mammalian expression vectors and transformed the L929 mammalian cell line to investigate in a heterologous system whether yeast promoters could control the expression of (a different yeast) desaturase gene in mammalian cells, modulate the lipid desaturation and alter the composition of membranes of mammalian cells.

MATERIALS AND METHODS

Cell culture. L929 mouse fibroblastoid cell line was cultured as monolayer in DMEM (Sigma Chemical Co., St. Louis, USA) medium supplemented with 10% fetal calf serum (Gibco BRL, Gaithersburg, USA) at 37°C in 5% CO₂ and 95% air. For fatty acid analysis and microviscosity measurements we used subconfluent cultures of cells.

Plasmids. Constructs were inserted in the mammalian expression vector pRc/CMV (Invitrogen BV, Leek, The Netherlands). We replaced the original cytomegalovirus promoter by HindIII-SalI digestion of the pRc vector with Δ^9 -desaturase promoters derived from *H. capsulatum* (14). 2.7 kb DNA fragments (for details see ref. 15) were cloned into the XbaI site of the pRc plasmid, containing either the wild type (G217B) or the mutant (Downs) *H. capsulatum* promoters and the *S. cerevisiae* desaturase (*Ole1*) gene (see Fig.1). The expression vectors were amplified in DH5 α *E. coli* cells.

Transformation and selection of mammalian cells. Transformations with the mammalian expression vectors were performed into L929 cell line using Lipofectamine (Gibco BRL, Gaithersburg, USA).

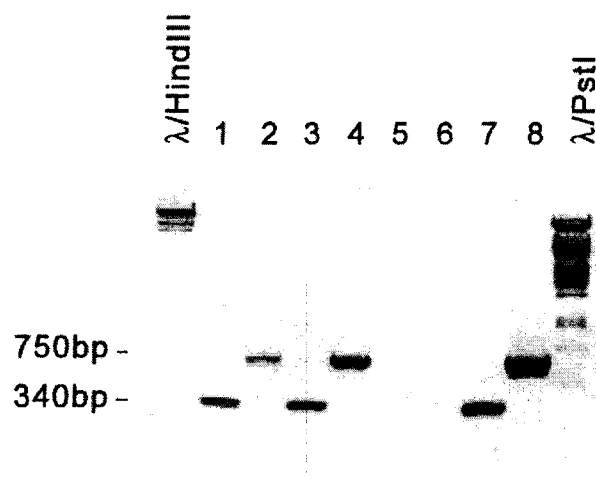


FIG. 2. Amplification of different fragments of the transforming vector from the transfected cell lines by polymerase chain reaction. With the A and B primers we amplified a fragment of the *Ole1* gene, 340 bp in length (lines 1, 3, 7). With the A and Sp6 primers we amplified an 800 bp fragment of the *Ole1* gene (lines 2, 4, 8). Lines 1,2: LG cell line; lines 3,4: LD cell line; lines 5,6: L929, lines 7,8: pRc/Downs/Ole1 transforming vector.

For each transformation 1-2 μ g DNA and 10⁵ cells were used. Transformant colonies were selected in the presence of 400 μ g/ml G418 (SKW, Budapest, Hungary) in the culture medium. 10-10 clones of stable transfectants were chosen for further characterization from each transformation. The code of L929 cell lines containing the pRc/G217B/Ole1 vector was LG, the ones with pRc/Downs/Ole1 are labeled with LD.

Amplification of genomic DNA by PCR. Cultured cells (5 \times 10⁶) were treated with trypsin and washed with PBS. Cells were lysed in a solution containing 4M guanidium-thiocyanate, 25 mM sodium-citrate (pH 7), 0.5 % N-lauroylsarcosine and 0.1 M mercapto-ethanol.

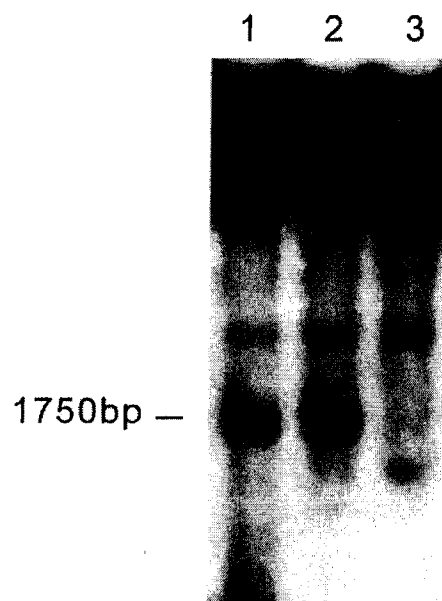


FIG. 3. Southern analysis of the control L929 cell line (line 3) and the transformed cell lines LD (line 2) and LG (line 1).

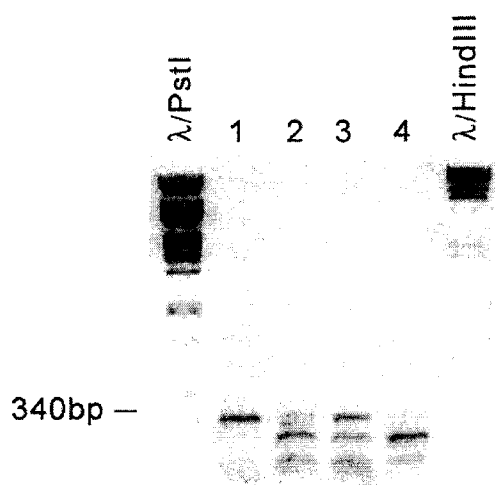


FIG. 4. Results of the RT-PCR reaction of *S. cerevisiae* (line 1), *LG* cells (line 2), *LD* cells (line 3) and the control L929 cells (line 4). We used the *B* reverse primer in the RT, and *A* and *B* primers in the PCR reactions.

The suspension was diluted with a buffer containing 0.5 M Tris-HCl (pH 7.0). Cell debris was collected with centrifugation for 2 minutes at 15 000 rpm, supernatant was extracted with phenol and chloroform and genomic DNA was precipitated overnight in ethanol. To amplify the target DNA we used *A* (5'TCT AGC ATA CGA CTT GAA GAA ATT 3') forward; *Sp6* and *B* (5'CCT TGA TAA CAG CCA CTC TCA 3') reverse primers. *A* and *B* primers were designed according to the *S. cerevisiae Ole1* coding sequence. We used a region of the yeast desaturase gene that has the lowest homology with the mouse desaturase gene. Sequences were obtained from GenBank (yeast *OLE1*: J05676; Mouse *SCD2*: M26270).

PCR was carried out in a volume of 25 μ l containing 100 ng genomic or plasmid DNA, 1 pmol/ μ l of each primer, 2.5 U Taq DNA Polymerase (Pharmacia Biotech, Uppsala, Sweden), 200 μ mol/l of each dNTP and 2.5 μ l reaction buffer. After denaturation for 5 min at 95°C, 30 cycles were carried out, each consisted of 1 min at 95°C, 1 min at 65°C and 2 min at 72°C. The last synthesis step was extended to 10

minutes. The amplified alleles were detected by running the DNA in 1% agarose, 1x TBE gel.

DNA probe. The probe used for the Southern analysis was an 800 bp *ApaI-EcoRI* fragment of the *S. cerevisiae* Δ^9 -desaturase gene derived from the cloning vector pRc/Downs/Ole1. The probe was labeled with [α - P^{32}] dCTP using the Pharmacia Oligolabelling Kit (Pharmacia Biotech, Uppsala, Sweden).

Southern analysis. 15 μ g DNA was digested with *EcoRI* and transferred onto Hybond N membranes (Amersham Intl. Little Chalfont, England). Prehybridization, hybridization and filter washing procedures were done as recommended by the manufacturer, at 65°C. The size of the restriction fragment that hybridized to the radioactive probe was determined by DNA molecular weight marker.

RT-PCR. Total RNA was prepared from yeast cultures according to Patriarca and Maresca (16). Mammalian cells (about 10^7) were washed with PBS and resuspended in 250 μ l TNE buffer containing 1 mM EDTA, 100 mM NaCl and 10 mM Tris-HCl (pH 8). 20 μ l solution of vanadyl nucleoside complex (Sigma, St. Louis, USA) and 24 μ l of Nonidet-P 40 were added to the solution. After centrifugation for 2 min, 250 μ l extraction buffer (200 mM Tris-HCl, pH 8, 0.35 M NaCl, 20 mM EDTA, 1% SDS) was added to the supernatant followed by extraction with phenol and chloroform and precipitation of RNA.

cDNA synthesis. 0.5 μ l M-MLV reverse transcriptase (Gibco BRL, Gaithersburg, USA), 10 mM DTT, 20 μ M dNTP mix (Pharmacia Biotech, Uppsala, Sweden), 1 pM *B* reverse primer and 5X 1st strand buffer were added to 200 ng DNase I (Gibco BRL, Gaithersburg, USA) treated RNA. Two μ l cDNA of each samples with *A* and *B* primers were amplified in polymerase chain reaction with an annealing temperature of 65°C.

Analysis of fatty acids. Lipids were extracted from washed cells by the method of Bligh and Dyer (17). Phospholipids were separated on precoated TLC plates (Merck 5721) developed with hexan/aether/glacial acetic acid (60:40:2). For the determination of the constituent fatty acids, aliquots of the total lipids or the phospholipids were subjected to methanolysis, the resultant methyl-esters were analyzed on Hewlett Packard gas chromatograph (HP 3396A) equipped with flame ionization detector on SP2230, 30cm long capillary column (Supelco). Quantitation was made by a Hewlett Packard (HP 3396A) integrator.

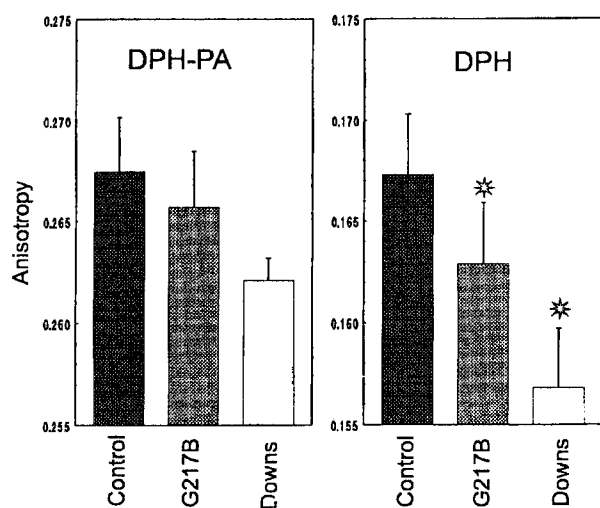
Microviscosity determination. Microviscosity of cell membranes were followed by measuring DPH (1,6-diphenyl-1,3,5-hexatriene)

TABLE 1

Total Lipid and Phospholipid Analysis of Fatty Acids in Transformed Cells in Comparison with the Control L929 Cells

| A. Fatty acid composition of total lipids | | | | | | | | | |
|--|------|------|------|------|------|------|-------|-------|-------|
| | 16:0 | 16:1 | 18:0 | 18:1 | 18:2 | 20:1 | 20:46 | 22:53 | 22:63 |
| L929 | 19.5 | 3.4 | 18.2 | 45.3 | 2.2 | 1.3 | 4.9 | 2.4 | 2.7 |
| LD | 15 | 4.6 | 15.5 | 53.3 | 1.8 | 1.2 | 4.4 | 1.9 | 2.4 |
| LG | 20.1 | 3 | 20.8 | 47.6 | 0.9 | 1.3 | 3.8 | 1 | 1.4 |
| B. Fatty acid composition of phospholipids | | | | | | | | | |
| | 16:0 | 16:1 | 18:0 | 18:1 | 18:2 | 20:1 | 20:46 | 22:53 | 22:63 |
| L929 | 18.8 | 3.7 | 18.4 | 45.7 | 1.9 | 1 | 5.1 | 2.5 | 2.8 |
| LD | 14.9 | 3.7 | 15.9 | 57.5 | 1 | 1.8 | 2.9 | 1.1 | 1.2 |
| LG | 17.5 | 3.3 | 17.4 | 50.9 | 1.6 | 1.3 | 4.3 | 1.7 | 2 |

(A) The total lipid analysis, that showed that the level of the monounsaturated fatty acids (palmitoleic (16:1) and oleic (18:1) acids) has increased while the level of the saturated palmitoyl (16:0) and stearoyl (18:0) acids have decreased in the transformed cell lines. (B) Results of the phospholipid analysis showed the same, i.e., the monounsaturated fatty acids are over-produced in the transformed clones.



* = $p < 0.05$ (Dunnett's test for paired data)

FIG. 5. Membrane fluidity changes in transformed L929 cells measured by DPH-PA and DPH. Control: L929 cell line, G217B: *LG* cell line, Downs: *LD* cell line. The membranes of the *LD* and *LG* clones showed significantly decreased microviscosity values compared with that of the control L929 cell line.

and DPH-PA (3-(p-(6-phenyl)-1,3,5-hexatrienyl) phenylpropionic acid) (Aldrich) fluorescence anisotropy. After harvesting cells were washed twice and resuspended in PBS. Concentration of the cell suspension was adjusted with PBS to $OD_{360}=0.07$ ($\sim 10^5$ cell/ml) in 3 ml volume, labeled by the addition of DPH or DPH-PA, and dissolved in tetrahydrofuran to a final concentration of $0.1 \mu\text{M}$. The final concentration of the organic solvent was 0.1% (vol %). Cells were incubated with DPH-PA for 10 min or with DPH for 30 min at 37°C . Steady state fluorescence measurements were carried out at 37°C using a Quanta Master QM-1 T-format luminescence spectrometer (Photon Technology Int. Inc., NJ, USA). Fluorescence anisotropy was calculated as described by Schlame et al. (19).

RESULTS AND DISCUSSION

L929 mammalian cells were transformed with DNA constructs in order to study the effects of the expression of the yeast Δ^9 -desaturase gene under the control of two *H. capsulatum* promoters. Promoters were isolated from two strains of *H. capsulatum*: the wild type, temperature-tolerant (G217B) and the non-virulent, temperature-susceptible (Downs) strains (6, 15).

In the Downs strain of *H. capsulatum* transcription of Δ^9 -desaturase gene is upregulated. This is in agreement with the previous finding that membranes of this strain contain higher level of oleic acid than wild type cell membranes (18). The coding sequences of the *H. capsulatum Ole1* alleles are virtually identical, but differences exist in specific regions of the promoters. (6).

Our experiments indicated that in transformed L929 clones the *S. cerevisiae* Δ^9 -desaturase gene was transcribed and translated under the control of both *H. capsulatum* promoters and the yeast enzyme was active in the mammalian cells. Transformed cells exhib-

ited altered fatty acid composition of membrane phospholipids and reduced microviscosity of their membranes.

The presence of the transforming sequences in the animal cells were detected by PCR (Fig. 2.) and Southern analysis (Fig. 3). Yeast gene was also transcribed in all transformant colonies, specific mRNA was detected by RT-PCR analysis (Fig. 4). The mutant promoter induced higher expression of the *Ole1* gene in animal cells grown at 37°C than regulatory sequence of the wild type cells. Both fungal promoters were functional in animal cells and RT-PCR detected an approx. 340 bp band in all transformed cells.

We measured fatty acid composition of total lipids and phospholipids of control vs. transfected cells. Table 1A and 1B shows that the values of palmitoleic acid (16:1) and oleic acid (18:1) of *LD* and *LG* cells are significantly higher than those of the non-transformed L929 cells. The ratio of monounsaturated fatty acids was the same in total lipids and phospholipids in the transformed cells, showing that oleic and palmitoleic acids produced by the yeast gene is not stored in lipid vesicles but assembled into phospholipids of cellular membranes.

According to biophysical measurements using DPH as probe, microviscosity of cellular membranes was significantly decreased in the case of *LD* and *LG* cells compared to that of the control cells (Fig. 5).

Our experiments proved that the yeast *S. cerevisiae* gene is expressed under the control of regulatory sequences of *H. capsulatum* in mammalian cells. At 37°C , where the animal cells are grown, the level of *Ole1* specific transcripts and the corresponding enzyme activities are higher in cells transformed with the mutant Downs promoter than in cells harboring the wild type *H. capsulatum* regulatory sequences. The fungal desaturase gene product exhibited enzymatic activity and modified the lipid content of membranes in the transformed cells. This is not very surprising as there is high homology in the nucleotide and protein sequences of the corresponding yeast and animal genes. The predicted structure of the enzymes are similar and both proteins seem to bound to membranes of the endoplasmic reticulum (4).

According to our data this cell system is a promising new tool to alter the fatty acid composition of phospholipids in membranes of mammalian cells and to study the effect of these modifications on most various membrane-related biological processes.

ACKNOWLEDGMENTS

We are grateful for Dr. S. Bottka for the synthesis of the oligonucleotides. This research was supported by OTKA (National Science Foundation) grants T13101 and T17685 to ED.

REFERENCES

1. Bloomfield, D. K., and Bloch, K. (1960) *J. Biol. Chem.* **235**, 337–344.
2. Tamura, Y., Yshida, Y., Sato, R., and Kumaoka, H. (1976) *Arch. Biochem. Biophys.* **175**, 284–294.
3. Ohba, M., Sato, R., Yoshida, Y., Bieglmayer, C., and Ruis, H. (1979) *Biochim. Biophys. Acta* **572**, 352–362.
4. Stuke, J. E., McDonough, V., and Martin, C. E. (1990) *J. Biol. Chem.* **265**, 20144–20149.
5. Nakashima, S., Zhao, Y., and Nozawa, Y. (1996) *Biochem. J.* **317**, 29–34.
6. Gargano, S., Di Lallo, G., Kobayashi, G. S., and Maresca, B. (1995) *Lipids* **30**, 899–906.
7. Kaerstner, K. H., Ntambi, J. M., Kelly, T. J., and Lane, M. D. (1989) *J. Biol. Chem.* **264**, 14755–14761.
8. Thiede, M. A., Ozols, J., and Strittmatter, P. (1986) *J. Biol. Chem.* **261**, 13230–13235.
9. Li, J. Ding, S. F., Fermor, B. F., Wood, C. B., and Gilmour, R. S. (1994) *Int. J. Cancer* **57**, 348–352.
10. Hazel, J. R., and Williams, E. E. (1990) *Progr. Lipid Res.* **29**, 167–227.
11. Stubbs, C., and Smith, A. D. (1984) *Biochim. Biophys. Acta* **779**, 89–137.
12. Stubbs, C. D., Kouyama, T., Kinoshita, K., and Ikegami, A. (1981) *Biochemistry* **20**, 2800–2810.
13. Coolbear, K. P., Berde, C. P., and Keogh, K. M. W. (1983) *Biochemistry* **22**, 167–171.
14. Tosco, A., Gargano, S., and Maresca, B. (1997) *Biochem. Biophys. Res. Comm.* **230**, 457–461.
15. Carratú, L., Franceschelli, S., Pardini, C. L., Kobayashi, G. S., Horváth, I., Vigh, L., and Maresca, B. (1996) *Proc. Natl. Acad. Sci. USA* **93**, 3870–3875.
16. Patriarca, E. J., and Maresca, B. (1990) *Exp. Cell Res.* **190**, 57–64.
17. Bligh, E. G., and Dyer, W. J. (1959) *Can. J. Biochem. Physiol.* **31**, 911–917.
18. Maresca, B., and Kobayashi, G. S. (1993) *Arch. Med. Res.* **24**, 247–249.
19. Schlame, M., Horváth, I., Török, Zs., Horváth, L., and Vigh, L. (1990) *Biochim. Biophys. Acta* **1045**, 1–8.

The *OLE1* Gene of *Saccharomyces cerevisiae* Encodes the $\Delta 9$ Fatty Acid Desaturase and Can Be Functionally Replaced by the Rat Stearoyl-CoA Desaturase Gene*

(Received for publication, June 12, 1990)

Joseph E. Stucky‡, Virginia M. McDonough§, and Charles E. Martin¶

From the Nelson Biological Laboratory, Bureau of Biological Research, Rutgers University, Busch Campus, Piscataway, New Jersey 08855-1059

Strains of *Saccharomyces cerevisiae* bearing the *ole1* mutation are defective in unsaturated fatty acid (UFA) synthesis and require UFAs for growth. A previously isolated yeast genomic fragment complementing the *ole1* mutation has been sequenced and determined to encode the $\Delta 9$ fatty acid desaturase enzyme by comparison of primary amino acid sequence to the rat liver stearoyl-CoA desaturase. The *OLE1* structural gene encodes a protein of 510 amino acids (251 hydrophobic) having an approximate molecular mass of 57.4 kDa. A 257-amino acid internal region of the yeast open reading frame aligns with and shows 36% identity and 60% similarity to the rat liver stearoyl-CoA desaturase protein. This comparison disclosed three short regions of high consecutive amino acid identity (>70%) including one 11 of 12 perfect residue match. The predicted yeast enzyme contains at least four potential membrane-spanning regions and several shorter hydrophobic regions that align exactly with similar sequences in the rat liver protein. An *ole1* gene-disrupted yeast strain was transformed with a yeast-rat chimeric gene consisting of the promoter region and N-terminal 27 codons of *OLE1* fused to the rat desaturase coding sequence. Fusion gene transformants displayed near equivalent growth rates and modest lipid composition changes relative to wild type yeast control implying a significant conservation of $\Delta 9$ desaturase tertiary structure and efficient interaction between the rat desaturase and yeast cytochrome b_5 .

In animal and fungal cells, monounsaturated fatty acids are synthesized via an aerobic process from saturated fatty acid precursors by a microsomal membrane-bound three-component enzyme system involving cytochrome b_5 , NADH-dependent cytochrome b_5 reductase, and the $\Delta 9$ fatty acid desaturase

(1-3). This complex catalyzes the insertion of a double bond between carbons 9 and 10 of the saturated fatty acyl substrates, palmitoyl (16:0)- and stearoyl (18:0)-CoA, yielding the monoenoic products palmitoleic (16:1) or oleic (18:1) acids. Although higher eukaryotes contain polyunsaturated fatty acids in their membranes, either synthesized endogenously via $\Delta 12$ and $\Delta 15$ desaturase reactions or obtained from their diet, the $\Delta 9$ reaction accounts for all *de novo* unsaturated fatty acid (UFA)¹ production in *Saccharomyces cerevisiae* (4).

Isolation and characterization of fatty acid desaturase enzymes has proved difficult due to their extraordinary hydrophobic nature and tight association with membranes. Although fatty acid desaturation was first described using the yeast $\Delta 9$ desaturase system, only animal $\Delta 9$ enzymes have been successfully purified to homogeneity (5, 6). At a genetic level, only the DNA sequence for the rat liver and mouse adipocyte genes have been reported and analyzed (7, 8). Those genes were found to encode proteins with 92% identical amino acid sequences.

The $\Delta 9$ desaturase from rat liver has been most extensively characterized. It is a protein consisting of 358 amino acids of which 62% are hydrophobic (7). The functional enzyme has an obligate phospholipid requirement and contains one molecule of non-heme iron (5). Effects of chemical modification on enzyme function has suggested that arginyl and tyrosyl residues are involved in the binding of the negatively charged CoA moiety of the substrate and in the chelation of the iron prosthetic group, respectively (9). A truncated rat liver $\Delta 9$ enzyme missing 26 residues from the N terminus is also membrane-bound and functional (10).

Yeast mutants bearing the *ole1* allele require oleic acid for growth and were believed to produce a defective $\Delta 9$ desaturase suggesting that *OLE1* was the structural gene encoding the enzyme (11). Recently, we isolated and characterized a yeast genomic fragment containing the *OLE1* gene of *S. cerevisiae* (12). Replacement of the wild type gene in haploid cells with a disrupted form of that fragment resulted in a UFA-requiring, nonreverting phenotype.

In this paper we report the DNA sequence of the *S. cerevisiae* *OLE1* gene and compare the deduced amino acid sequence of the yeast $\Delta 9$ fatty acid desaturase with that of the rat liver stearoyl-CoA desaturase primary sequence. Although the proteins encoded are highly divergent, the rat $\Delta 9$ desaturase gene functions efficiently in *S. cerevisiae* in place of the native yeast gene. Furthermore, predicted structural features of the two proteins suggest a model for the topology of the $\Delta 9$ fatty acid desaturase in the ER membrane.

* This work was supported by National Science Foundation Grant DMB84-17802, Biomedical Research Group Grant RR-07058-21 from the Public Health Service, and by a grant from the Bureau of Biological Research Charles and Johanna Busch Memorial Fund. The costs of publication of this article were defrayed in part by the payment of page charges. This article must therefore be hereby marked "advertisement" in accordance with 18 U.S.C. Section 1734 solely to indicate this fact.

The nucleotide sequence(s) reported in this paper has been submitted to the GenBank™/EMBL Data Bank with accession number(s) J05676.

‡ Supported by a Charles and Johanna Busch predoctoral fellowship.

§ Supported by an Arthur McCallum predoctoral fellowship.

¶ To whom correspondence should be addressed. Tel.: 201-932-4081 or 201-873-2752.

¹ The abbreviations used are: UFA, unsaturated fatty acid; ORF, open reading frame; ER, endoplasmic reticulum; kb, kilobase(s).

MATERIALS AND METHODS

DNA Manipulations, Media, and Stain—All recombinant DNA manipulations were according to standard methods (13, 43). Plasmid amplifications and bacterial transformations were performed using either *Escherichia coli* strain HB101 or XL1 Blue (Stratagene). Yeast transformations were by the method of Ito *et al.* (14). Growth analysis was performed in synthetic dextrose medium supplemented with the appropriate amino acids (23). The genotype of yeast strain L8-14C is: α , *ole1* Δ ::*LEU2*, *leu2-3*, *leu2-d112*, *ura3-52*, *his4*.

DNA Sequencing—Overlapping DNA fragments lying within the *OLE1* open reading frame were subcloned into pBluescript vectors (Stratagene) in two orientations for sequencing in either direction. Single-stranded DNA sequencing templates were prepared by methods supplied by Stratagene. The M13(-20) primer was hybridized to single-stranded DNA templates and DNA sequencing was performed by the dideoxy chain termination method of Sanger *et al.* (15) using the modified T7 DNA polymerase, Sequenase (U. S. Biochemical Corp.). In two cases, *OLE1* internal oligonucleotides were synthesized to facilitate DNA sequence analysis.

DNA Sequence and Deduced Primary Sequence Analysis—*OLE1* DNA sequence and the deduced primary sequence analysis was performed using the Genetics Computer Group (GCG) sequence analysis software package (16). Amino acid sequence of the rat liver stearyl-CoA desaturase was obtained from GenBank. Primary sequence comparison of the yeast and rat liver $\Delta 9$ desaturases was performed using the BestFit analysis program. Hydropathy analysis was according to Kyte and Doolittle (17).

Construction of Modified *ole1* Alleles—Alleles *ole1-33* and *ole1-107*, containing stop codons in the 5' region of the coding sequence, were constructed similarly. YEp352/*OLE4.8* was partially digested with *SalI* or *NcoI*, the cohesive ends were made blunt, and plasmids were religated. Following amplification in *E. coli*, plasmid samples were subject to restriction enzyme analysis. Candidates lacking the relevant restriction site were subject to DNA sequence analysis for verification.

Construction of Episomal and Centromeric Plasmids Bearing the Rat Liver Stearyl-CoA Desaturase Gene—A 1.2-kb rat liver $\Delta 9$ desaturase cDNA fragment encoding residues 3–358, stop codon, and 136 base pairs of the 3'-untranslated region was removed from plasmid pDs3-358 (10) by digestion with *BamHI* and *SacI* and inserted into the multiple cloning site of episomal plasmid YEp352. A 1.0-kb yeast genomic fragment encompassing the promoter region, translation initiation codon, and the first 27 codons of the *OLE1* was isolated via *HindIII/SalI* digestion and ligated in-frame with the rat desaturase fragment in YEp352. In this final construct, an eight-codon linker derived from the multiple cloning site regions of pUC8 and YEp352 separates the yeast N-terminal codons from the rat desaturase sequence. The predicted size of the fusion gene product is 391 amino acid residues. The yeast-rat fusion gene was then recovered via *HindIII/DraI* digestion and ligated into YCp50 using *HindIII* and *NruI* restriction sites. Plasmids bearing the fusion gene were amplified in *E. coli* strain XL1-Blue and used to transform the yeast *ole1* gene-disrupted strain L8-14C.

Lipid Isolation and Fatty Acid Analysis—Lipids were extracted from whole yeast cells by direct saponification (18). Fatty acid methyl esters were prepared by transmethylation with boron trifluoride (19) and analyzed by gas chromatography using a 30-meter capillary column SP-2330 (Supelco) in a Hewlett-Packard 5710A chromatograph as previously reported (12).

RESULTS AND DISCUSSION

General Features of the *OLE1* Structural Gene—In a previous report it was shown that a cloned 4.8-kb *HindIII* yeast genomic fragment, but not two subclones of that fragment terminating at a central *KpnI* region, complemented the *ole1* mutation of *S. cerevisiae* (12). From that *KpnI* junction, overlapping subclones were used to "walk" through the observed open reading frame (ORF) in both directions yielding the sequence strategy presented in Fig. 1. Both strands were sequenced through the entire ORF without ambiguity.

The DNA and deduced amino acid sequence of *OLE1* and flanking nucleotide sequence is shown in Fig. 2. The ORF is 1530 nucleotides long. Translation of the entire ORF would produce a 510-amino acid polypeptide having an approxi-

mately molecular mass of 57.4 kDa containing 49.2% hydrophobic and 25.7% charged (10.0% acidic and 15.7% basic) amino acid residues. No consensus *N*-glycosylation sites are present in the deduced amino acid sequence of *OLE1* and the protein does not appear to contain a cleavable N-terminal signal sequence.

Yeast TATA promoter elements are commonly found 40–120 base pairs upstream from transcription initiation sites (20) with an average mRNA leader sequence of 52 nucleotides (21). The *OLE1* promoter region has two consensus TATA promoter elements (TATAAA and TATATA) located at positions –30 and –156 relative to the ORF. A transcription initiation event, directed from the TATATA element located at –156, could yield a transcript having features consistent with the above observations. However, transcription initiation directed from the TATAAA promoter element located at –30 could result in an atypically short, nontranslated leader sequence relative to the first in-frame ATG. Furthermore, there are three additional in-frame ATG codons within the first 400 base pairs of the *OLE1* ORF at positions 56, 61, and 116 that could also serve as potential translation start sites (see Fig. 1). Due to the close proximity of the first ATG codon to the TATA promoter element at –30 and comparison with the rat desaturase (discussed below) that showed no significant similarities in the first 140 amino acids, we were prompted to test for functional *OLE1* products initiating from these downstream sites. Two modified *ole1* alleles were constructed (see "Materials and Methods") that shifted the ORF and introduced translation stop codons at either position 33 (*ole1-33*) or 107 (*ole1-107*). Both in-frame stop codons were positioned before the next available ATG sequence. The *ole1* gene-disrupted yeast strain L8-14C, bearing the deletion allele *ole1* Δ ::*LEU2*, was transformed with either of the above alleles on an episomal plasmid and tested for the ability to grow in the absence of exogenous UFAs. (Strains bearing this *ole1* allele were previously shown (12) to completely lack $\Delta 9$ desaturase activity as determined by product formation and have limited and finite growth potential (4–5 generations) in UFA-free medium.) In both cases the transformed strain grew only when UFAs were added to the growth medium, which is consistent with the first in-frame ATG codon functioning as the primary site of translation initiation.

Yeast and Rat Liver $\Delta 9$ Enzyme Amino Acid Analysis—A computer search of homologies to all current entries in GenBank/EMBL protein data bases identified a single data

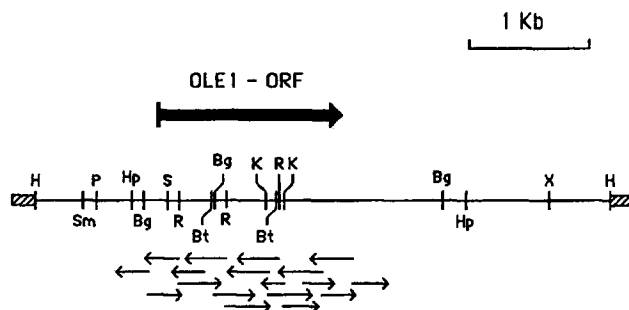


FIG. 1. *OLE1* restriction map and sequencing strategy. Primary restriction sites mapping the 4.8-kb yeast DNA fragment containing *OLE1*: Bg, BglII; Bt, BstEII; H, HindIII; Hp, HpaI; K, KpnI; R, EcoRI; S, SalI; Sm, SmaI; P, PstI; and X, XhoI. The position and direction of the 1530-base-long ORF encoding the $\Delta 9$ enzyme is indicated by the large arrow above the map. Small arrows below the map indicate by size and direction the *OLE1* subclones used to sequence the entire ORF and flanking regions.

| | | | | | |
|------|---|-----------------|------|--|------|
| 1 | ACACTCAACAAACCTTATCTAGTGCACACAGGCTGTCTTACGAGCTTGTCTCACTC | 60 | 1141 | GTCACTTCAACTCTTATCTGTGGTACTTTTCAACGACTATATGGGTGGTTGATCTAT | 1200 |
| 61 | AGACACACCTATCCCTATTGTTACGGCTATGGGATGGACACAAAGGTGGAATAATAG | 120 | | ValIleProThrLeuIleCysGlyTyrPhePheAsnAspTyrMetGlyGlyLeuIleTyr | |
| 121 | TAGTTAACAATATATGACGCAATCATCGGCTCCTGGCTCATCGAGTCTTGCAATACAGC | 180 | 1201 | GCGGGTTTATCTGTGCTTTGTTCATTCAACAGCTACTTTGGCATTAACTCCATGGCT | 1260 |
| 181 | ATATACATATATATATGCGGSCAGATCTTGATTCATTATTGTTCTATTTCATCTTTCC | 240 | | AlaGlyPheIleArgValPheValIleGlnGlnAlaThrPheCysIleAsnSerMetAla | |
| 241 | TACTTCTGTTTCCGTTTATATTGTTATCTAGTAGATAGAACATCATAGTAATAGATAG | 300 | 1261 | CATTACATCGGTACCAACCATTCGATGACAGAAGACCCCTCGTACAACGGATTA | 1320 |
| 301 | TTGTGGTGATCATATTATAACAGCACTAAACATTACACAAAGATGCCAACTCTGGA | 360 | | HisTyrIleGlyThrGlnProPheAspArgArgTyrProArgAspAsnTrpIleThr | |
| | | MetProThrSerGly | 1321 | GCCATTGTTACTTTCGGTGAAGTTACCAACTCCACCACGAATCCCAACTGATTAC | 1380 |
| 361 | ACTACTATTGAATTGATTGACGACCAATTCCAAAGGATGACTCTGCCAGCAGTGGCATT | 420 | | AlaIleValThrPheGlyGluGlyTyrHisAsnPheHisHisGluPheProThrAspTyr | |
| | ThrThrIleGluLeuIleAspAspGlnPheProLysAspSerAlaSerSerGlyIle | | 1381 | AGAAACGCTATTAAAGTGTACCAATACGACCACTAAGGTTATCATCTATTGACTTCT | 1440 |
| 421 | GTCGACGAAGTCCGCTTAACGAAGCTAAATTTTGGTCTGCTTGAATAAGAAGCA | 480 | | ArgAsnAlaIleLysTrpTyrGlnTyrAspProThrLysValIleIleTyrLeuThrSer | |
| | ValAspGluValAspLeuThrGluAlaAsnIleLeuAlaThrGlyLeuAsnLysLysAla | | 1441 | TTAGTTGGTCTAGCATACCACTTGAAGAAATCTCTCAAAATGCTATTGAAGAAGCTTC | 1500 |
| 481 | CCAAGAATTGTCAACGGTTTGGTCTTAAATGGGCTCCAAGGAATGGTTCCGCTGGA | 540 | | LeuValGlyLeuAlaTyrAspLeuLysPheSerGlnAsnAlaIleGluGluAlaLeu | |
| | ProArgIleValAsnGlyPheGlySerLeuMetGlySerLysGluMetValSerValGlu | | 1501 | ATTCACAAAGCAAAAGAGATCAATAAAAGAGGCTAAGATTAACTGGGTCCAGTT | 1560 |
| 541 | TTGCACAAGAGGCAACGAAAGCAATTCGATCGTCTGCTAGAAAGGACAAAC | 600 | | IleGlnGlnGlnLysLysIleAsnLysLysLysAlaLysIleAsnTrpGlyProVal | |
| | PheAspLysLysGlyAsnGluLysLysSerAsnLeuAspArgLeuLeuGluLysAspAsn | | 1561 | TTGACTGATTGCCAATGTGGGCAACAAACCTTCTTGGCTAAGTCTAAGGAAACAG | 1620 |
| 601 | CAAGAAAAGAGGCAAGTAAACATAAATTCACATCTCCGACCAACCATGGATTTGAAT | 660 | | LeuThrAspLeuProMetTrpAspLysGlnThrPheLeuAlaLysSerLysGluAsnLys | |
| | GlnGluLysGluGluAlaLysThrLysIleHisIleSerGluGlnProTrpThrLeuAsn | | 1621 | GGTTTGGTATCATTTCTGCTATTGTTTACGACGATCTGCTATATCTCTGAACATCCA | 1680 |
| 661 | AACTGGCACAACATTGAACTGGTGAACATGGTCTTGTGTTGGTATGCCAATGATT | 720 | | GlyLeuValIleIleSerGlyIleValHisAspValSerGlyTyrIleSerGluHisPro | |
| | AsnTrpHisGlnHisLeuAsnTrpLeuAsnMetValLeuValCysGlyMetProMetIle | | 1681 | GGTGGTGAATCTTAATTAACATGCAATAGTAAAGGCTACCAAGCTTTCAGTGGT | 1740 |
| 721 | GTTTGGTACTTCGCTCTCTGTTAAAGTACCTTTCGATTAAACGTTTTCCTTTCTCC | 780 | | GlyGlyGluThrLeuIleLysThrAlaLeuGlyLysAspAlaThrLysAlaPheSerGly | |
| | GlyTrpTyrPheAlaLeuSerGlyLysValProLeuHisLeuAsnValPheLeuPheSer | | 1741 | GGTGTCTACGCTCACTCAATGCCGCTCAAAATGTCTTGGCTGATGAGAGTGGCTGTT | 1800 |
| 781 | GTCTTCTACTACGCTGCTGGTGGTGTCTTCTATTACTGCGGTACCATAGATTGGTCT | 840 | | GlyValTyrArgHisSerAsnAlaAlaGlnAsnValLeuAlaAspMetArgValAlaVal | |
| | ValPheTyrTyrAlaValGlyGlyValSerIleThrAlaGlyTyrHisArgLeuTrpSer | | 1801 | ATCAAGGAAAGTAAAGTCTGCTATTAGATGGCTAGTAGAGAGGTGAATCTACGAA | 1860 |
| 841 | CACAGATCTTACTCCGCTACTGCCATTGAGATTATTCTACGTATCTCGGTTGTGCT | 900 | | IleLysGluSerLysAsnSerAlaIleArgMetAlaSerLysArgGlyGluIleTyrGlu | |
| | HisArgSerTyrSerAlaHisIleTrpProLeuArgLeuPheTyrAlaIlePheGlyCysAla | | 1861 | ACTGGTAAGTCTTTTAAAGCATCATTACAATAACAAACTGCAACTACCATTAATAAA | 1920 |
| 901 | TCCGTTGAAGGCTCCGCTAAATGGTGGGCACTCTCACAGAATTCACATCGTTACACT | 960 | | ThrGlyLysPhePheEnd | |
| | SerValGluGlySerAlaLysTrpTrpGlyHisSerHisArgIleHisHisArgTyrThr | | 1921 | AAATTTGAAAATCATAAATTAATAAAAAAAAAAATCAATTGAATTTTTTTTTTCATGATT | 1980 |
| 961 | SATACCTTGACAGATCTTATGACGCTCGTACAGGCTATGACTTCCACATGGGATGG | 1020 | | ACGTTTTCGACATTTTCTCTTTTCTCTCTTATTACGATTACCTTTTATTATTATT | 2040 |
| | AspThrLeuArgAspProTyrAspAlaArgArgGlyLeuTrpTyrSerHisMetGlyTrp | | 2041 | TTTCATTTTAGTATTTTATCTTCTGCTATTATGATAGAAATTTTCATTTTCATTAGA | 2100 |
| 1021 | ATGCTTTTGAAGCAAAATCCAAATACAGGCTAGAGCTGATATACGATATGACTGAT | 1080 | | TTTCAGATTGGTTATCTTTTTCATTTATATATCTTTTGCATAAGTTTCAGCTTAAGTTC | 2160 |
| | MetLeuLeuLysProAsnGlnLysTyrLysAlaArgAlaAspIleThrAspMetThrAsp | | 2161 | TATTTTATTATTTTCTTTTCTGGGCGCTGCAGCAATAGATATGGATGGCTTACTGCATC | 2220 |
| 1081 | GATTGGACATTAGATTCCAAACAGACACTACATCTTGTGATGTTATTAACGGCTTTC | 1140 | | 2221 TCTTCAAAATTCACAGTCATGCTCAGCTTAAGTTCTCAACCTTTT 2267 | |
| | AspTrpThrIleArgPheGlnHisArgHisTyrIleLeuLeuMetLeuLeuThrAlaPhe | | | | |

FIG. 2. Nucleotide and encoded amino acid sequence of the $\Delta 9$ fatty acid desaturase structural gene, *OLE1*. Two consensus yeast TATA elements preceding the 1530-base-long ORF and the first four in-frame methionine-specific codons are underlined. An *OLE1* internal region of 258 amino acids displaying significant identity to the rat liver $\Delta 9$ enzyme is delimited by asterisks. Potential membrane-spanning regions are highlighted with lines above nucleotide and amino acid sequences.

base entry, the rat liver $\Delta 9$ desaturase, with significantly similarity to the *OLE1* gene product (Fig. 3). The aligned sequences show 36% identity and are greater than 60% similar over the region encompassing the C-terminal 260 amino acids of the shorter rat protein. No significant similarities exist over the N-terminal 141 amino acids of the yeast and 99 amino acids of the rat sequences. The yeast open reading frame extends 113 amino acids beyond the C-terminal end of the rat sequence. Within the region of high amino acid similarity there are three segments, having a minimum length of 10 residues, of very high identity (>70%) beginning at *OLE1* amino acid positions 156, 331, and 368. The most highly conserved of these is the first region where 17 of 23 identities are observed including one stretch containing 11 of 12 perfect matches.

The most conserved amino acid type within the compared region of the yeast protein is histidine with 10 of 14 (71.4%) residues in perfect alignment. Two other amino acid residues, proline and arginine, also show greater than 50% total identity. Arginine residues of the rat liver enzyme have been previously identified as being involved in substrate binding

| | | | |
|-------|-----|---|-----|
| yeast | 141 | VFLSVFYAVGGVSIITAGYHRLNSHRSYSAHWFLRLFYAIFGCASVEGS | 190 |
| rat | 99 | TLWGIFLYLSALGITAGAHRLNSHRTYKARLPLRLFLIANTAFQND | 148 |
| yeast | 191 | AKWGHSHRIHRTITLLEDPDARRGLWSHNGWLLKGNPKYKARA | 238 |
| rat | 149 | VYENARDERAHKPSETHADPHNSRGFPFSHVGLLVKRHPVKEGKG | 198 |
| yeast | 239 | .DITMDTDWTRFQHRHYLLMLTAFVPTLTCGYFFND.YNGGLIYA | 286 |
| rat | 199 | LNSDLKAEKLVFQRRYKPLGLLNCFLPLTPVPYWGGETFLSLFVS | 248 |
| yeast | 287 | GFIRVFVQDQTCINSRSLVIGTQPFDRPTPRDMITAIIVTCEYHN | 336 |
| rat | 249 | PLRVTYLVNATWLVNSAHLGYRYPQKNGISRENLVSLGSGVEGFHN | 298 |
| yeast | 337 | PHHEFTDYRNALWYQDPTKVITYLTSVLGLAYDLKFSQNALEALI | 386 |
| rat | 299 | YHAFPPDYSAEYRWHNFTTFIDONALGLAYDRKVKSKAAV.LARI | 347 |
| yeast | 387 | QOEQKINKKK | 397 |
| rat | 348 | KRTGGSHRSS | 358 |

FIG. 3. Amino acid sequence comparison of the yeast and rat liver $\Delta 9$ fatty acid desaturases. A 257-residue internal region of the yeast $\Delta 9$ enzyme is aligned with the rat liver stearoyl-CoA desaturase. Comparison was prepared by the GCG sequence analysis program BestFit. Identical residue matches are indicated by connecting solid lines. Two or one point between residues indicate decreasing amino acid similarity. Percent similarity value is based on the number of identical and two-point amino acid comparisons. Segments showing high identity (>70%) are indicated with lines above those regions.

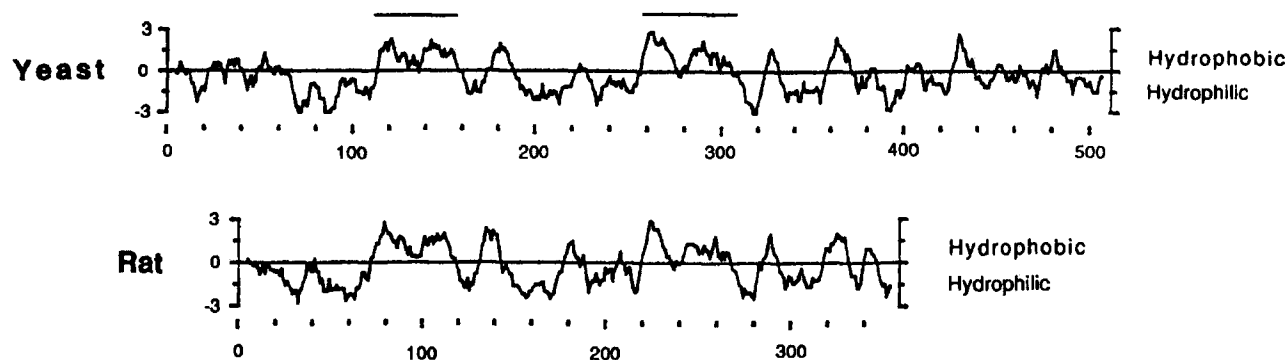


FIG. 4. Hydropathy analysis of yeast and rat liver $\Delta 9$ enzymes. Aligned Kyte-Doolittle (17) hydropathy profiles of the yeast and rat liver $\Delta 9$ desaturase proteins. The presumptive double membrane-spanning sequences are indicated by bold lines above those regions.

(9). Its significance as a highly conserved amino acid supports this finding. Although the role of histidyl residues in the fatty acid desaturases has not been examined, their highly conserved appearance also suggests an important contribution to enzyme function.

Structural Analysis and Proposed Topology of the Yeast $\Delta 9$ Enzyme—Striking similarities were also observed in the hydropathic characteristics of the two enzymes (Fig. 4). Both proteins contain two long hydrophobic regions (~50 residues) that could potentially form two membrane traversing loops, each consisting of two transmembrane segments. Chou-Fasman algorithms predict β -turn forming potential in the central portions of each loop in both the yeast and rat liver proteins. Inspection of the primary sequences at those sites reveals the presence of multiple helix-breaking amino acids that could serve to disrupt α -helical structure in order to form the looped structures. These hydrophobic regions are at identical positions in the aligned yeast and rat sequences. At least three smaller hydrophobic regions (each <7 amino acids) are also found at identical positions in the two proteins. The regions of high consecutive amino acid identity, however, are not within the hydrophobic sequences. The first region is located between the two "transmembrane loop regions," the second and third identity regions are located at the C-terminal part of the protein past the second "transmembrane loop." Neither extension of the N- and C-terminal domains of the yeast appears significantly hydrophobic and an examination of the amino acid distribution in those regions further suggests that they do not contribute to the integral membrane domains of the protein. A proposed model of the topology of the yeast protein in the ER membrane is given in Fig. 5. Assuming that the membrane-spanning regions are confined to the predicted hydrophobic sequences that are greater than 50 amino acids long, the arrangement places most of the protein on the cytosolic side of the ER membrane. Furthermore, all three regions of high consecutive identity would be located on that side of the membrane which is consistent with its proposed site of action (22).

Growth and Fatty Acid Content of Gene-disrupted Yeast Transformed with the Rat Liver $\Delta 9$ Desaturase—The significant sequence and predicted structural similarities observed between the yeast and rat $\Delta 9$ proteins prompted us to test whether the rat enzyme could functionally replace the yeast enzyme in *S. cerevisiae*, although there are additional residues at the N- and C-terminal ends of the yeast peptide sequence that are not found on the rat protein. A yeast-rat fusion gene was constructed (see "Materials and Methods") placing codons 3–358 of the rat gene in-frame with the initial 27 codons

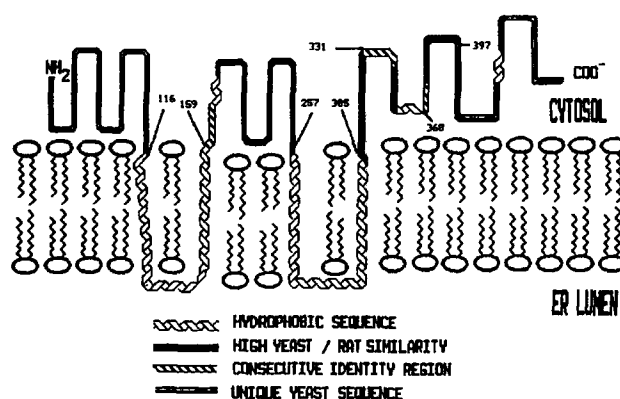


FIG. 5. Model for the orientation of the yeast desaturase in the ER membrane. The numbers identify amino acid positions in the yeast open reading frame.

of the yeast gene and promoter sequences separated by an 8-codon linker region. This fusion gene was placed on a multi-copy episomal and single copy centromere-based (CEN) vectors and introduced into the *ole1* gene-disrupted yeast strain, L8-14C. Fusion gene transformants were analyzed for growth and lipid composition relative to the same gene-disrupted strain transformed with the plasmid bearing native *OLE1* gene.

Yeast transformants bearing either the native *OLE1* or the yeast-rat fusion desaturase gene (two isolates) on an episomal plasmid were found cured of the UFA requirement and, surprisingly, showed identical growth rates (Fig. 6A) indicating significant conservation of $\Delta 9$ desaturase tertiary structure and an ability of the rat enzyme to interact with the yeast cytochrome *b₅*. In addition, because the rat protein is 113 residues shorter than the yeast desaturase at the C-terminal end and yet can functionally substitute for the yeast enzyme in *S. cerevisiae*, it appears that this extension of the yeast protein may be nonessential for catalytic functions. We cannot exclude the possibility, however, that the additional residues may be involved in other functions that influence its catalytic efficiency or optimize interactions with other components of the desaturase system.

An analysis of stationary phase cellular lipid compositions revealed, however, significant differences in the percentage of 16-carbon fatty acid species in the yeast-rat fusion gene transformants relative to the wild type control and, as a result, a modest decrease in the percent total UFA (Table I). The lower percentage of 16:1 and increased 16:0 species found in

FIG. 6. Growth characteristics of transformed *S. cerevisiae*. Growth curves were determined for L8-14C transformants containing either the native *OLE1* gene or the yeast-rat $\Delta 9$ fusion gene on the episomal plasmid YEp352 (A) or the CEN plasmid YCp50 (B).

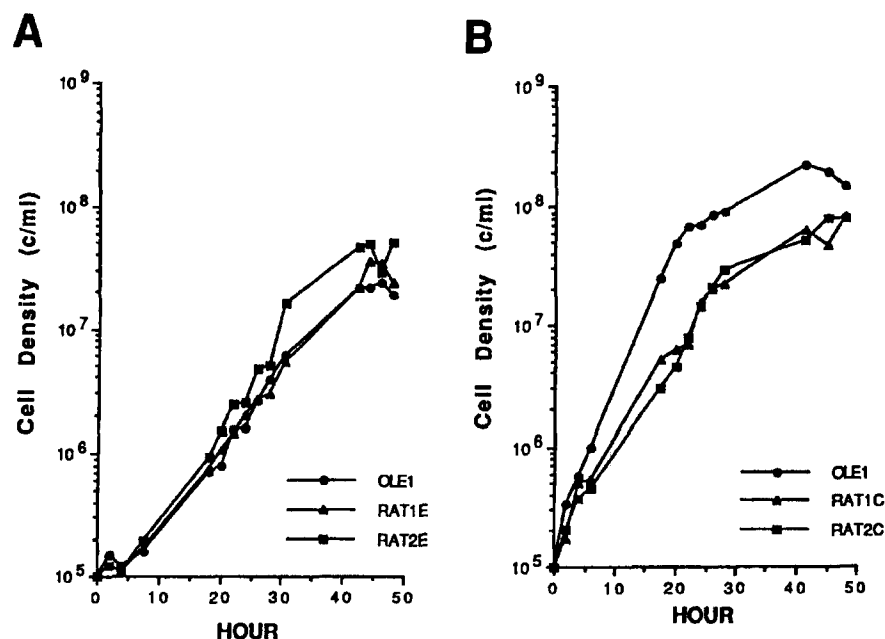


TABLE I

Fatty acid composition of transformed *S. cerevisiae*

Stationary phase L8-14C cells transformed with *OLE1* or the yeast-rat $\Delta 9$ chimeric gene on multiple (episomal) or single (CEN) copy number plasmids were harvested and cellular lipids analyzed as described under "Materials and Methods."

| Plasmid type and transformant | Fatty acids | | | | | |
|-------------------------------|-------------|-------|-------|-------|-------|-------|
| | 14:0 | 16:0 | 16:1 | 18:0 | 18:1 | UFA |
| | % | | | | | |
| Episomal | | | | | | |
| <i>OLE1</i> | 1.95 | 21.92 | 41.70 | 4.65 | 29.77 | 71.47 |
| RAT1E | 1.40 | 33.00 | 28.77 | 4.61 | 32.21 | 60.98 |
| RAT2E | 1.41 | 30.94 | 27.42 | 4.73 | 35.51 | 62.93 |
| CEN | | | | | | |
| <i>OLE1</i> | 1.16 | 18.38 | 34.05 | 9.10 | 37.32 | 71.36 |
| RAT1C | 5.58 | 40.67 | 21.22 | 8.70 | 23.82 | 45.04 |
| RAT2C | 7.23 | 39.71 | 15.83 | 10.89 | 26.35 | 42.18 |

those strains may reflect a preference of the rat $\Delta 9$ enzyme for the 18:0-CoA substrate over 16:0-CoA.

Although a yeast-rat $\Delta 9$ desaturase fusion gene is capable of functionally replacing the native *OLE1* of *S. cerevisiae* when present on a high copy number plasmid, a more stringent test of the efficiency of the rat protein in yeast would be to examine cells transformed with a single copy of the fusion gene. Cells containing the chimeric gene on CEN plasmid YCp50 showed growth rates that are reduced approximately 65% relative to wild type (Fig. 6B).

Similarly, the lipid composition of CEN plasmid-bearing yeast transformants differed markedly between those containing the chimeric gene and those containing the cloned yeast gene (Table I). The relative UFA levels were reduced approximately 38% in cells containing the rat gene coding sequence and the compensatory relative increase in saturated fatty acids resulted in a doubling of the 16:0 content and increased 14:0 levels, but no significant change in the level of 18:0. Thus, the yeast-rat $\Delta 9$ desaturase fusion gene can functionally replace the native *OLE1* of *S. cerevisiae*, although its action results in striking differences in cellular fatty acid compositions.

In previous studies using gene disruption and lipid analytical methods (12) we provided evidence suggesting that the *OLE1* gene encoded the yeast $\Delta 9$ fatty acid desaturase. The deduced *OLE1* amino acid sequence and physical comparisons of the yeast and rat liver proteins given here provide further proof that the *OLE1* locus contains the authentic structural gene for the desaturase. The aligned regions of consecutive identity between these two proteins from widely divergent sources suggests that they may represent conserved regions with similar function. The finding that the rat $\Delta 9$ fatty acid desaturase gene can complement *OLE1* in *S. cerevisiae* although the two proteins have only 36% identity suggests that there is conserved functional interaction among cytochrome *b₅*-mediated desaturase systems. Thus, ER-bound $\Delta 9$ enzymes from other organisms and possibly other cytochrome *b₅*-mediated desaturases, such as the $\Delta 12$ and $\Delta 15$, may also function in yeast.

Acknowledgment—We wish to thank Philipp Strittmatter for plasmids containing the rat stearoyl-CoA desaturase gene.

REFERENCES

- Bloomfield, D. K., and Bloch, K. (1960) *J. Biol. Chem.* **235**, 337–345
- Tamura, Y., Yoshida, Y., Sato, R., and Kumaoka, H. (1976) *Arch. Biochem. Biophys.* **175**, 284–294
- Ohba, M., Sato, R., Yoshida, Y., Bieglmayer, C., and Ruis, H. (1979) *Biochim. Biophys. Acta* **572**, 352–362
- Schweizer, E. (1984) in *Fatty Acid Metabolism and Its Regulation* (Numa, S., ed) pp. 59–83, Elsevier Scientific Publishing Co., New York
- Strittmatter, P., Spatz, L., Corcoran, D., Rogers, M. J., Setlow, B., and Redline, R. (1974) *Proc. Natl. Acad. Sci. U. S. A.* **71**, 4565–4569
- Prasad, M. R., and Joshi, V. C. (1979) *J. Biol. Chem.* **254**, 6362–6369
- Thiede, M. A., Ozols, J., and Strittmatter, P. (1986) *J. Biol. Chem.* **261**, 13230–13235
- Ntambi, J. M., Buhrow, S. A., Kaestner, K. H., Christy, R. J., Sibley, E., Kelly, T. J., Jr., and Lane, M. D. (1988) *J. Biol. Chem.* **263**, 17291–17300
- Enoch, H. G., and Strittmatter, P. (1978) *Biochemistry* **17**, 4927–

- 4932
10. Strittmatter, P., Thiede, M. A., Hackett, C. S., and Ozols, J. (1988) *J. Biol. Chem.* **263**, 2532-2535
 11. Resnick, M. A., and Mortimer, R. K. (1966) *J. Bacteriol.* **92**, 597-600
 12. Stukey, J. E., McDonough, V. M., and Martin, C. E. (1989) *J. Biol. Chem.* **264**, 16537-16544
 13. Maniatis, T., Fritsch, E. F., and Sambrook, J. (1982) in *Molecular Cloning: A Laboratory Manual*, Cold Spring Harbor Laboratory, Cold Spring Harbor, NY
 14. Ito, H., Fukuda, Y., Murata, K., and Kimura, A. (1983) *J. Bacteriol.* **153**, 163-168
 15. Sanger, F., Nicklen, S., and Coulson, A. R. (1977) *Proc. Natl. Acad. Sci. U. S. A.* **74**, 5463-5467
 16. Devereux, J., Haeberli, P., and Smithies, O. (1984) *Nucleic Acids Res.* **12**, 387-395
 17. Kyte, J., and Doolittle, R. F. (1982) *J. Mol. Biol.* **157**, 105-132
 18. Kates, M. (1972) *Techniques of Lipidology*, Elsevier Scientific Publishing Co., New York
 19. Morrison, W. R., and Smith, L. M. (1964) *J. Lipid Res.* **5**, 600-608
 20. Struhl, K. (1989) *Annu. Rev. Biochem.* **58**, 1051-1077
 21. Cigan, A. M., and Donahue, T. F. (1987) *Gene (Amst.)* **59**, 1-18
 22. Jeffcoat, R., Brawn, P. R., Safford, R., and James, A. T. (1977) *Biochem. J.* **161**, 431-437
 23. Sherman, F., Fink, G. R., and Hicks, J. B. (1982) *Methods in Yeast Genetics*, Cold Spring Harbor Laboratory, Cold Spring Harbor, NY